University of Twente

Structure-preserving integrators for Molecular Dynamics

L.A. van Goor

Committee:
Prof. dr. ir. B.J. Geurts
Dr. ir. M. Bokdam
Dr. ir. E. Luesink
A. Franken, MSc.
Prof. dr. C. Filippi
Dr. F.L. Schwenninger

Mathematics of Multiscale Modeling and Simulation (3MS)
Computational Chemical Physics (CCP)
University of Twente
Enschede
The Netherlands

May, 2023

Abstract

Fast and accurate time integrators for Molecular Dynamics (MD) simulations are needed to investigate the properties of materials without the experimental costs. This thesis illustrates the implementation and benefits of a structure-preserving time-integration method for structured MD models. We compare the Trapezoidal Munthe-Kaas (TMK) method, a Lie group integrator, with the widely used Verlet method for MD simulations. The Verlet method fails to conserve additional symmetry present in model simulations, leading to the development of asymmetry and inaccurate particle trajectories. In contrast, the TMK method, implemented with Flaschka variables, conserves additional symmetry of model simulations and exhibits qualitatively different behavior compared to the Verlet method. Preserving the structure and conserving the constants of motion in the governing equations through MD simulations can provide significant advantages. We demonstrate the effectiveness of the TMK method through multiple small and generic MD models that feature different potential forces, including the Lennard-Jones potential. Our approach could easily be extended to real MD simulations, which indicates the promising application of the TMK method for MD.

Contents

Chapter 1

Introduction

Fast and accurate time integrators for Molecular Dynamics (MD) simulations are needed to investigate the properties of materials without the experimental costs. In this thesis, two time integration methods are compared. We compare the commonly used energy-preserving Verlet method (Verlet, 1967) to the Trapezoidal Munthe-Kaas (TMK) method, a structure-preserving Lie-group integrator (Engø and Faltinsen, 2001). The TMK method, implemented with Flaschka variables (Flaschka, 1974a), shows qualitatively different behavior as compared to the Verlet method. This indicates possible advantages that can be obtained in MD simulations to explicitly preserve structures, symmetries, and conserved quantities in the governing equations. We illustrate the new time integrator with a number of MD models.

The evolution of a physical system can often be described with differential equations. Sometimes we can find the exact solution to these equations and calculate their outcomes at any given moment in time. However, more often than not, the exact analytical solution is not available to us. Instead, we approximate the evolution of a system using time steps and discrete approximations of the governing continuous-time equations (Hairer et al., 2006). The adopted time integration scheme captures how this is done. Depending on the scheme's construction, different numerical errors are made, impacting the calculated outcomes' reliability.

We focus on an N-body system consisting of an interacting set of molecules. With MD simulations, we want to predict the motion of those molecules as governed by a force field. If we can predict a material's (changing) geometric structure, we can predict many of its properties (Hook and Hall, 2013). Experimentally investigating the properties of many different materials is expensive. Instead, we would seek methods that enable accurate MD simulations to predict their characteristics (Frenkel and Smit, 2001). The general class to which this type of system belongs is the class of Hamiltonian systems. An analytical solution for such systems cannot be constructed for the N-body problem (Valtonen and Karttunen, 2006). Therefore, a numerical scheme and time integrator are employed. The commonly used method is the Verlet method.

The Verlet method is one of the most famous time integrators for MD simulations. This method has been reinvented throughout history under various names, including the Strömer, Leapfrog, and

Encke methods (Hairer et al., 2003). One of the first demonstrations of this method is given in the Principia, written by Newton himself in 1687. Nowadays, this scheme is extensively used in MD simulations (Coretti et al., 2022),(Lindahl, 2015). The Verlet scheme has many great properties, like energy conservation, symplecticity, and time-reversal symmetry. These properties and its simple formulation make it an excellent integrator for Hamiltonian systems. Other well-known integrators, like the fourth-order Runge-Kutta method, do not preserve energy or require a much more complicated and expensive implementation (Hairer et al., 2006). We will elaborate further on this in Chapter 2. However, Verlet is also known to have some issues, which may result in qualitative differences between the true and the computed system orbits. Although there is some evidence of true orbits close to computed system orbits, this has not been proven in general. In (Frenkel and Smit, 2001) the following is stated:

"Our trust in MD simulations as a tool is based largely on belief ... let us say that there is clearly still a corpse in the closet".

In this thesis, we will show that the Verlet scheme may fail qualitatively for a generic type of MD-like system. We will also demonstrate another structure-preserving integrator, the TMK method, which does not fail in these instances.

We argue that another integrator, the TMK method, is a promising integrator for MD simulations that does not have the same complications. The method is also energy-preserving like the Verlet method but preserves additional structure. We expect that this method is more accurate and ultimately less costly due to its structure-preserving properties. Structure and symmetry have been connected to the conservation of quantities ever since the famous theorem of Noether (Noether, 1971). Structure-preserving integrators can be constructed via Lie-group methods as described in (Engø and Faltinsen, 2001), based on methods such as the RKMK developed by (Munthe-Kaas, 1999). This is further described in Chapter 2. Traditionally, these integrators are used in highly symmetric Lie-Poisson problems, like the heavy-top or the rigid body (Marsden and Ratiu, 1999). This thesis uses structure-preserving methods to calculate MD simulations instead. To our knowledge, this has not been investigated before. Furthermore, we will show that the TMK method does not fail in a class of MD systems where the Verlet integrator fails.

This thesis aims to develop more accurate MD methods using the structure-preserving TMK method instead of the famous Verlet method. One of the challenges lies in comparing the outcomes of the TMK method with the outcomes of the Verlet method. We employ simple potentials to compare the behavior of the two integrators. The models build up from a two-particle system towards an n-dimensional system with periodic boundary conditions. This way, we can identify the two integrators' characteristic behavior and extend the conclusions to larger systems. A fourth-order Runge-Kutta method is used as a reference for the numerical solutions. In conclusion, the study demonstrates the possibilities of structure-preserving methods in MD simulations.

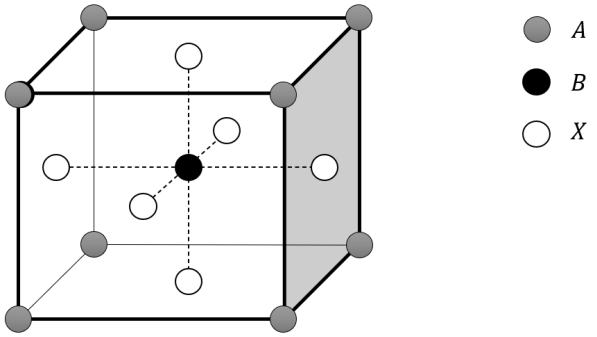

Figure 1.1: A unit cell of a cubic perovkite structure.

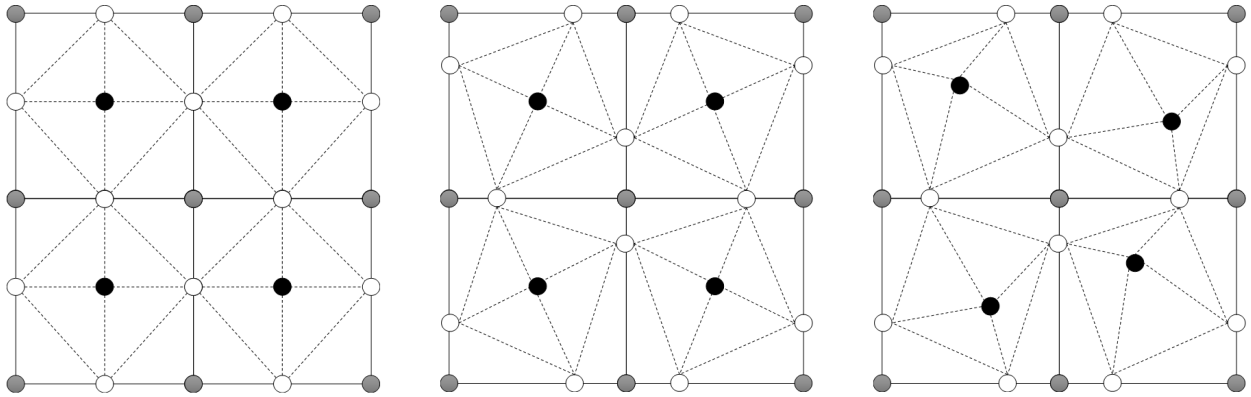

Figure 1.2: Phases of perovskite. From left to right; Cubic, Tetragonal, Orthorhombic.

Motivation

The motivation for this work stems from a particular type of material for MD simulations, namely the group of perovskites. In this section, we will motivate the interest in perovskites, briefly describe their lattice structure, and illustrate the importance of accurate simulations for these structured MD systems.

Materials with perovskite structures have demonstrated many properties, like superconductivity and ferroelectricity (Hook and Hall, 2013). Furthermore, certain perovskites are photovoltaics, materials that transform light into electricity, making them interesting materials for solar cells. Research has increased the power conversion efficiency of perovskite materials from 2.2 to 20.5 percent between 2006 and 2020 (Gao et al., 2019). Solar cells are only one of the many applications of perovskites. Other applications show that perovskites can act as lasers (Dereń et al., 2008), as LEDs Stranks and Snaith (2015), and for photoelectrolysis (Luo et al., 2014).

Perovskites are materials with a certain lattice structure ABX_3 where A, B are positively charged ions, cations, while the X is a negatively charged ion, an anion. The expected structure of a unit cell in the cubic phase is sketched in figure 1.1. Under certain conditions, like decreasing temperature, a perovskite can undergo a displacive phase transition and distort to a tetragonal structure with less symmetry. Such a phase transition can occur again when even less energy is available in the system, where even more symmetry loss leads to an orthorhombic structure. The structures of the cubic, tetragonal, and orthorhombic phases are sketched in figure 1.2.

Depending on the phase of the perovskite structure, the material has different characteristics. For example, $BaTiO_3$ does not have an electric polarization in the absence of an applied field when it is in the cubic phase. However, in the tetragonal and orthorhombic phases, there is a spontaneous electric polarization (Hook and Hall, 2013). Researchers can determine the suitability of particular perovskites for specific applications by predicting phase transitions and long-time stability. Determining this experimentally is costly. Therefore, accurate simulations of perovskites, respecting symmetries in the crystal structure are needed.

In order to perform MD simulations, we need to define the forces present in the system. Traditionally, the force field is approximated through density functional theory (DFT) calculations at each time step during the simulation. DFT calculations use the local electron density and incorporate quantum effects to calculate a force field. These calculations are accurate but costly. Ways to circumvent this cost with machine learning have been investigated (Lahnsteiner and Bokdam, 2022). Another possible approximation of the forces is to use DFT-informed potentials. In (Schelling et al., 2001),(You et al., 2023), and (Qu et al., 2021), force fields are calculated via interatomic potentials based on DFT calculations. This way, a system can be integrated in time with fewer DFT calculations. The interatomic potentials may be the sum of only a few classical force terms multiplied by parameters, which are fitted using a DFT database. The used force terms include Coulomb forces, Lennard-Jones potential forces, and exponential Toda-like forces. The results of this approach also predict the phase transitions and are cheaper to calculate.

The force fields are commonly integrated in time with the Verlet method. The Verlet method calculates the movement of each molecule separately, which is costly, and the exact trajectories are likely not recovered. (See Chapter 2). It makes little sense to have accurate force approximations but inaccurate time integration. The symmetries in the perovskite structure can be exploited to overcome these problems. The use of TMK in MD simulations to conserve symmetries is pursued in this thesis. To investigate the performance of the two integrators, i.e., Verlet and TMK, we will employ simulations of potential models with a quadratic, Toda, and Lennard-Jones potential. As these types of potentials are generic and also appear in the DFT-informed potential models, the simulations will indicate the quality of the integrators for real MD simulations.

Outline

The organization of this thesis is as follows. Chapter 2 of this thesis consists of an overview of the Verlet and Trapezoidal Munthe-Kaas (TMK) methods and gives a summary of the Runge-Kutta

methods since these are the basis of the TMK method. Furthermore, the chapter will provide the reader with enough information or references to other sources to understand the methods. In Chapter 3 the approach to implement TMK for MD for one-dimensional models is sketched. Chapter 4 discusses the simulations demonstrating differences in the numerical methods and simulations that resemble the perovskite structure. The thesis will be discussed and concluded in Chapter 5. Ideas for further research are given in Chapter 6.

Chapter 2

Time-integration methods

We are interested in the differences in performance of two types of time integrators for molecular systems. We study the accuracy and computational cost difference between the widely used Verlet method and a Lie group integrator, the structure-preserving Trapezoidal Munthe-Kaas method (TMK). In this chapter, we introduce the structure of both methods and discuss some of their features, such that we can employ and compare these methods for our simulations.
First, we will introduce and discuss the Verlet method in section 2.1. Next, we discuss the Runge-Kutta methods in section 2.2, since the methods form the basis of the Munthe-Kaas methods and are therefore used as a benchmark for all simulations in this thesis. Next, we provide some background information on Lie-group integrators in section 2.3. Finally, in section 2.4 the Munthe-Kaas integrators and specifically the TMK integrator are discussed. We will use a time-independent step size for simplicity, but all integrators allow for adaptive time-stepping.

2.1 Verlet method

As mentioned in the introduction, the Verlet method is also known as the Strömer, Leapfrog, or Encke methods. The different names result from the same method being reinvented multiple times throughout history in different fields. The method even appears in the Principia written by Newton himself in 1687 (Hairer et al., 2003) To this day, the Verlet method is used extensively as a basis for Molecular Dynamics simulations (MD), for example, in the new algorithm of (Coretti et al., 2022). Also, MD software packages, like GROMACS (Lindahl, 2015), have the Verlet method as their basis. GROMACS is used to calculate the stability of materials (Michl et al., 2019), enzyme simulations (Yu and Dalby, 2020), and Free Energy calculations (Gotzias, 2022). Like GROMACS, there are many optimized software packages to perform MD simulations for which a Verlet method is still at the basis of the software. A demonstration of these software packages' huge role in MD simulations is the existence of a Wikipedia article dedicated to the comparison between the different software, of which many, if not all, use Verlet. [1] The popularity of this integrator is not without reason. This section will introduce the scheme and mention some of its features.

[1] `https://en.wikipedia.org/wiki/Comparison_of_software_for_molecular_mechanics_modeling`

The scheme

The Verlet method is a time integration scheme used to evaluate equations of the form:

$$\ddot{q} = f(q) \tag{2.1}$$

Or, equivalently, as:

$$\dot{v} = f(q), \quad \dot{q} = v \tag{2.2}$$

In principle, any equation of this form can be solved with the Verlet method. However, in anticipation of our application to molecular dynamics, let us use q, v to denote the position and velocity of a particle respectively. Let us denote the discretized versions of these variables and the function $f(q)$ by:

$$v(t = t_0 + n\Delta t) = v_n \tag{2.3}$$
$$q(t = t_0 + n\Delta t) = q_n \tag{2.4}$$
$$f(q_n) = f_n, \tag{2.5}$$

The Verlet method uses a staggered grid to evaluate this type of system, splitting the evaluation of velocity v and position q at intermediate and integer time steps, respectively. Each step of the scheme is given by:

$$v_{n+\frac{1}{2}} = v_{n-\frac{1}{2}} f_n \Delta t \tag{2.6}$$
$$q_{n+1} = q_n + v_{n+\frac{1}{2}} \Delta t \tag{2.7}$$

This formulation of the method poses a challenge for the initialization of the scheme, as the velocity is not defined at $t = t_0$. Commonly, a 'kick-drift-kick' form of the method is employed that solves the initialization of the staggered grid. Even though strictly the velocity only needs to be evaluated at the intermediate time steps, in the 'kick-drift-kick' form it is also calculated at the integer time steps. The velocity 'kick' is split into two kicks from v_n to $v_{n+\frac{1}{2}}$ to v_{n+1}. This solves the computation of the first $v_{\frac{1}{2}}$ term.

Below, the 'kick-drift-kick' form of the Verlet method is given, which is further illustrated schematically in figure 2.1. Now that we know the structure of the Verlet algorithm, we can identify some of its features.

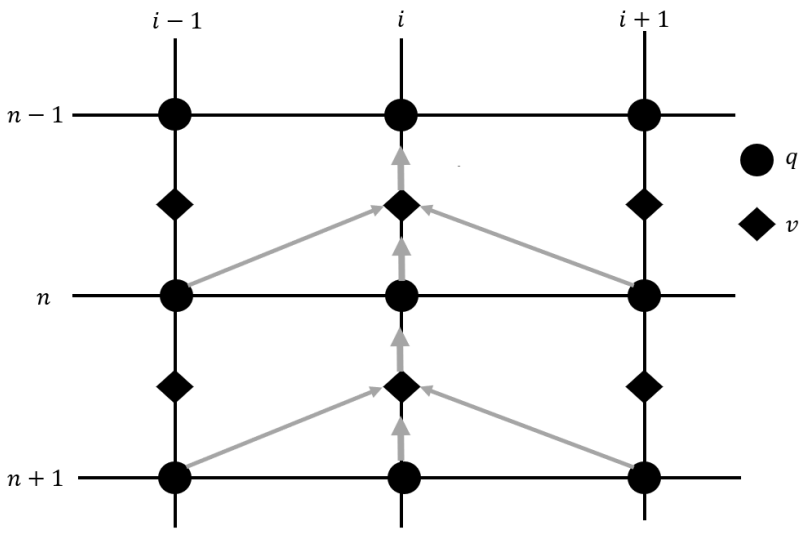

Figure 2.1: Staggered grid of the Verlet scheme. i indicating the ith grid point of the spatial discretization, n indicating the nth grid point of the temporal discretization. Blue and Red indicate the points at which the momentum and position are defined respectively.

Integrator 1 - Verlet
For systems of the form in equation 2.2, the positions and velocities at each new time step, $t_{n+1} = t_n + \Delta t$, are computed with the Verlet scheme as follows:

$$\begin{aligned} v_{n+\frac{1}{2}} &= v_n + \frac{1}{2} f_n \Delta t \\ q_{n+1} &= q_n + v_{n+\frac{1}{2}} \Delta t \\ v_{n+1} &= q_{n+\frac{1}{2}} + \frac{1}{2} f_{n+1} \Delta t \end{aligned} \tag{2.8}$$

where Δt is the time step size.

Note that one commonly writes $\ddot{q} = f(q) = A(q)$. The function $A(q)$ is called the acceleration function.

Features

The Verlet method has numerous characteristics that make it a popular method. These include its second-order convergence, reversibility with respect to time, preservation of linear first integrals, preservation of some quadratic integrals, and symplecticity (Hairer et al., 2003). Due to these features, Verlet is near-preserving the total energy and exactly preserving total linear and angular momentum for the N-body Hamiltonian system. While remaining a simple scheme with little com-

putational cost, it has excellent long-time behavior.

Firstly, it is a relatively simple scheme, with only one additional explicit step than the basic Euler forward method, but with an improved order of convergence of order two. This makes it a computationally cheap but rapidly converging method.

Secondly, the Verlet integrator is symmetric with respect to time. This implies that it is also reversible. After the next time-step is calculated, t_{n+1}, we can apply the same integrator to calculate a time-step backward,t_n, and obtain the same state in phase space up to rounding errors as we initially started with. This implies that the method exactly retains the time-reversal symmetry of a Hamiltonian system.

Furthermore, the Verlet method is a symplectic integrator. Hamiltonian systems have a symplectic phase space structure. The symplectic integrator preserves this structure. One could also state that the flow of a Hamiltonian system is a symplectic transformation. Therefore, preserving the symplecticity is connected to preserving the Hamiltonian nature of the system.

Let us demonstrate this in some more detail. For some Hamiltonian system $Q = (q_1, q_2, ..., q_n)$ the phase space can be identified as the cotangent bundle $T^*Q = (q_1, q_2, .., ., p_1, p_2, ..., p_n)$. The phase space is an underlying symplectic structure, namely, it is a symplectic manifold. This means that the phase space is a smooth manifold that is symplectic with respect to a closed non-degenerate 2-form. The 2-form is given as:

$$\omega = \sum_{i=1}^{n} dp_i \wedge dq_i \tag{2.9}$$

Where the wedge operator is the product of the exterior algebra. In coordinates, the 2-form is given by:

$$\omega(e_k, e_l) = \sum_{i=1}^{n} \det \begin{bmatrix} q_i(e_k) & q_i(e_l) \\ p_i(e_k) & p_i(e_l) \end{bmatrix}, \quad q, p \text{ given in the basis } e_k, e_l \in \mathbb{R}^{2n} \tag{2.10}$$

This can be written as:

$$\omega(\xi, \eta) = \xi^T J \eta, \quad \text{with } J = \begin{bmatrix} 0 & I \\ -I & 0 \end{bmatrix} \tag{2.11}$$

Any transformation A that preserves this form is a symplectic transformation. This condition can be written as:

$$A^T J A = J \quad \rightleftarrows \quad \omega(A\xi, A\eta) = \omega(\xi, \eta), \quad \forall \xi, \eta \in \mathbb{R}^{2n} \tag{2.12}$$

A symplectic transformation acting on ξ, η in a one-dimensional system is sketched in figure 2.2. A Hamiltonian system inherently contains a symplectic structure, which can be formulated in the following Theorem (Hairer et al., 2006):

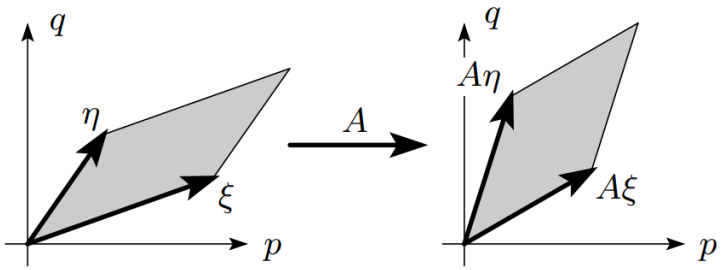

Figure 2.2: Symplecticity (area preservation) of a linear mapping. (Hairer et al., 2006)

Theorem 3.1
Let $f : U \to \mathbb{R}^{2n}$ be continuously differentiable. Then, $\frac{d}{dt}((p,q)) = f((p,q))$ is locally Hamiltonian if and only if its flow $\phi_t((p,q))$ is symplectic for all $(p,q) \in U$ and for all sufficiently small t.

Note that the flow dictates the mapping that advances the solution in time:

$$\phi_t(p_0, q_0) = (p(t, p_0, q_0), q(t, p_0, q_0)) \tag{2.13}$$

If an integrator does not preserve the symplectic geometry, the numerical solution is no longer a Hamiltonian flow. Fortunately, the Verlet method is symplectic, as proven by (De Vogelaere, 1956).

Symplectic methods have a linear global error growth and long-time near-preservation of first integrals as opposed to quadratic error growth and drifting first integrals of non-symplectic methods[2] (Hairer et al., 2003). As the total energy is a first integral, it must be near-preserved within some error bounds by the Verlet method. Bounds have been constructed from the symmetry and symplecticity of the Verlet method by (Benettin and Giorgilli, 1994) and (Hairer and Lubich, 2000). The error bounds are given by equation 2.14. This means that although the method does not preserve the exact total energy, the energy will not drift for long-time simulations but will remain within these bounds.

$$|H(p_n, q_n) - H(p_0, q_0)| \leq C(\Delta t)^2 + C_N(\Delta t)^N t, \quad \text{for} \quad 0 \leq t = n\Delta t \leq (\Delta t)^{-N} \tag{2.14}$$

where N is a arbitray positive integer, C and C_N are independent of $t, \Delta t$.

The near-preservation of the total energy, the Hamiltonian, may be explained via the modified equation. Through backward analysis in (Hairer et al., 2003) it is shown that the Verlet method does not solve the exact system, but rather a perturbation of the system. This can be formulated in a modified equation. The Hamiltonian that is conserved exactly by the Verlet method is the modified equation's Hamiltonian, which is commonly referred to as the shadow Hamiltonian. For short times,

[2] A first integral is some function $I((p,q))$ that is constant, or invariant along the solution, such that $I'((p,q))f((p,q)) = 0$ for all (p,q), where $f((p,q)) = \left(\frac{dp}{dt}, \frac{dq}{dt}\right)$ and $I'((p,q)) = \left(\frac{\partial I}{\partial p}, \frac{\partial I}{\partial q}\right)$.

the real Hamiltonian only varies with $O(h^2)$ from this shadow Hamiltonian. The long-term behavior is captured in the error bound in equation 2.14.

As mentioned, the Verlet method is symplectic and, therefore, near-preserving of first integrals. However, we can make an even stronger statement. We can state that the Verlet method exactly preserves linear first integrals (Hairer et al., 2003). This implies that the Verlet method conserves total linear momentum. Furthermore, a certain type of quadratic first integrals is also conserved by the Verlet method. For Hamiltonian systems, quadratic first integrals of the following form are conserved by the Verlet method:

$$I(p, q) = p^\top (Bq + b) \tag{2.15}$$

were B is a constant square matrix, b a constant vector and I the first integral.
For the N-body Hamiltonian system, this means that the Verlet method preserves total angular momentum but not the Hamiltonian.

The Verlet method is not unconditionally stable, and we require a sufficiently small time step to assure stability. A commonly used criterion for the time step size as compared to the highest eigenfrequency of the system is given in equation 2.17. This criterion is derived from the solution of a harmonic oscillator and ensures that the eigenvalues of the propagation matrix are modulus one for constant Δt (Hairer et al., 2003). The propagation matrix, or sometimes called the amplification matrix of a numerical method applied to a continuous system A is given by

$$(p_{n+1}, q_{n+1}) = A((p_n, q_n)) \tag{2.16}$$

The eigenvalues of this matrix should be smaller or equal to 1 to prevent exploding numerical errors. This is a stability criterion.

$$|\Delta t \omega| \leq 2 \tag{2.17}$$

where ω is the largest eigenfrequency of the system.

In conclusion, the Verlet method is stable for sufficiently small time steps and remains near-energy preserving for long-time simulations. Furthermore, for the N-body system, total linear momentum and total angular momentum are conserved exactly by Verlet. These excellent features, in combination with its low computational costs, make the Verlet method a seemingly ideal time-integration method for large MD simulations. However, the Verlet method does not conserve all first integrals of a system, which might lead to incorrect solutions such as the calculated trajectory.

2.2 Runge-Kutta methods

Runge-Kutta methods form the basis of many time-integration methods. For example, the Munthe-Kaas methods are essentially Runge-Kutta methods constructed on manifolds. Furthermore, the fourth-order Runge-Kutta method is used as a reference method for the performed simulations.
Runge-Kutta methods, as defined in definition 3.1, are time integration schemes used to solve equations of the form:

$$\dot{y} = f(t, y), \quad y(t_0) = y_0 \tag{2.18}$$

This holds for y in vector form. Therefore, we can solve systems of the form of equation 2.1 rewritten in the form of equation 2.2 with a Runge-Kutta method.

$$\dot{\mathbf{y}} = \begin{bmatrix} \dot{v} \\ \dot{q} \end{bmatrix} = \begin{bmatrix} f(q) \\ v \end{bmatrix} = \mathbf{f}(q, v), \quad \begin{bmatrix} v(t_0) \\ q(t_0) \end{bmatrix} = \begin{bmatrix} v_0 \\ q_0 \end{bmatrix} \tag{2.19}$$

Let us review the definition of a Runge-Kutta method:

Definition 3.1
An s-stage **Runge-Kutta method** is given by:

$$k_i = f\left(t_0 + c_i h,\, y_0 + h\sum_{j=1}^{s} a_{ij}k_j\right), \quad i = 1, ..., s \tag{2.20}$$

$$y_1 = y_0 + h\sum_{i=1}^{s} b_i k_i \tag{2.21}$$

where b_i, a_{ij}, c_i are real numbers.

In each time step of the Runge-Kutta method, the solution of the system is approximated by a polygonal line. The line is composed of s parts with varying slopes. The number of parts, s, are called the stages of the Runge-Kutta method. The slopes and portion of each part of the line are determined by the constants (a_{ij}, c_i, b_i). This is visualized for some three-stage explicit method in figure 2.3. Since the constants characterize the method, a method can be described entirely by a Butcher Tableau as follows:

$$\begin{array}{c|ccc} c_1 & a_{11} & \cdots & a_{1s} \\ \vdots & \vdots & & \vdots \\ c_s & a_{s1} & \cdots & a_{ss} \\ \hline & b_1 & \cdots & b_s \end{array} \tag{2.22}$$

The Runge-Kutta methods can be explicit or implicit. For explicit methods, the matrix $\mathbf{A} = (a_{ij})$ is strictly triangular. If the $\mathbf{A}$ is not strictly triangular, the coefficients k_i cannot be calculated explicitly, and the method is implicit.
An arbitrary combination of coefficients in the Butcher Tableau will generally not produce a reasonable numerical method. Several conditions on these coefficients are needed for stability, consistency, and convergence, but this will not be further explored in this thesis. The reader is referred to the book (Hairer et al., 2006) for further information.

If the coefficients of the Butcher Tableau satisfy equation 2.23, then the corresponding Runge-Kutta method conserves quadratic first integrals and it is symplectic.

$$b_i a_{ij} + b_j a_{ji} = b_i b_j, \quad \text{for all } i, j = 1, .., s. \tag{2.23}$$

Numerous numerical methods can be classified as Runge-Kutta methods. Famous examples are the Euler forward method, the Crank-Nicholson method, and Heun's method. The Butcher Tableau's

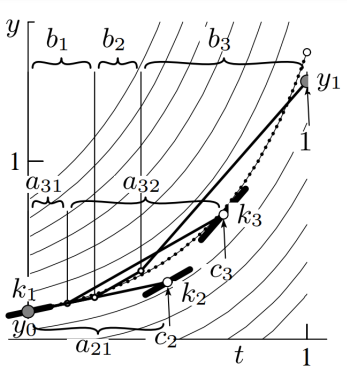

Figure 2.3: A three-stage explicit Runge-Kutta time step.(Hairer et al., 2006)

of these examples are shown in equation 2.24.

$$\begin{array}{c|c} 0 & 0 \\ \hline & 1 \end{array}, \quad \begin{array}{c|cc} 0 & 0 & 0 \\ 1 & 1/2 & 1/2 \\ \hline & 1/2 & 1/2 \end{array}, \quad \begin{array}{c|cc} 0 & 0 & 0 \\ 1 & 1 & 0 \\ \hline & 1/2 & 1/2 \end{array}, \tag{2.24}$$

One of the most famous Runge-Kutta methods is the fourth-order Runge-Kutta method (RK4). This method is celebrated for its fourth-order global error $O(h^4)$ and thus its fast convergence. Therefore, RK4 is often used in large simulations. Because of its accuracy, we will use RK4 as a reference method in simulations. The Butcher tableau of this method is given by:

$$\begin{array}{c|cccc} 0 & 0 & 0 & 0 & 0 \\ 1/2 & 1/2 & 0 & 0 & 0 \\ 1/2 & 0 & 1/2 & 0 & 0 \\ 1 & 0 & 0 & 1 & 0 \\ \hline & 1/6 & 2/6 & 2/6 & 1/6 \end{array} \tag{2.25}$$

As can be seen in the tableau, the matrix $\mathbf{A} = (a_{ij})$ is strictly triangular, which implies that the method is explicit. No explicit Runge-Kutta method is energy preserving (Celledoni et al., 2009). By the Butcher Tableau in 2.25, we note that the RK4 method is explicit and thus can not be energy-conserving. Instead, a drift in total energy may be expected. This causes issues for long-time simulations, which should be considered when using this method. Furthermore, it is not symplectic by equation 2.23, making it unsuitable for solving Hamiltonian systems. The RK4 method is also formulated below.

Integrator 2 - Fourth-order Runge-Kutta (RK4)
For systems of the form in equation 2.18, the solution at each new time step, $t_{n+1} = t_n + \Delta t$, is computed with the RK4 scheme as:

$$y_{n+1} = y_n + \frac{\Delta t}{6}(k_1 + 2k_2 + 2k_3 + k_4) \tag{2.26}$$

with:

$$\begin{aligned} k_1 &= f(t_n, y_n) \\ k_2 &= f\left(t_n + \frac{\Delta t}{2}, y_n + \frac{\Delta t}{2}k_1\right) \\ k_3 &= f\left(t_n + \frac{\Delta t}{2}, y_n + \frac{\Delta t}{2}k_2\right) \\ k_4 &= f\left(t_n + \Delta t, y_n + \Delta t k_3\right) \end{aligned}$$

where Δt is the time step size.

2.3 Lie group theory

Despite the many appealing features of the Verlet algorithm, we would like to consider a different time-integration method. Since the Verlet method does not conserve all possible constants of motion or symmetries of the system, another method might be more suited for calculations on a system with additional structure. Therefore, we introduce a Runge-Kutta Munthe-Kaas method, which solves the equation with a Runge-Kutta method on a manifold. Specifically, the Trapezoidal Munthe-Kaas (TMK) method will be used, as this method is also energy-conserving. Since the 1990s, Lie group integrators have been developed more systematically and extensively by, among others, (Crouch and Grossman, 1993) and (Munthe-Kaas, 1999). These time-integration methods are based on a coordinate-independent description of the equations, which will be detailed in this section. Since Lie group integrators have not yet seen general application-based implementations, we explore how these integrators can be applied to molecular systems in Chapter 3.

The essence of this chapter is captured in Figure 2.6. The Verlet method solves a differential equation $\mathbb{R}^n$ in some space. To apply the TMK method, the differential equation is first transformed to a Lie group formulation, $G = M$. Then, the differential equation is solved by locally transforming it to a differential equation on the Lie algebra $\mathfrak{g}$.

In other words, Lie group integrators integrate differential equations over the Lie group. A Hamiltonian system can be described in a Lie group formulation. This approach differs from simply integrating the canonical Hamiltonian formulation. The advantages of this approach become apparent whenever the Hamiltonian problem has an additional structure such as invariance under a

specific action. For these Hamiltonian problems, the group formulation can reduce dimensions whilst exactly preserving the additional structure. By integrating over a Lie group in the corresponding Lie algebra, the solution satisfies the Lie group structure. Therefore, by an appropriate choice of Lie group, symmetries of the system that are incorporated in the group can be preserved. By the famous paper Noether (Noether, 1971), the continuous symmetries of the system dictate the existence of corresponding conserved values. Thus, preserving symmetry and structure is essential to integrate a system appropriately.

For a general introduction to Lie group integrators, the reader is referred to (Hairer et al., 2006). A particularly clear overview of Lie group integrators is given by (Celledoni et al., 2014). A more theoretical introduction on Lie groups and algebras can be found in (Holm et al., 2009) and more formally in (Marsden and Ratiu, 1999).

In the following subsections, we will introduce the most important notions of a Lie group, Lie algebra, and introduce some group actions. With these notions, we can describe how a Hamiltonian system can be described in a Lie group formulation. This background knowledge will be useful for the construction and use of the TMK integrator.

The Lie group

The origin of the Lie group stems from a desire to construct a collection of continuous transformations. A minimal structure of this collection on which differentiability and continuity can be defined was constructed by (Lie, 1874). Let us look at the definition of a group:

Definition 3.2
A **group** G is a non-empty set together with a binary composition law, here denoted with the dot $\cdot$, that has the following properties:

1. **Closure.** The composition of any two elements, $g, h \in G$ is called the product and is in itself an element of G:
$$g, h \in G \quad \Longrightarrow \quad g \cdot h \in G \tag{2.27}$$

2. **Associativity.** The composition law is associative:
$$g, h, k \in G \quad \Longrightarrow \quad ((g \cdot h) \cdot k) = (g \cdot (h \cdot k)) \tag{2.28}$$

3. **Identity**. There exists an element called the unit or identity, denoted by e or I, such that:
$$g \cdot e = e \cdot g = g, \quad \forall g \in G \tag{2.29}$$

4. **Inverses.** Every element $g \in G$ has an inverse denoted by g^{-1} which is also in G, such that:
$$g^{-1} \cdot g = g \cdot g^{-1} = e \tag{2.30}$$

Clearly, a group is a set with an operation that upholds certain laws. To be able to consider differentiability and continuity, the group needs to also be a smooth manifold. Specifically, we will consider an n-dimension topological manifold that is also smooth. The definition of a (smooth) manifold is quite technical and deserves more background information than provided here. Therefore, the reader is referred to (Marsden and Ratiu, 1999) or (Holm et al., 2009) for more information[3]. However, we can give an intuitive description of a smooth manifold.

Intuitive description smooth manifold
A **manifold** is a (topological) space that locally resembles $\mathbb{R}^n$. Such, one can construct a complete collection of transformations called charts that map the manifold to open subsets of $\mathbb{R}^n$. A smooth manifold has the property that any smooth function in the domain of one such chart, ϕ_k, must also be smooth in the same domain mapped by any other chart ϕ_m.

With the definition of a group and of a smooth manifold, we can finally define a Lie group, as done by (Marsden and Ratiu, 1999), or (Holm et al., 2009):

Definition 3.3
A **Lie group** is a smooth manifold G that has a group structure consistent with its manifold structure in the sense that the group multiplication

$$\mu : \quad G \times G \to G, \quad g \cdot h \to gh, \tag{2.31}$$

is a C^∞ map. *(Infinitely differentiable).*

The Lie algebra

Having obtained some notion of a Lie group, being a smooth manifold with smooth group multiplication, we must look further into the Lie algebra. Tangent spaces, as defined by (Holm et al., 2009), enable us to describe the Lie algebra, a vector space that can be closely related to the Lie group. A sketch of the tangent space notion is given in Figure 2.4.

Definition 3.4
Let M be an submanifold of $\mathbb{R}^n$. A **tangent vector** to M is $g'(0)$ for some smooth path $g : \mathbb{R} \to M$ such that $g(0) = x$. The **tangent space** to M at point x is the set of all tangent vectors based at x, denoted T_xM. Every tangent space is a vector space.

With the notion of the tangent space, a Lie algebra corresponding to a Lie group can be defined:

[3]For the curious reader, there is a very nice lecture series available on Youtube of Fredic Schuller that provides a clear explanation of the topic. `https://www.youtube.com/@FredericSchuller`.

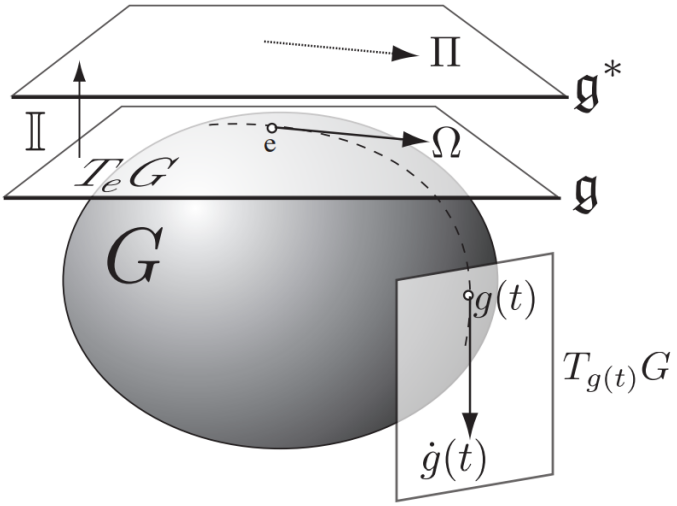

Figure 2.4: The Lie algebra sketched as the tangent space at the identity element of the group manifold G. The manifold is sketched as a sphere, but it need not be this shape. Also, the dual Lie algebra corresponding to the Lie algebra on which the solution is calculated is sketched. From (Holm, 2011).

Definition 3.5
A **Lie algebra** $\mathfrak{g}$ is the tangent space at the identity T_eG of a Lie group G, together with the corresponding Lie bracket.

A Lie algebra is a tangent space equipped with an operation, the Lie bracket. This operation has to uphold some properties as follows:

Definition 3.6
The **Lie bracket** is an operation denoted by $[\cdot, \cdot]$ on elements in the Lie algebra. It satisfies bilinearity, alternativity, and the Jacobi identity.

The corresponding Lie algebra is unique for a Lie group up to isomorphisms. However, a Lie algebra can be constructed without a Lie group or/and belong to multiple Lie groups. Furthermore, in this thesis, we only consider finite-dimensional Lie algebras. The elements of any finite-dimensional Lie algebra can be mapped to the Lie group via the exponential map.

Definition 3.7
The **exponential map** maps an element of the Lie algebra to the Lie group:

$$\exp : \mathfrak{g} \to G \tag{2.32}$$

The dual space of the Lie algebra will be denoted by $\mathfrak{g}^*$ and referred to as the dual Lie algebra. In this thesis, only finite-dimensional Lie algebras are considered, which are finite dimensional vector spaces. Since the dual of any finite-dimensional vector space exists, the dual of the considered Lie algebra exists too.

Tangent bundle

Another notion that will be useful is that of the tangent bundle and cotangent bundle.

Definition 3.8
Let M be an submanifold of $\mathbb{R}^n$. The **tangent bundle** of M denoted by TM, is the union of all the tangent spaces to M:

$$TM = \bigcup_{x \in M} T_x M \tag{2.33}$$

The cotangent bundle is the dual space of the tangent bundle denoted by T^*M.

Group actions

Group action on the group

The actions of a Lie group on an element of the Lie group should follow the rules of a group. A Lie group action on the Lie group itself can be defined as the left translation, $L_g : G \to G$ given by $h \to gh$. Also, a right translation can be identified, as $R_g : G \to G$ as $h \to hg$.

Group action on a manifold

A group G can also act on a manifold. For example, the set of invertible linear transformations in $\mathbb{R}^n$ is a (matrix) Lie group. It remains to show how exactly a group action on a manifold is defined. Let us look at the definition as given by (Marsden and Ratiu, 1999):

Definition 3.9
Let M be a manifold, and let G be a Lie group. A smooth left action of a Lie group G on a manifold M is a smooth mapping $\Phi : G \times M \to M$ such that:

(i) $\Phi(e, x) = x$ for all $x \in M$;
(ii) $\Phi(g, \Phi(h, x)) = \Phi(gh, x)$ for all $g, h \in G$ and $x \in M$.

The left action of the group $g \in G$ on a point in the manifold $x \in M$ could also be expressed at the tangent level by some infinitesimal action of a Lie group element $\xi \in \mathfrak{g}$. To be more precise, a smooth path at the element x in time can be constructed with the Lie group element:

$$t \to (\exp(t\xi))x \quad = path \quad \in M \tag{2.34}$$

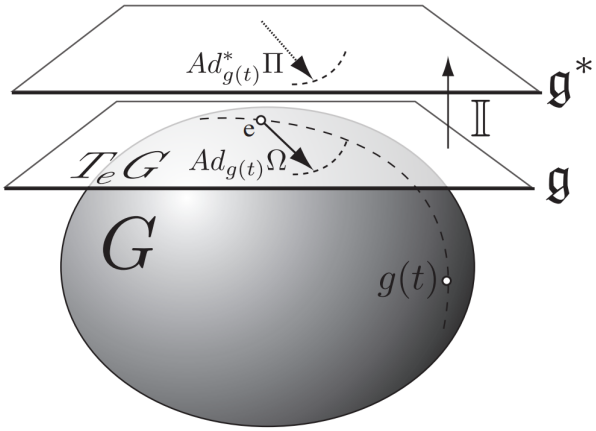

Figure 2.5: The Adjoint and Coadjoint actions working on the Lie algebra and dual Lie algebra, respectively. From (Holm, 2011).

At each point, $x \in M$ a tangent vector to this smooth path can be identified and is called the infinitesimal generator associated with ξ at $x \in M$. The infinitesimal generator is given by:

$$\xi_M(x) := \frac{d}{dt}\bigg|_{t=0} \textit{(path)} \ \in T_xM \tag{2.35}$$

By definition, the Lie algebra $\mathfrak{g}$ consists of the tangent space of the Lie group at the identity of the Lie grou,p and with elements of the Lie algebra, we can describe the infinitesimal action $\xi_M(x) \in \mathfrak{g}$ on $x \in M$ that generates the Lie group action. The infinitesimal action of $\mathfrak{g}$ on M is given by:

$$\mathfrak{g} \times M \to TM, \quad (\xi, x) \to \xi_M(x) \tag{2.36}$$

Group action on the Lie algebra

Another group action is the action of the group on the Lie algebra or the dual of the Lie algebra. These actions are called the Adjoint Action and Coadjoint Action of G on $\mathfrak{g}$ and $\mathfrak{g}^*$ given in equation 2.37 and 2.38. The actions are sketched in Figure 2.5.

$$\mathrm{Ad} \ : G \times \mathfrak{g} \to \mathfrak{g}, \qquad \mathrm{Ad}_g(\xi) = T_eI_g(\xi) = T_e(R_{g^{-1}} \circ L_g)\xi \tag{2.37}$$

$$\mathrm{Ad}^* : G \times \mathfrak{g}^* \to \mathfrak{g}^*, \quad \left\langle \mathrm{Ad}^*_g\mu, \xi \right\rangle = \langle \mu, \mathrm{Ad}_g\xi \rangle \tag{2.38}$$

for all $\mu \in \mathfrak{g}^*$, $\xi \in \mathfrak{g}$, $g \in G$, and $\langle \cdot, \cdot \rangle : \mathfrak{g}^* \times \mathfrak{g} \to \mathbb{R}$ is the natural pairing.

Similarly to the infinitesimal action of the group action, the Coadjoint or Adjoint action can also be expressed by Lie algebra elements related to the tangent vectors at the Lie algebra or the dual Lie algebra element on which the Coadjoint or Adjoint acts. These infinitesimal actions are called the

adjoint and coadjoint operators and are defined as:

$$\mathrm{ad} : \mathfrak{g} \times \mathfrak{g} \to \mathfrak{g}, \qquad \mathrm{ad}_\xi(\eta) = (\xi, \eta) \to \left.\frac{d}{dt}\right|_{t=0} \mathrm{Ad}_{\exp t\xi}(\eta) \tag{2.39}$$

$$\mathrm{ad}^* : g \times \mathfrak{g}^* \to \mathfrak{g}^*, \quad \left\langle \mathrm{ad}^*_\xi \mu, \eta \right\rangle = \langle \mu, \mathrm{ad}_\xi \eta \rangle \tag{2.40}$$

for all $\eta, \xi \in \mathfrak{g}$, $\mu \in \mathfrak{g}^*$.

Matrix Lie groups

In this thesis, we consider a particular type of Lie group known as a matrix Lie group. The elements of these groups can be represented by matrices, where matrix multiplication is used as the composition law. Moreover, the exponential map for matrix Lie groups is given by the exponential of matrices.

$$\exp : \mathfrak{g} \to G \tag{2.41}$$

$$\exp(\xi) = I + \frac{\xi}{1!} + \frac{\xi^2}{2!} + ... \tag{2.42}$$

for an element $\xi \in \mathfrak{g}$, with I being the identity matrix.

For matrix Lie groups, the Lie bracket is given by the matrix commutator:

$$[\xi, \eta] = \xi\eta - \eta\xi, \quad \xi, \eta \in \mathfrak{g} \tag{2.43}$$

The Adjoint action, Coadjoint action, adjoint operator, and coadjoint operator for matrix Lie groups are given by (Holm et al., 2009):

$$\mathrm{Ad}_R \xi = R\xi R^{-1} \tag{2.44}$$

$$\mathrm{Ad}^*_{R^{-1}} \mu = R^{-T} \mu R^T \tag{2.45}$$

$$\mathrm{ad}_\xi \eta = [\xi, \eta] \tag{2.46}$$

$$\mathrm{ad}^*_\xi \mu = -[\mu, \xi^\top] \tag{2.47}$$

for all $R \in G$, $\xi, \eta \in \mathfrak{g}$, $\mu \in \mathfrak{g}^*$ and with $[\cdot, \cdot]$ the Lie bracket.

Differential equations and Lie groups

We can introduce differential equations on a manifold using the following theorem.

Theorem 3.2
Let M be a real n-dimensional manifold. The problem $\dot{x} = f(x)$ is a differential equation on the manifold M if and only if

$$f(x) \in T_x M \quad \text{for all } x \in M \tag{2.48}$$

Using this theorem and the exponential map, (Hairer et al., 2006) showed that the tangent space of the matrix Lie group G at element g is the action of some Lie algebra element to the group element. Therefore, the whole tangent space at g can be constructed with Lie group elements ξ:

$$T_gG = \{\xi g \,|\, \xi \in \mathfrak{g}\} \tag{2.49}$$

Using theorem 3.1, for a matrix Lie group, we note that the differential equation must be in the tangent space of the group:

$$\dot{g} = f(g) \in T_gG \tag{2.50}$$

However, it was just stated that the tangent space at g can be constructed with elements of the Lie algebra. Therefore, we note that $f(g)$ must be equal to ξg for some element of the Lie algebra. Which Lie algebra element this is depends on g and we write $\xi(g)$ to indicate that the Lie algebra element is now a function dependent on g. Using this, we can write down the following theorem (Hairer et al., 2006):

Theorem 3.3
Let G be a matrix Lie group and $\mathfrak{g}$ its Lie algebra. If $\xi(g) \in \mathfrak{g}$ for all $g \in G$, then the solution of:

$$\dot{g} = \xi(g)g \tag{2.51}$$

satisfies $g(t) \in G$ for all t.

This implies that the differential equation stays on the Lie group and that we can write the differential equation as a Lie algebra action. This is used in the Runge-Kutta Munthe-Kaas (RKMK) methods.

From Hamiltonian system to Lie group formulation

As introduced, the phase space of a Hamiltonian system has a symplectic structure. In particular, the phase space of a Hamiltonian system may be described on the cotangent bundle of the real space $T^*\mathbb{R}^m$, which has an underlying symplectic structure.

$$H : T^*\mathbb{R}^m \to \mathbb{R} \tag{2.52}$$

We can transform the motion of the Hamiltonian system to a formulation on the cotangent bundle of a Lie group G instead of the cotangent bundle of $\mathbb{R}^m$.

$$H : T^*G \to \mathbb{R} \tag{2.53}$$

The specific Lie group applicable depends on the symmetries and invariances of the Hamiltonian system in question. Let us sketch the mapping of the Hamiltonian problem to Lie group formulation and Lie algebra formulation in figure 2.6. For completeness, the Lagrangian formulation is included as well.

Lie-Poisson structure

A large class of Hamiltonian problems can be formulated using Lie-Poisson formalism. The symplectic structure relates to a Lie-Poisson structure. Namely, the Hamilton's equations for a given $H : T^*M \to \mathbb{R}$ are equivalent to (Holm et al., 2009):

$$\dot{F} = \{F, H\}, \quad \text{for all differentiable } F : T^*M \to \mathbb{R} \tag{2.54}$$

Where $\{\cdot, \cdot\}$ are the canonical Poisson brackets on T^*M. For a system with $(q^1, q^2, ..., q^n, p_1, ..., p_n)$ the canonical Poisson brackets are given by:

$$\{F, G\} = \frac{\partial F}{\partial q^i}\frac{\partial G}{\partial p_i} - \frac{\partial F}{\partial p_i}\frac{\partial G}{\partial q^i} \tag{2.55}$$

A more general Poisson bracket than the canonical Poisson bracket can be defined for other structures. In fact, any dual Lie algebra carries a Poisson bracket. For further information see (Holm et al., 2009).

Let us demonstrate briefly how a canonical Hamiltonian formulation is rewritten to a Lie-Poisson system. A Hamiltonian system can be described in canonical coordinates on the phase space as:

$$\frac{dp}{dt} = -\frac{\partial H}{\partial q}, \quad \frac{dq}{dt} = \frac{\partial H}{\partial p} \tag{2.56}$$

where $H = H(p, q)$ and $p, q \in \mathbb{R}^n$. Alternatively, with $\mu = (p; q) \in \mathbb{R}^n$ we can write:

$$\frac{d\mu}{dt} = -J\nabla H(\mu) \tag{2.57}$$

where $J(\mu)$ is a skew-symmetric matrix given by:

$$J = \begin{bmatrix} 0 & I_n \\ -I_n & 0 \end{bmatrix} \tag{2.58}$$

As discussed in section 2.1, the Hamiltonian system has a symplectic structure in phase space, described by:

$$w(\xi, \eta) = \xi^T J \eta \tag{2.59}$$

Let us now change from the canonical formulation to the Lie-Poisson formulation. The skew-symmetric matrix J was constant for the canonical system but will depend linearly on elements of $\mathfrak{g}^*$ in what follows. Furthermore, let μ be an element of the dual Lie algebra $\mathfrak{g}^*$. Let us express μ and $J(\mu)$ for finite dimensional systems on the basis of the dual algebra, $\{e_k\}_{k=1}^d$, where d is the dimension of the system and C_{ij} are the structure constants.

$$\mu = \sum_{k=1}^{d} \mu_k e_k, \quad (J(\mu))_{ij} = \sum_{k=1}^{d} C_{ij}^k \mu_k \tag{2.60}$$

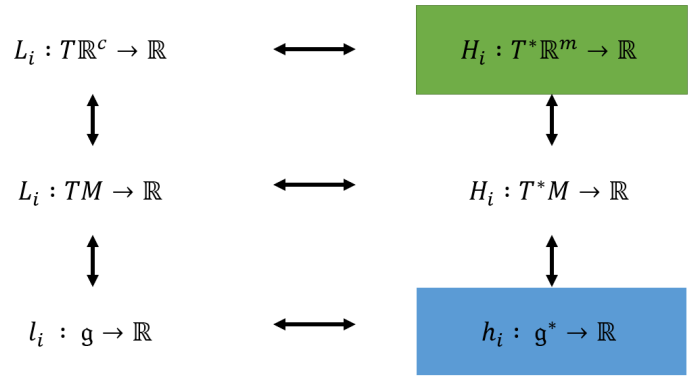

Figure 2.6: Lagrangian and Hamiltonian formulation on Euclidean space, manifolds (Lie groups), and the Lie algebra. Green denotes the application of Verlet, Blue of TMK. The horizontal arrows indicate the (reduced) Lagrange transforms.

As mentioned, any Lie algebra carries a linear Poisson. It can be shown that this implies the following[4]:

$$\mathrm{ad}^*_\sigma \mu = -J(\mu)\sigma \tag{2.61}$$

for any $\sigma \in \mathfrak{g}$ and any $\mu \in \mathfrak{g}^*$.

For the Lie-Poisson equations associated with a Hamiltonian, we can therefore write the differential equation as:

$$\frac{d\mu}{dt} = \mathrm{ad}^*_{\nabla H}\mu = -J(\mu)\nabla H \tag{2.62}$$

These are the Lie-Poisson equations.

Casimirs

On the dual Lie algebra, we will define the Poisson bracket as done in (Engø and Faltinsen, 2001):

$$\{F, G\}(\mu) = \nabla F(\mu)^\top J(\mu) \nabla G(\mu) \tag{2.63}$$

Any function F for which $\{F, G\} = 0$ for all other functions G on the manifold is called a Casimir. The first integrals as defined in section 2.1 are Casimirs.

2.4 Trapezoidal Munthe-Kaas method

In the previous subsection, we introduced matrix Lie groups, their actions and we have rewritten an ODE on a matrix Lie group. In this subsection, we describe the Trapezoidal Munthe-Kaas method,

[4]The reader is referred to (Luesink et al.,2022).

which is a method for solving differential equations on the Lie group while adhering to the group structure. First, the Runge-Kutta Munthe-Kaas (RKMK) methods are described. Then, the TMK method, which is an RKMK method, is discussed.

For derivations of the methods, see the original papers (Munthe-Kaas, 1999) and (Engø and Faltinsen, 2001). Another paper providing a particularly clear and more extensive overview for the learning reader is (Iserles et al., 2000). The method can be extended to stochastic processes as described by (Luesink et al., 2021).

The RKMK methods

Munthe-Kaas has developed methods to integrate ODEs on manifolds with Runge-Kutta methods (Munthe-Kaas, 1999). These are now known to be the Runge-Kutta Munthe-Kaas methods (RKMK). At each time step, a RKMK method constructs an ODE on a Lie algebra and advances that ODE. The result is then transformed into the result on the manifold. The strength of the RKMK approach lies in the achievable order of accuracy. The order of accuracy of the RKMK methods can be as high as that of the underlying Runge-Kutta method. Since Runge-Kutta methods of any order can be constructed, the approach of Munthe-Kaas leads to arbitrarily high-order methods on manifolds. Due to this property, the RKMK methods greatly impacted the field of Lie group integrators. We will review the RKMK methods for Lie groups only, but the reader should know that the RKMK methods apply to more general manifolds.

We have seen in the previous subsection that ODEs on Lie groups can be rewritten to functions on the Lie algebra. This step is crucially needed for the RKMK methods to hold. For clarity, we will rewrite this in a slightly different notation once more, although essentially the same is stated in the previous section, now we will allow for time dependency in the notation.[5]

Let us consider an ODE on a Lie group of the following form:

$$\dot{g} = f(t, g), \quad g(0) = g_0, \quad f : \mathbb{R} \times G \to G \tag{2.64}$$

The ODE can be rewritten for matrix Lie groups with a function $\tilde{f}$ mapping to the Lie algebra instead of the Lie group.

$$\dot{g} = \tilde{f}(t, g)g, \quad g(0) = g_0, \quad \tilde{f} : \mathbb{R} \times G \to \mathfrak{g} \tag{2.65}$$

With this notion, we can jump to the main point of the RKMK methods. Namely, the differential equation can be transformed into a differential equation on the Lie algebra for small time steps. The derivation from equation 2.65 to this result can be reviewed in the sources mentioned above.

[5] In the approach by Munthe-Kaas this is regarded to be an assumption.

The solution of equation 2.65 for small $t \geq 0$ is given by:

$$g(t) = \exp(\sigma(t))g_0 \tag{2.66}$$

where $\sigma \in \mathfrak{g}$ satisfies:

$$\dot{\sigma} = \mathrm{dexp}^{-1}_{\sigma(t)}(f(t,g)), \quad \sigma(0) = 0 \tag{2.67}$$

In other words, the solution of the system can be found by solving the differential equation on the Lie algebra at each time step. The solution of this differential equation is transformed into the solution of the original differential equation with the exponential map.

The operator $\mathrm{dexp}^{-1}_{\sigma}$ stems from the inverse of the differential of the exponential mapping and is a mapping given by:

$$\mathrm{dexp}^{-1}_{\sigma} \; : \; \mathfrak{g} \to \mathfrak{g} \tag{2.68}$$

$$\mathrm{dexp}^{-1}_{\sigma} = \sum_{k=0}^{\infty} \frac{B_k}{k!} \mathrm{ad}^k_{\sigma} \tag{2.69}$$

where B_k is the k-th Bernoulli number.

In the RKMK method, the inverse map is approximated by a summation to $q-1$, where q is the desired order of the scheme with the following expression:

$$\mathrm{dexpinv}(\sigma, v, q) = \sum_{k=0}^{q-1} \frac{B_k}{k!} \mathrm{ad}^k_{\sigma}(v) \tag{2.70}$$

Munthe-Kaas showed that an RKMK method remains on the manifold and has an order of convergence of at least q for any Lie group action on any manifold. Below, we will give the algorithm of the RKMK method.

RKMK method for Lie groups
For ODEs on Lie groups of the form 2.64, the Runge-Kutta Munthe-Kaas method computes the solution at each new time step $t_1 = t_0 + \Delta t$ with an s-stage Runge-Kutta method. A single (time) step of the method is given by:

$$
\begin{aligned}
&g(t) = g_0 \\
&\text{for} \qquad\qquad i = 1, 2, ..., s \\
&\qquad\qquad \sigma_i = \Delta t \sum_{j=1}^{s} a_{ij} \tilde{k}_j \\
&\qquad\qquad k_i = f(\Delta t c_i, \exp(\sigma_i) g_0) \\
&\qquad\qquad \tilde{k}_i = \text{dexpinv}(\sigma_i, k_i, q) \\
&\text{end} \\
&\sigma = \Delta t \sum_{j=1}^{s} b_j \tilde{k}_j \\
&g(t + \Delta t) = \exp(\sigma) g_0
\end{aligned}
$$

where $g_0, g \in M$, $\sigma_i, k_i, \tilde{k}_i \in \mathfrak{g}$ and a_{ij}, b_i, c_i are s-stage Runge-Kutta coefficients. The function $f(\cdot, \cdot)$ is the function as given by the ODE in equation 2.64

The TMK method

(Engø and Faltinsen, 2001) have applied the RKMK methods to Lie-Poisson systems, preserving Casimirs as well as the Hamiltonian. The connection and transformation of canonical Hamiltonian equations and the Lie-Poisson structure have been discussed along with the theory in section 2.3. Let us show how the Lie-Poisson equation is solved with the RKMK method where the trapezoidal rule is used as the Runge-Kutta method.

Let us denote the Lie-Poisson equation in terms of the coadjoint operator on the dual Lie group, as in equation 2.62:

$$\dot{\mu} = \text{ad}^*_{\nabla H(\mu)} \mu \tag{2.71}$$

for $h \in G$, $\mu \in \mathfrak{g}^*$.
It is shown by (Luesink et al., 2021) that the solution of this equation is given by:

$$\mu(t) = \text{Ad}^*_g \mu_0 \tag{2.72}$$

for some $g \in G$.

With the RKMK method, we locally represent the solution to the differential equation with $g = \exp(\sigma)$ for some Lie algebra element $\sigma \in \mathfrak{g}$:

$$\mu(t) = \mathrm{Ad}^*_{\exp(\sigma)}\mu_0, \quad \text{for small } t \geq 0 \tag{2.73}$$

Which leads to the differential equation on the Lie algebra of the form:

$$\dot{\sigma} = \mathrm{dexp}^{-1}_{\sigma}\left(\nabla H(\mu)\right) \tag{2.74}$$

Since we transformed the Hamiltonian system to an equation on the Lie algebra, we can use the RKMK method to solve this system in terms of sigma. For the Runge-Kutta coefficients, we use the trapezoidal method. This method is only second order, so we can truncate the summation in the inverse of the differential of the exponential map to $q = 2$. For $q = 2$, the operator dexp_{-1} reduces to the identity operator, and we condense the calculation of σ to the following (trapezoidal) form:

$$\sigma_n = \frac{1}{2}\Delta t\left(\nabla H(\mu_n) + \nabla H(\mu_{n+1})\right) \tag{2.75}$$

The resulting scheme is implicit. By the approach of (Engø and Faltinsen, 2001) we solve this iteratively with the Chord method. This method is an approximate version of the Newton-Raphson method. Instead of calculating and inverting the Jacobian term Df for each iteration, the Chord method approximates it with the initial Jacobian $Df(0)^{-1}$.

$$\sigma^{[k+1]} = \sigma^{[k]} - \left(Df(\sigma^{[k+1]})\right)^{-1} f(\sigma^{[k]}, \mu_n) \quad \text{Newton-Raphson method iteration} \tag{2.76}$$

$$\sigma^{[k+1]} = \sigma^{[k]} - \left(Df(0)\right)^{-1} f(\sigma^{[k]}, \mu_n) \quad \text{Chord method iteration} \tag{2.77}$$

The TMK method is given as follows:

Integrator 3 - Trapezoidal Munthe-Kaas (TMK) method
For systems of the form in equation 2.62, the solution at each new time step, $t_{n+1} = t_n + \Delta t$, is computed with the TMK method to order q as follows.

$$Df(0) = I + \frac{\Delta t}{2}D^2H(\mu_n)J(\mu_n)$$
$$\sigma = 0$$
while error $>$ tolerance :
$$k = k + 1$$
$$\sigma^{[k+1]} = \sigma^{[k]} - \left(Df(0)\right)^{-1} f(\sigma^{[k]}, \mu_n)$$
$$\text{error } = |\sigma^{[k+1]} - \sigma^{[k]}|$$
$$g = \exp(\sigma)$$
$$\mu_{n+1} = \mathrm{Ad}^*_g\mu_n$$

where Δt is the (constant) time step size and $f(\sigma)$ is given by:

$$f(\sigma, \mu) = \sigma - \Delta t\left(\nabla H\left(\frac{1}{2}\mu + \frac{1}{2}\exp(\mathrm{ad}^*_\sigma)\mu\right)\right) \tag{2.78}$$

Features of the TMK method

The TMK method has particular features that make it a suitable integrator for Hamiltonian systems. It preserves the Casimirs exactly[6]. Also, energy preservation of TMK is demonstrated in (Engø and Faltinsen, 2001) as well as a linear global error growth. Furthermore, by (Munthe-Kaas, 1999), the TMK method stays on the manifold. Therefore, any symmetries assumed by the group structure will be preserved.

The TMK method appears to have many features that the Verlet method has. In addition, one should note that the TMK method preserves the additional structure of the group and all constants of motion related to this structure. In contrast, we have seen that the Verlet method only preserves linear first integrals and some quadratic first integrals. Additional constants of motion and symmetries will not be preserved with the Verlet method but will be preserved with the TMK method.

Example: The rigid body

A classic example that demonstrates the excellent performance of the TMK method is the rigid body with a fixed point (Marsden and Ratiu, 1999). A rigid body consists of three or more mass points of which the distances within the body do not change; a non-deformable body. Furthermore, it is fixed at one point in some inertial frame. Therefore, we can reduce the dynamics to rotational motion around the fixed point. The rigid body can be described as a Lie-Poisson system on the Lie algebra $\mathfrak{so}(3)$ associated with the rotation group $SO(3)$, consisting of rotation matrices $\mathbf{R}$. The elements of the Lie algebra $\mathfrak{so}(3)$ are traceless, skew-symmetric matrices $\hat{\xi} \in \mathbb{R}^{3\times 3}$. All matrix Lie group rules apply as the Lie group is a matrix Lie group. The Lie algebra can be denoted in vector representation in $\mathbb{R}^3$ via the hat map as follows:

$$(\hat{}) : \mathbb{R}^3 \to \mathfrak{so}(3), \quad \xi = (\xi_1, \xi_2, \xi_3) \to \hat{\xi} = \begin{bmatrix} 0 & -\xi_3 & \xi_2 \\ \xi_3 & 0 & -\xi_1 \\ -\xi_2 & \xi_1 & 0 \end{bmatrix} \tag{2.79}$$

The Hamiltonian of the rigid body is given by the kinetic energy:

$$H = \frac{1}{2}\boldsymbol{\pi} \cdot \boldsymbol{I}^{-1}\boldsymbol{\pi} \tag{2.80}$$

where $\boldsymbol{\pi} \in \mathbb{R}^3$ is the angular momentum vector and $\boldsymbol{I} = \text{diag}(I_1, I_2, I_3) \in \mathbb{R}^{3\times 3}$ is the matrix representation of the moment of inertia tensor.
The equation of motion is given by:

$$\dot{\boldsymbol{\pi}} = \boldsymbol{\pi} \times \boldsymbol{I}^{-1}\boldsymbol{\pi} \tag{2.81}$$

The Casimir of the rigid body is given by:

$$C = \boldsymbol{\pi} \cdot \boldsymbol{\pi} \tag{2.82}$$

The Casimir as well as the total energy should remain constant. The TMK method is energy preserving and Casimir preserving. We expect the solution to have a conserved Hamiltonian as well as

[6] In fact, it preserves the coadjoint orbit and, therefore the Casimirs. However, we have not introduced this notion.

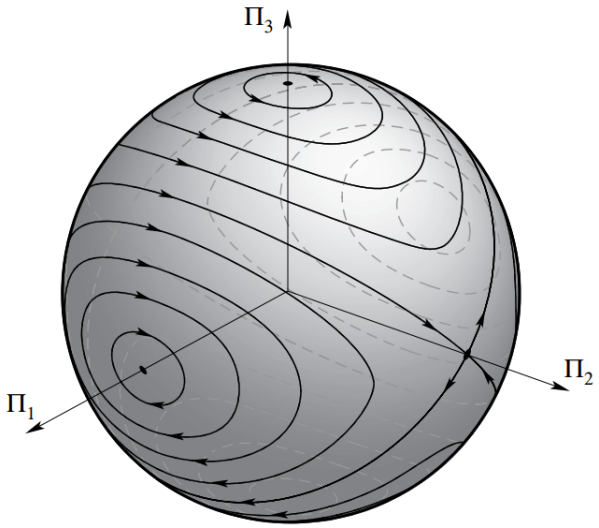

Figure 2.7: Intersection lines of level set H with sphere of radius $||\boldsymbol{\pi}||$ from (Marsden and Ratiu, 1999).

a conserved Casimir. Therefore, the solution for the angular momentum should at all times be on the intersection of level sets of the Casimir and the Hamiltonian, specified by the initial condition. A sketch of possible solution orbits on the sphere is given in Figure 2.7.

The numerical solution is computed an initial intertia of $\boldsymbol{I}_0 = \text{diag}\left(\frac{7}{8}, \frac{5}{8}, \frac{1}{4}\right)$, and initial angular momentum of $\boldsymbol{\pi} = (0.875, 0.625, 0.250)^T$ with TMK and RK4. The initial conditions are scaled s.t. $I = \frac{\boldsymbol{I}_0}{||\boldsymbol{I}_0||}$, $\boldsymbol{pi} = \frac{\boldsymbol{\pi}}{||\boldsymbol{\pi}||}$. The time step is set to $\Delta t = 0.1$. The solutions are plotted in Figure 2.8.

From the figures, one can see that the RK4 method has a drift in both the Casimir and the Hamiltonian, while, using the TMK method, they remain constant up to machine precision. We should not trust the RK4 method for long-time accurate simulations as this drift will build up the error. The change in $\boldsymbol{\pi}$ is still small enough that it appears to remain on the sphere of radius $||\boldsymbol{\pi}||$ for both methods for this short-time simulation. However, for long-time simulations, the non-conservation of the Casimir and Hamiltonian will result in visible incorrect errors.

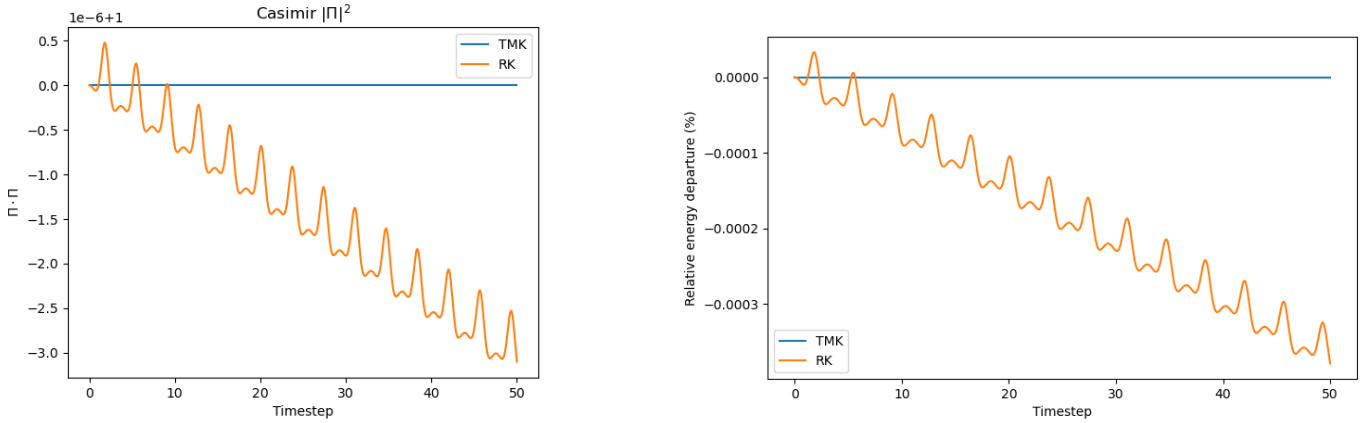

Figure 2.8: Casimir and total energy of a rigid body as a function of time for TMK and RK.

Chapter 3

TMK for MD - Methodology

The purpose of this section is twofold. First of all, we want to inform the reader of our choice of models for the N-body system. This is done in section 3.1 by describing the geometry of the models and the chosen potentials. Secondly, we describe our implementation of the trapezoidal Munthe-Kaas (TMK) integrator for Molecular Dynamics (MD) simulations. In section 3.2 we will introduce the Flaschka variables that are employed. Then, in section 3.3 the choice of Lie group is described, and its link to the physical system is explained. Also, a step-by-step plan of how to obtain all the needed expressions to implement the TMK method is given. Finally, in section A.1, an example is given for $n = 3$ particles on a line.

In this chapter, we describe our approach to implementing TMK for MD. However, this is not by any means the only approach possible. The TMK method is used in this thesis as it has many beneficial properties that make it a good choice for MD simulations. Other MD simulation methods are discussed in Chapter 2. For other possible approaches that might be of interest to implement a Lie group integrator for MD, see Chapter 6.

3.1 Setup

We consider a one-dimensional lattice with point particles in which neighboring particles interact via a potential. The models are Hamiltonian systems of the form 3.1 and are implemented as particles on a line and ring by imposing free and periodic boundary conditions. The setup is sketched in figure 3.1. In the one-dimensional setting, these are the only two topologically inequivalent cases.

The total energy of the system is given by the Hamiltonian H:

$$H = \sum_{k=1}^{n} \frac{1}{2} p_k^2 + V(r_k) \tag{3.1}$$

where n is the total number of particles, p_k is the momentum of the kth particle. We consider equal masses of unity, which implies that $p_k = v_k$, where v_k is the velocity of the kth particle. Furthermore,

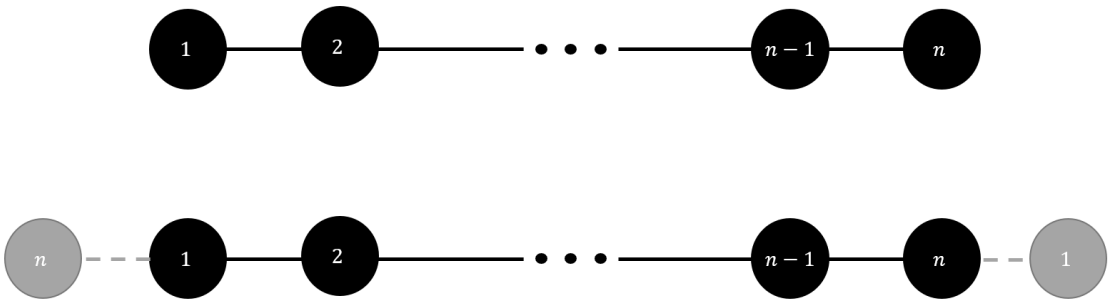

Figure 3.1: Sketch of one-dimensional lattice models with n particle without periodic boundary conditions (top), and with periodic boundary conditions (bottom).

r_k is the distance between two neighboring particles given by:

$$r_n = q_k - q_{k-1}, \quad \begin{cases} k = 2, 3, ..., n \text{ for free BC,} \\ k = 1, 2, ..., n \text{ for periodic BC.} \end{cases} \tag{3.2}$$

where q_k is the distance of the kth particle with respect to its equilibrium distance. The positions are sketched in figure 3.2

The dynamics of the system are governed by Newton's equations with a potential V:

$$m_k \ddot{q}_k = -\frac{\partial V}{\partial q_k}, \quad k = 1, 2, ..., n \tag{3.3}$$

This is equivalent to Hamilton's canonical equations for the Hamiltonian, given by:

$$\dot{q} = \frac{\partial H}{\partial p}, \quad \dot{p} = -\frac{\partial H}{\partial q} \tag{3.4}$$

Both notations are also equivalent to the Euler-Lagrange equations for certain Langrangians[1] denoted by:

$$\frac{d}{dt}\left(\frac{\partial L}{\partial \dot{q}}\right) - \frac{\partial L}{\partial q} = 0 \tag{3.5}$$

where the Lagrangian is related to the Hamiltonian as:

$$H(q, p) := p \cdot (\dot{q})(q, p) - L(q, \dot{q}(q, p)) \tag{3.6}$$

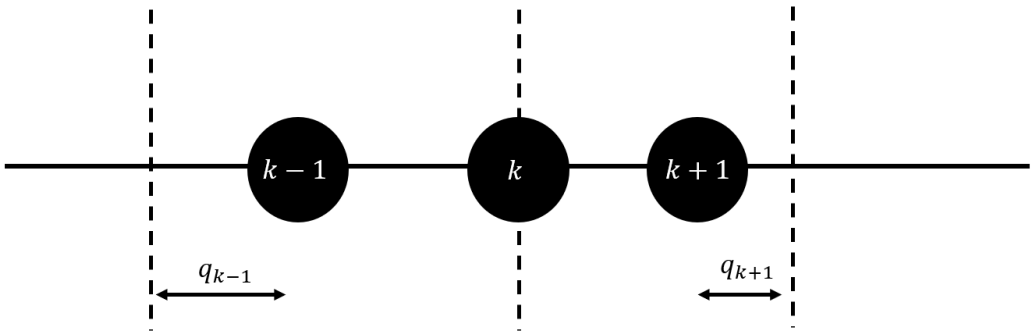

Figure 3.2: Positions of particles q with respect to their equilibrium position in the lattice indicated with a dashed line. Here, $q_k = 0$, $q_{k+1} < 0$, $q_{k-1} > 0$.

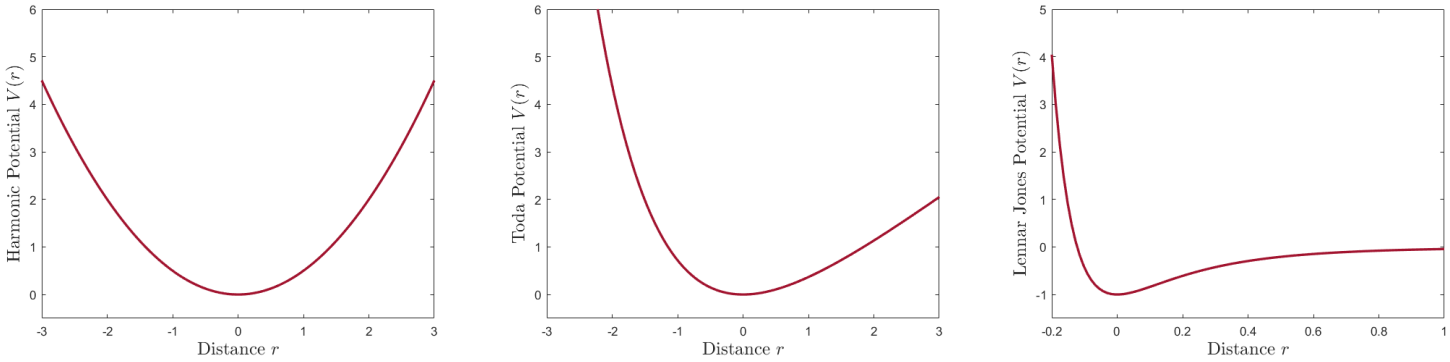

Figure 3.3: Interatomic potentials $V(r)$ as a function of the distance between particles with respect to their equilibrium distance, r. From left to right: the Toda potential, the quadratic potential of the harmonic oscillator, and the Lennard-Jones potential.

The Potentials

The potentials that are considered are the quadratic potential for the harmonic oscillator, the Toda potential [2], and the Lennard-Jones potential, as given in equations 3.7-3.9. The potentials are functions of the distance r with respect to the equilibrium distance $\tilde{r}$ between the particles.[3]The three potentials and resulting accelerations as a function of r are plotted in figure 3.3.

$$V_{Harm}(r) = \frac{1}{2}r^2 \tag{3.7}$$

$$V_{Toda}(r) = e^{-r} + r - 1 \tag{3.8}$$

$$V_{LJ}(r) = 4\left[\left(\frac{1}{r}\right)^{12} - \left(\frac{1}{r}\right)^{6}\right] \tag{3.9}$$

The Harmonic oscillator potential is a quadratic function in r. The quadratic function is symmetric with respect to r_{eq} and tends to infinity as r tends to $\pm\infty$. Because of this, particles can not escape this potential in case of energy conservation. The one-dimensional harmonic oscillator, $n = 2$, is an integrable system in one dimension of which the analytical solution is known. This fact allows us to compare numerical methods with the analytic solution.

The Toda potential contains an exponential function and a term that is linear in r. For $r > r_{eq}$, the linear term dominates the potential, and the potential increases linearly with r. The exponential term dominates for $r < r_{eq}$, resulting in a steep, exponentially increasing barrier. This ensures strong short-range repulsion between particles and a softer long-range attraction. The Toda lattice is a well-studied system that is integrable for any n. Due to this asymmetry and exponentially increasing potential on one side, trajectories with sharper corners and, thus, more numerical errors are expected.

The Lennard-Jones potential consists of rational polynomial terms down to order minus twelve. These result in a strong short-range repulsive and soft long-range attractive force. Unlike the Harmonic and Toda potential, due to the asymptotic approach to zero for $r \to \infty$, particles with enough energy can escape from this potential.

The simulations start from the two-body system with the Harmonic potential, for which we expect little numerical errors and smooth trajectories, to the most chaotic situation, for eight-body systems with the Lennard-Jones potential, for which interesting behavior and errors are expected. Furthermore, we will consider free and periodic boundary conditions for an increasing number of particles.

[1]Hyperregular Lagrangians to be precise. See (Holm et al., 2009).

[2]A one-dimensional chain connected by Toda potentials is a famous completely integrable system known as the Toda lattice.(Toda, 1970)

[3]It should be noted that the potentials are functions of r_n, where $r_{eq} = 0$ corresponds to the equilibrium distance of the potential for the Harmonic oscillator and Toda lattice, while $r_{eq} = 2^{\frac{1}{6}}$ corresponds to the equilibrium distance for the Lennard-Jones potential. Such, the positions are denoted with respect to their true equilibrium distance in the lattice as sketched in figure 3.2. We can write $r_n = (q_n - q_{n-1}) -$ for Toda and Harmonic, and $r_n = (q_n - q_{n-1}) + 2^{\frac{1}{6}}$ for the Lennard-Jones potential.

3.2 Flaschka variables

In our approach to implementing a Lie group integrator for MD-like simulations, we use Flaschka variables. These variables were first introduced in (Flaschka, 1974a) and (Flaschka, 1974b) to demonstrate the complete integrability of the Toda lattice. Namely, using Flaschka variables, the dynamics of the Toda lattice could be represented by the evolution of Lax pairs. With the Lax pair, it can be shown that the dynamics of the n-particle Toda lattice are governed by n distinct real eigenvalues that are preserved in time. Therefore, the system has a full set of conservatives and is integrable.

However, Flaschka variables are more than a trick to show integrability. In (Bloch et al., 2017), the Flaschka transformations are generalized to an abstract Flaschka transformation concept. Many exciting properties of the abstract Flaschka transformation are shown, and its use for many different problems is demonstrated. Even the rigid body problem could be rephrased as a Toda system up to some parameterization. These results indicate the generalization and possibilities of the Flaschka transformation beyond the Toda lattice. In this thesis, we will employ this transformation for all potentials.

Flaschka variables transform a Hamiltonian expressed in canonical coordinates (p, q) to a system expressed in Flaschka variables a, b. This transformation is given by:

$$a_k = \frac{1}{2} e^{-(q_{k+1}-q_k)/2} \tag{3.10}$$

$$b_k = -\frac{1}{2} p_k \tag{3.11}$$

for $k = 1, ..., n$.

For the different potentials, the Hamiltonian expressions under Flaschka transformation are given by equation 3.12-3.14[4]:

$$H_{Toda} = \sum_{k=1}^{n} \frac{1}{2} b_k^2 + \sum_{k=2}^{m+1} a_k^2 + \frac{1}{2} \ln\left(\frac{1}{2a_k}\right) - \frac{1}{4} \tag{3.12}$$

$$H_{Harm} = \sum_{k=1}^{n} \frac{1}{2} b_k^2 + \sum_{k=2}^{m+1} \frac{1}{2} \ln\left(\frac{1}{2a_k}\right)^2 \tag{3.13}$$

$$H_{LJ} = \sum_{k=1}^{n} \frac{1}{2} b_k^2 + \sum_{k=2}^{m+1} \left(2 \ln\left(\frac{1}{2a_k}\right) + 2^{\frac{1}{6}}\right)^{-12} - \left(2 \ln\left(\frac{1}{2a_k}\right) + 2^{\frac{1}{6}}\right)^{-6} \tag{3.14}$$

where n is the number of particles in the chain and m is the number of connections. For periodic boundary conditions $m = n$, otherwise $m = n = 1$.

[4]Note that the Hamiltonians are scaled by a factor 1/4.

3.3 Choice of group structure

Since we would like to improve MD simulations by conservating any additional structure of the system, the implementation of a Lie group In order to implement a Lie group integrator, we need to construct a suitable Lie group. For example, we have seen that the dynamics of the rigid body were invariant under rotations in three dimensions, and therefore the $SO(3)$ group was applicable. Now, we are considering a one-dimensional chain of particles in Flaschka variables. The construction of the Lie group and its action will be described in five steps. These steps are carried out for the $n = 3$ and $n = 2$ models with and without boundary conditions. We can generalize the resulting expressions to the n particle system. For one $n = 3$ model, the steps and calculations are demonstrated in section A.1, as well as the construction for arbitrary n.

Step 1. The state of the system

Let us consider the one-dimensional lattice model as described in section 3.1. The state of the system can completely be described by a b coefficient for each particle and an a coefficient for each interaction. This can be expressed by the following vector in $\mathbb{R}^{2n-1}$:

$$\mu = (a_1, a_2, ..., a_{n-1}, b_1, b_2, ..., b_n) \in \mathbb{R}^{2n-1} \tag{3.15}$$

In case of periodic boundary conditions the vector becomes $\mathbb{R}^{2n}$ with an additional a_n term:

$$\mu = (a_1, a_2, ..., a_{n-1}, a_n, b_1, b_2, ..., b_n) \in \mathbb{R}^{2n-1} \tag{3.16}$$

Step 2.1 Transformations of the system

After each time step, the state of the system is updated. However, the underlying structure of the system must be respected. The allowed set of state vectors the system can be in arises from considering transformations under which the system is invariant. Following the Toda lattice approach of (Holm and Lucas, 2013) let us consider scaling transformations of the a variable and shearing transformations of the b variable:

$$S: \quad (a_1, a_2, ..., a_{n-1}) \to \left(e^{\beta_1-\beta_2}a_1, e^{\beta_2-\beta_3}a_2, ..., e^{\beta_{n-1}-\beta_n}a_{n-1}\right) \tag{3.17}$$

$$W: \quad (b_1, b_2, ..., b_n) \quad \to (b_1 - \alpha_1 a_1, b_2 + \alpha_1 a_1 - \alpha_2 a_2, ..., b_n + \alpha_{n-1}a_{n-1}) \tag{3.18}$$

Such that the state vector under these transformations is given by:

$$\tilde{\mu} = \left(e^{\beta_1-\beta_2}a_1, e^{\beta_2-\beta_3}a_2, ..., e^{\beta_{n-1}-\beta_n}a_{n-1}, b_1 - \alpha_1 a_1, b_2 + \alpha_1 a_1 - \alpha_2 a_2, ..., b_n + \alpha_{n-1}a_{n-1}\right)$$

Step 2.2 Physical interpretation of Transformations

Note that the interacting particle system is invariant under the change to Flaschka variables. Also, note that the choice of these transformations does not dictate the way the state vector changes in time. The values of coefficients β and α are not set by the choice of group structure. Instead, the choice of these transformations merely dictates the allowed configurations of the system. The

most naive choice would be to allow any scaling and translation of a and b. However, there is more structure in the physical system, which can be put into the transformations. Let us discuss how this has been done for the scaling and shearing transformations separately.

By construction, the Flaschka variable a_k is related to the positions of the particles given by q_k, q_{k+1}. Similarly, the variable $a_{k\pm1}$ are related to $q_{k-1}, q_k, q_{k+1}, q_{k+2}$. Therefore, we know that there is a relation between the states a_k and $a_{k\pm1}$, dictated by the allowed positions q. This relation can be constructed into the transformation. In the physical system, any set of positions q might be a solution. Let us consider the translation freedom of q:

$$(q_1, q_2, ..., q_n) \rightarrow (q_1 + \beta_1, q_2 + \beta_2, ...q_n + \beta_n) \tag{3.19}$$

The scaling transformation of the Flaschka variables a_k corresponds to a translation transformation of the positions q. This is demonstrated below by the Flaschka transformation of the translation transformation of q_k and q_{k+1}, which results in a scaling transformation of the Flaschka variable a_k

$$\begin{aligned} FL(T(q_k)) &= FL(q_k + \beta_k) && (3.20)\\ &= \frac{1}{2} e^{-((q_{k+1}+\beta_{k+1})-(q_k+\beta_k))/2} && (3.21)\\ &= e^{\beta_k - \beta_{k+1}} a_k && (3.22)\\ &- e^{\beta_k - \beta_{k+1}} FL(q_k) && (3.23)\\ &= S(FL(q_k)) && (3.24) \end{aligned}$$

where T is the translation transformation, S the scaling transformation and FL the Flaschka transformation.

We restrict the transformation by only allowing scaling of the form $e^{\beta_k - \beta_{k+1}}$. Such, we implement the structure of a_k to $a_{k\pm1}$ imposed by the relation of the variables to $q_k, q_{k\pm1}$.

For the interpretation of the transformation of the momentum variable, b, let us consider the line of particles. The momenta of the particles change in time due to the nearest neighbor potential forces present. The perturbed distance between two particles creates a potential felt by each of the two particles. Since the masses of all particles are equal, the contribution of this potential to the momentum of the two involved particles must be equal. Therefore, the structure between the momenta of neighboring particles up to the initial momenta must be present. In other words, the momenta of neighboring particles did not change independently. Therefore, instead of allowing any transformation of the momenta, we can restrict the transformation R to be a function of the left and right displacements as follows:

$$R(p_k) = -2p_k + c_k \left(\frac{1}{2} e^{-(q_k - q_{k-1})/2} \right) - c_{k+1} \left(\frac{1}{2} e^{-(q_{k+1} - q_k)/2} \right) \tag{3.25}$$

where c_k is some multiplication factor.

For the Flaschka variables b this transformation is given by:

$$FL(R(p_k)) = FL\left(-2p_k + c_k\left(\frac{1}{2}e^{-(q_k-q_{k-1})/2}\right) - c_{k+1}\left(\frac{1}{2}e^{-(q_{k+1}-q_k)/2}\right)\right) \tag{3.26}$$

$$= FL\left(-2p_k + c_k a_k - c_{k+1}a_{k+1}\right) \tag{3.27}$$

$$= b_k - \frac{1}{2}c_k a_k + \frac{1}{2}c_{k+1}a_{k+1} \tag{3.28}$$

$$= b_k - \alpha_k a_k + \alpha_{k-1}a_{k-1} \tag{3.29}$$

$$= W(b_k) \tag{3.30}$$

where $\alpha_k = -\frac{1}{2}c_k$ is some multiplication factor.

It can be noted that the shear transformation of b_k corresponds to another shear transformation of p_k, denoted by W and R respectively. By shear transforming the momenta in this fashion, each momentum can be changed with respect to its initial conditions, but with the limitation that the change in momentum of the particle is the same as the change in momentum of its neighbors with respect to their inter distance.

Note once more that the shear and scaling transformations do not dictate the dynamics of the line of particles since the values of α and β are not determined here. The transformations under which the system is invariant merely describe the allowed geometric structures allowed in the simulation.

Step 3. Lie group and groups element

The transformations described in step 2 result in a semi-direct product Lie group $G = S \otimes W$. For more information on semi-direct product groups see (Holm et al., 2009) or (Marsden and Ratiu, 1999). We consider a group element $g \in G$ in following matrix representation, such that $G = S \otimes T \in GL$:

$$g = \left[\begin{array}{ccccc|c} e^{\beta_1-\beta_2} & & & & & \\ & e^{\beta_2-\beta_3} & & & & \\ & & \ddots & & & O_{(n-1)\times n} \\ & & & & e^{\beta_{n-1}-\beta_n} & \\ \hline -\alpha_1 & & & & & \\ \alpha_1 & -\alpha_2 & & & & \\ & \alpha_2 & \ddots & & & I_{n\times n} \\ & & \ddots & -\alpha_{n-1} & & \\ & & & \alpha_{n-1} & & \end{array}\right]_{(2n-1)\times(2n-1)}$$

The top left matrix is a diagonal matrix with $e^{\beta_k-\beta_{k+1}}$ on the diagonal and describes an element of the scaling group S. The bottom left matrix has $-\alpha_k$ on the diagonal and α_k on the lower sub-diagonal and is an element of the shearing group W. $I_{n\times n}$ is an identity matrix of size n by n.

$O_{(n-1)\times n}$ is a matrix filled with zeros of size $n-1$ by n. [5]

In the case of periodic boundary conditions, the dimension of the problem is increased by one, accounted for by the extra interaction term a_n. The group element represented in matrix form becomes:

$$g = \left[\begin{array}{ccccccc|c} e^{\beta_1-\beta_2} & & & & & & & \\ & e^{\beta_2-\beta_3} & & & & & & \\ & & \ddots & & & & & O_{n\times n} \\ & & & e^{\beta_{n-1}-\beta_n} & & & & \\ & & & & e^{\beta_n-\beta_1} & & & \\ \hline -\alpha_1 & & & & & \alpha_n & & \\ \alpha_1 & -\alpha_2 & & & & & & \\ & \alpha_2 & \ddots & & & & & I_{n\times n} \\ & & \ddots & -\alpha_{n-1} & & & & \\ & & & \alpha_{n-1} & -\alpha_n & & & \end{array}\right]_{2n\times 2n}$$

Step 4. Lie algebra element

The Lie algebra $\mathfrak{g}$ of a matrix Lie group G is identified with the tangent space at the identity T_IG. Hence, one can construct the Lie algebra element $\xi \in \mathfrak{g}$ of G as done by (Holm and Lucas, 2013) as:

$$\xi := \left[g^{-1}\dot{g}\right]_{t=0} \tag{3.31}$$

For notational convenience, we will introduce vector representation in $\mathbb{R}^{2n-1}$ for the Lie algebra and the dual Lie algebra. This can be done if there is an isomorphism from the Lie algebra and its dual to the vector space $\mathbb{R}^{2n-1}$. For more information see Chapter 5.3 of (Holm et al., 2009). [6] The matrix structure of the Lie algebra including the identification of the vector elements is given by:

$$\xi = \left[\begin{array}{ccccccc|c} \xi_n-\xi_{n+1} & & & & & & & \\ & \xi_{n+1}-\xi_{n+2} & & & & & & \\ & & \ddots & & & & & O_{(n-1)\times n} \\ & & & \xi_{2n-2}-\xi_{2n-1} & & & & \\ \hline -\xi_1 & & & & & & & \\ \xi_1 & -\xi_2 & & & & & & \\ & \xi_2 & \ddots & & & & & O_{n\times n} \\ & & \ddots & -\xi_{n-1} & & & & \\ & & & \xi_{n-1} & & & & \end{array}\right]_{(2n-1)\times(2n-1)}$$

[5] Note that the matrix structure of the group element is typical for a semi-direct product group. For comparison: the $SE(3)$ group, a semi-direct product group of $\mathbb{R}^3$ and $SO(3)$, has the form $\begin{bmatrix}\mathbf{R} & \mathbf{v}\\ 0 & 1\end{bmatrix}$ where $\mathbf{R} \in SO(3)$, $\mathbf{v} \in \mathbb{R}^3$.

[6] Note that the vector representation of a Lie algebra is not at all uncommon. A commonly known example is the hat representation of the $\mathfrak{so}(3)$ Lie algebra.

where ξ is an element of the Lie algebra $\mathfrak{g}$. Here, the matrix form is displayed, in which the elements of the vector representation are identified. The Lie algebra element is represented with the vector $(\xi_1, \xi_2, ..., \xi_{2n-1}) \in \mathbb{R}^{2n-1}$, of which the elements are identified as denoted in the matrix.

In the case of the periodic boundary conditions, the matrix Lie algebra element can be written as:

$$\xi = \left[\begin{array}{ccccccc|c} \xi_{n+1}-\xi_{n+2} & & & & & & & \\ & \xi_{n+2}-\xi_{n+3} & & & & & & \\ & & \ddots & & & & & O_{n\times n} \\ & & & \xi_{2n-2}-\xi_{2n-1} & & & & \\ & & & & \xi_{2n-1}-\xi_n & & & \\ \hline & -\xi_1 & & & & \xi_n & & \\ & \xi_1 & -\xi_2 & & & & & \\ & & \xi_2 & \ddots & & & & O_{n\times n} \\ & & & \ddots & -\xi_{n-1} & & & \\ & & & & \xi_{n-1} & -\xi_n & & \end{array}\right]_{2n\times 2n}$$

The structure of the dual Lie algebra elements, $\mu \in \mathfrak{g}^*$, are of a similar structure to the Lie algebra elements, but transposed. The dual Lie algebra elements can be represented with vectors as well $(\mu_1, \mu_2, ..., \mu_{2n-1})$, of which the entries are identified in the matrix representation of a dual Lie algebra element:

$$\mu = \left[\begin{array}{ccccc|ccc} \mu_n-\mu_{n+1} & & & & & -\mu_1 & \mu_1 & \\ & \mu_{n+1}-\mu_{n+2} & & & & & -\mu_2 & \mu_2 \\ & & \ddots & & & & & \ddots \\ & & & & \mu_{2n-2}-\mu_{2n-1} & & & -\mu_{n-1} \\ \hline & O_{n\times(n-1)} & & & & & O_{n\times n} & \end{array}\right]$$

Note that the letter μ has been used for both a state vector and for an element of $\mathfrak{g}^*$. We identify the Flaschka variables as the entries of the vector representation of μ:

$$(a_1, a_2, ..., a_{n-1}, b_1, b_2, ..., b_n) = (\mu_1, \mu_2, ..., \mu_{2n-1}) \tag{3.32}$$

Step 5. Lie group actions

As described in chapter 2, the TMK method employs the coadjoint action of the Lie group G on the Lie algebra $\mathfrak{g}$ and the adjoint operator of Lie algebra $\mathfrak{g}$ on itself. These can be constructed as follows (Holm et al., 2009):

1. Compute the Adjoint action of the Lie group G on the Lie algebra $\mathfrak{g}$. For matrix Lie algebras this is given by:

$$\mathrm{Ad}_g\xi : G \times \mathfrak{g} \to \mathfrak{g} \tag{3.33}$$

$$\mathrm{Ad}_g\xi = g\xi g^{-1} \tag{3.34}$$

and identify its vector elements $(\mathrm{Ad}_\xi\eta)_1, (\mathrm{Ad}_\xi\eta)_2, ..., (\mathrm{Ad}_\xi\eta)_n$, in the vector representation of the lie algebra $\mathfrak{g}$.

2. Use the relation for the Coadjoint action of Lie group G on the dual Lie algebra $\mathfrak{g}^*$ to find the elements of the Coadjoint action. The relation is given by:

$$\left\langle \mathrm{Ad}_g^*\mu, \xi \right\rangle = \langle \mu, \mathrm{Ad}_g\xi \rangle \tag{3.35}$$

3. Write the Coadjoint action in matrix form.

4. Compute the adjoint operator of Lie algebra $\mathfrak{g}$ on itself. For matrix Lie algebras this is given by the commutator:

$$\mathrm{ad}_\xi\eta : \mathfrak{g} \times \mathfrak{g} \to \mathfrak{g} \tag{3.36}$$
$$\mathrm{ad}_\xi\eta = [\xi, \eta] = \xi\eta - \eta\xi \tag{3.37}$$

and identify its vector elements $(\mathrm{ad}_\xi\eta)_1, (\mathrm{ad}_\xi\eta)_2, ..., (\mathrm{ad}_\xi\eta)_n$, in the vector representation of the lie algebra $\mathfrak{g}$.

A demonstrative example of the step-by-step process is given in section A.1 of the Appendix. From the example, the structure of the Coadjoint action and adjoint operator become apparent. From this, we can construct expressions for the Coadjoint action and adjoint operator for any one-dimensional n-particle system with or without boundary conditions.

Adjoint operator structure

For the Lie algebra corresponding to the group $S \odot W$, the adjoint operator $\mathrm{ad}_\xi\eta$ in vector representation is given by:

$$\begin{bmatrix} (\mathrm{ad}_\xi\eta)_1 \\ (\mathrm{ad}_\xi\eta)_2 \\ \vdots \\ (\mathrm{ad}_\xi\eta)_{n-1} \\ (\mathrm{ad}_\xi\eta)_n \\ (\mathrm{ad}_\xi\eta)_{n+1} \\ \vdots \\ (\mathrm{ad}_\xi\eta)_{2n-1} \end{bmatrix} = \begin{bmatrix} \xi_1(\eta_n - \eta_{n+1}) - \eta_1(\xi_n - \xi_{n+1}) \\ \xi_2(\eta_{n+1} - \eta_{n+2}) + \eta_2(\xi_{n+1} - \xi_{n+2}) \\ \vdots \\ \xi_{n-1}(\eta_{2n-2} - \eta_{2n-1}) + \eta_{n-1}(\xi_{2n-2} - \xi_{2n-1}) \\ 0 \\ 0 \\ \vdots \\ 0 \end{bmatrix} \tag{3.38}$$

For the same algebra, but incorporating periodic boundary conditions, the Coadjoint action can be represented in vector notation as:

$$\begin{bmatrix} (\mathrm{ad}_\xi\eta)_1 \\ (\mathrm{ad}_\xi\eta)_2 \\ \vdots \\ (\mathrm{ad}_\xi\eta)_n \\ (\mathrm{ad}_\xi\eta)_{n+1} \\ (\mathrm{ad}_\xi\eta)_{n+2} \\ \vdots \\ (\mathrm{ad}_\xi\eta)_{2n} \end{bmatrix} = \begin{bmatrix} \xi_1(\eta_{n+1}-\eta_{n+2})-\eta_1(\xi_{n+1}-\xi_{n+2}) \\ \xi_2(\eta_{n+2}-\eta_{n+3})+\eta_2(\xi_{n+2}-\xi_{n+3}) \\ \vdots \\ \xi_n(\eta_{2n-1}-\eta_{2n})+\eta_n(\xi_{2n-1}-\xi_{2n}) \\ 0 \\ 0 \\ \vdots \\ 0 \end{bmatrix} \tag{3.39}$$

Coadjoint action structure

For the group $S \odot W$, and corresponding Lie algebra, the Coadjoint action $\mathrm{Ad}^*_g\xi$ in vector representation is given by:

$$\begin{bmatrix} (\mathrm{Ad}^*_g\xi)_1 \\ (\mathrm{Ad}^*_g\xi)_2 \\ \vdots \\ (\mathrm{Ad}^*_g\xi)_{n-1} \\ (\mathrm{Ad}^*_g\xi)_n \\ (\mathrm{Ad}^*_g\xi)_{n+1} \\ \vdots \\ (\mathrm{Ad}^*_g\xi)_{n+k} \\ \vdots \\ (\mathrm{Ad}^*_g\xi)_{2n-2} \\ (\mathrm{Ad}^*_g\xi)_{2n-1} \end{bmatrix} = \begin{bmatrix} \mu_1 e^{\beta_2-\beta_1} \\ \mu_2 e^{\beta_3-\beta_2} \\ \vdots \\ \mu_{n-1}e^{\beta_n-\beta_{n-1}} \\ \mu_1 e^{\beta_2-\beta_1}\alpha_1+\mu_n \\ -\mu_1 e^{\beta_2-\beta_1}\alpha_1+\mu_2 e^{\beta_3-\beta_2}\alpha_2+\mu_{n+1} \\ \vdots \\ -\mu_k e^{\beta_{k+1}-\beta_k}\alpha_k+\mu_{k+1}e^{\beta_{k+2}-\beta_{k+1}}\alpha_{k+1}+\mu_{n+k} \\ \vdots \\ -\mu_{n-2}e^{\beta_{n-1}-\beta_{n-2}}\alpha_{n-2}+\mu_{n-1}e^{\beta_n-\beta_{n-1}}\alpha_{n-1}+\mu_{2n-2} \\ -\mu_{n-1}e^{\beta_n-\beta_{n-1}}\alpha_{n-1}+\mu_{2n-1} \end{bmatrix} \tag{3.40}$$

For the same group, but incorporating periodic boundary conditions, the Coadjoint action can be represented in vector notation as:

$$\begin{bmatrix} (\mathrm{Ad}^*_g\xi)_1 \\ (\mathrm{Ad}^*_g\xi)_2 \\ \vdots \\ (\mathrm{Ad}^*_g\xi)_n \\ (\mathrm{Ad}^*_g\xi)_{n+1} \\ (\mathrm{Ad}^*_g\xi)_{n+2} \\ \vdots \\ (\mathrm{Ad}^*_g\xi)_{n+k} \\ \vdots \\ (\mathrm{Ad}^*_g\xi)_{2n-1} \\ (\mathrm{Ad}^*_g\xi)_{2n} \end{bmatrix} = \begin{bmatrix} \mu_1 e^{\beta_2-\beta_1} \\ \mu_2 e^{\beta_3-\beta_2} \\ \vdots \\ \mu_n e^{\beta_1-\beta_n} \\ -\mu_n e^{\beta_1-\beta_n}\alpha_n+\mu_1 e^{\beta_2-\beta_1}\alpha_1+\mu_{n+1} \\ -\mu_1 e^{\beta_2-\beta_1}\alpha_1+\mu_2 e^{\beta_3-\beta_2}\alpha_2+\mu_{n+2} \\ \vdots \\ -\mu_{k-1}e^{\beta_k-\beta_{k-1}}\alpha_{k-1}+\mu_k e^{\beta_{k+1}-\beta_k}\alpha_k+\mu_{n+k} \\ \vdots \\ -\mu_{n-2}e^{\beta_{n-1}-\beta_{n-2}}\alpha_{n-2}+\mu_{n-1}e^{\beta_n-\beta_{n-1}}\alpha_{n-1}+\mu_{2n-1} \\ -\mu_{n-1}e^{\beta_n-\beta_{n-1}}\alpha_{n-1}+\mu_n e^{\beta_1-\beta_n}\alpha_n+\mu_{2n} \end{bmatrix} \tag{3.41}$$

Chapter 4

Qualitative symmetry breaking in structured MD simulations

As described in Chapter 2, the Verlet method does not conserve all possible conserved quantities of a system or its additional symmetries. Therefore, to obtain more accurate simulations, a Lie group integrator that can preserve symmetries and the corresponding constants of motion is considered. The Trapezoidal Munthe-Kaas (TMK) method is used because of its structure preservation and energy conservation. In this chapter, we apply the Verlet, RK4, and TMK methods to a range of model simulations and compare the outcomes. For all simulations performed in this thesis, the time step size Δt is chosen rather small to ensure meeting the stability criteria.

In the following sections, we will investigate the implementation of the TMK method and compare its solutions with those of the Verlet and RK4 methods for several models. First, we will demonstrate the possible issues arising from symmetry loss with the Verlet method in section 4.1. The way we will compare outcomes of the simulations is discussed in section 4.2. In section 4.3, we will demonstrate the loss of symmetry in some model simulations integrated with the Verlet method and compare them to the same simulations but integrated with the TMK and RK4 methods. This is done with several models with and without periodic boundary conditions as described in Chapter 3.

4.1 Symmetry loss with the Verlet method

So far, we have not demonstrated that the shortcomings of the Verlet method lead to any issues. Let us do so with the following example. Consider six particles surrounding a center particle at $(x, y, z) = (0, 0, 0)$. The six particles are symmetrically positioned and have the same distance to the center particle of $\sqrt{x^2 + y^2 + z^2}$. The initial momenta are zero for all particles. The initial positions are indicated in Figure 4.1 by stars. Each particle experiences a Lennard-Jones potential force from all the other particles present. The structure of this example is inspired by the structure and symmetry of a perovskite unit cell without the A cations.

As we calculate the time evolution of this system, four particles overcome the attractive poten-

tial force of the other particles and break free with constant velocities. This is shown in figure 4.1, in which the distance to the center $(0, 0, 0)$ is denoted as the radius, and trajectories of this distance are plotted. For two of the four escaping particles, the escape happens at $t \approx 37$. The two other escaping particles demonstrate a similar escape at $t = 55$. Meanwhile, a system of three particles oscillating on a line remains.

As the initial configuration of this three-dimensional setting is symmetric, each particle should experience the same net force but in different directions. At each moment in time, the potential and kinetic energy of each particle surrounding the center particle should be equal. The system has no reason to change its symmetries. However, in the simulation calculated with the Verlet method, it does change to a less symmetric system which demonstrates a true fundamental issue with the popular Verlet algorithm.

A similar phenomenon is observed in a two-dimensional setting. Suppose we place three particles on a two-dimensional plane with equal distances r as sketched in figure 4.2. In that case, the system breaks into a binary system moving in a direction opposite to the direction in which the escaped particle moves. The initial distances between the particles are given by:

$$r_i = \sqrt{(x_i - x_{i-1})^2 + (y_i - y_{i-1})^2} \tag{4.1}$$

$$r_1 = r_2 = r_3 \tag{4.2}$$

$$r_1 = \left(1.5 + 2^{\frac{1}{6}}\right) \tag{4.3}$$

Escape from the n-body problem

For the general three-body problem, this type of escape is not at all uncommon. For example, in systems of self-gravitating bodies, it is statistically speaking certain that at one point in time, a system of three bodies will break into a binary system moving in the opposite direction of the escaped body (Manwadkar et al., 2021). As described by (Valtonen and Karttunen, 2006), the three-body system is chaotic, inherently unstable, and only for a small part of the initial value space, the escape phenomenon should not occur—for example, the symmetric initial conditions. However, symmetric initial conditions might be more common for structured materials than for bodies in space, and this small part of the initial value space might be more important than considered before, especially in the case of simulation of material properties of n interacting bodies.

One should note that a symmetric escape for the Lennard-Jones potential is also perfectly possible when the initial energies are large enough. Furthermore, if the system is not symmetric, the system's energy can be passed on to some particle that can, in turn, escape the potential. However, if the system is symmetric, this type of energy transfer is not physical and should not lead to an asymmetric escape. As such, these constitute fundamental tests of time integrators for dynamical systems, which clearly indicate possible issues for particular integrators.

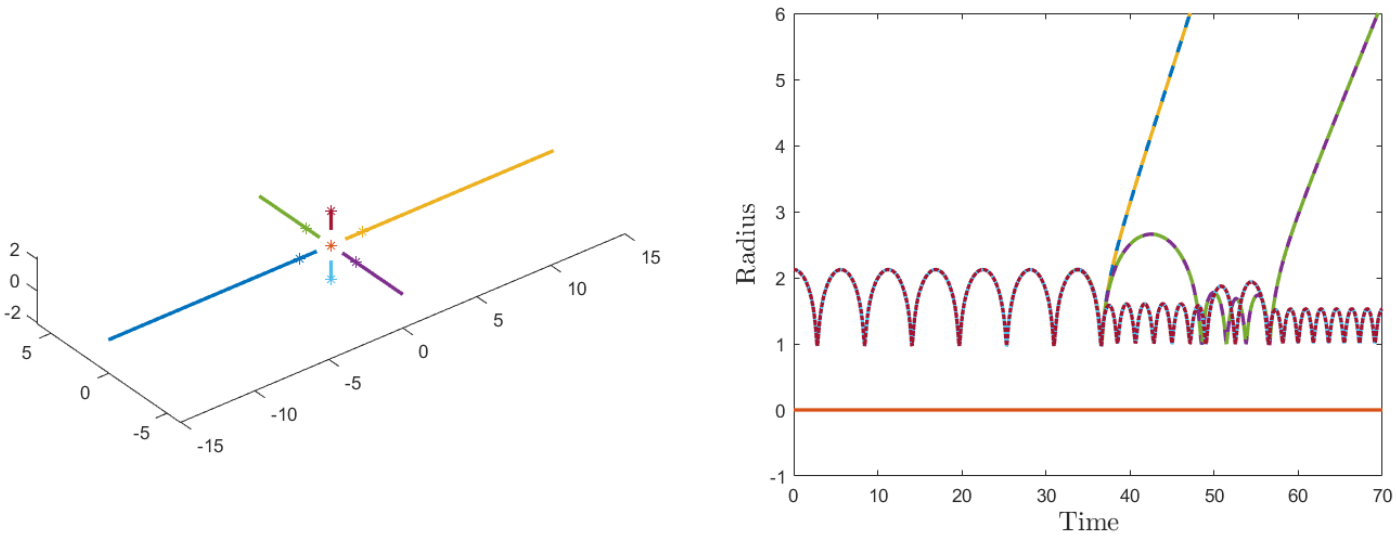

Figure 4.1: Position (x, y, z) and radius plot $\sqrt{x^2 + y^2 + z^2}$ for a 3D model with $n = 7$ particles with initial positions such that $\sqrt{x^2 + y^2 + z^2} = \left(1 + 2^{\frac{1}{6}}\right)$ and initial velocities $v_{1,2,\ldots,7} = 0$ centered around a particle at $(0, 0, 0)$ integrated with the Verlet method with $\Delta t = 10^{-3}$.

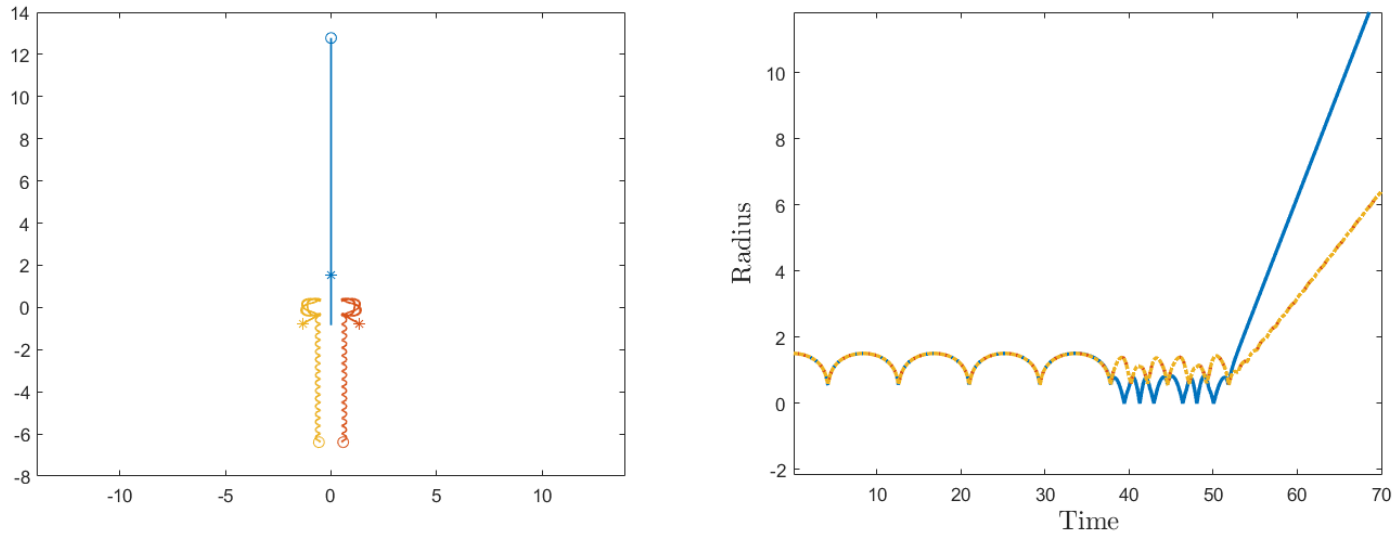

Figure 4.2: Position (x, y) and radius plot $\sqrt{x^2 + y^2}$ for a 2D model with $n = 3$ particles with initial distances of $r_{1,2} = 1.5 + 2^{\frac{1}{6}}$ and initial velocities $v_{1,2,3} = 0$ centered around $(0, 0)$ integrated with the Verlet method with $\Delta t = 10^{-3}$.

4.2 Characterizing simulations and outcomes

In order to compare different integrators, multiple one-dimensional models are considered, which enable us to distinguish between proper capturing of the dynamics and qualitative deviations due to numerical shortcomings. The total linear momentum and total energy should be conserved (within error bounds) for both integrators as described in Chapter 2. Therefore, we should check these observables, but we do not expect any irregularities for either integrator. The change in the Hamiltonian will be given in ratio to the initial total energy:

$$\text{Relative Energy change } = \frac{H(t) - H(0)}{H(0)} \tag{4.4}$$

The change in total linear momentum is given absolutely, as it is often equal to zero in our models:

$$\text{Momentum change } = P(t) - P(0) \tag{4.5}$$

Additionally, we can inspect and compare the particle trajectories computed with the different integrators. It has been observed in the previous section that the trajectories do not need to be identical, which can inform us of what method results in the correct behavior. However, only inspecting the trajectories might not always give us valuable information. Especially for larger chaotic systems, it is less clear which trajectory is correct, as small errors may lead to completely different trajectories as stated by the Lyapunov instability.

Therefore, we will also measure the conservation of symmetry by the time-integration schemes. Along the line of symmetry present in the initial conditions, the difference in the trajectories or energies in time can be plotted as a measure of symmetry.
For example, in the case of three particles of which the outer two are perturbed with the same amount, a line of symmetry in the middle particle can be identified. This is sketched in figure 4.3 Such, we can measure symmetry for this setup by:

$$|r_1 - r_2| = |q_2 - q_1 + q_3 - q_2| \tag{4.6}$$

$$|E_1 - E_3| = |V(r_1) + \frac{1}{2}p_1^2 - V(r_2) - \frac{1}{2}p_3^2| \tag{4.7}$$

Similarly for other numbers of particles and symmetry lines, a difference between the left and right displacement w.r.t. the symmetry line is used as a measure of the (a)symmetry.

4.3 Demonstration TMK application and advantages

This section aims to demonstrate the application and advantages of the TMK method for MD simulations. We will start by demonstrating the working and implementation of the TMK method for a two-particle model for several potentials in subsection 4.3.1. The results of the Verlet, RK4, and TMK methods will be similar. This will enhance our trust in the TMK method. In subsection 4.3.2 the escape phenomenon for a three-particle model with varying initial conditions is investigated with the TMK and Verlet methods. The loss of symmetry with the Verlet method is not observed with

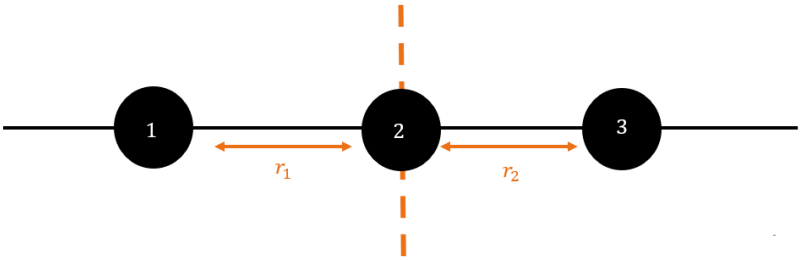

Figure 4.3: Three particles with a symmetry line for $(q_2 - q_1) = r_1 = r_2 = (q_3 - q_2)$.

the TMK method. Then, in section 4.3.3, a five-particle system with periodic boundary conditions and structural symmetry is employed to demonstrate a similar phenomenon of symmetry loss with periodic boundary conditions. In section 4.3.3 the same five-particle model is used, and it is shown that decreasing the time step size does not overcome the asymmetry build-up with the Verlet method. Finally, a more chaotic, eight-particle model with periodic boundary conditions is employed in subsection 4.3.4. This model shows us that the loss of symmetry of the Verlet method can be measured even when the periodicity of the displacements can not be identified. Furthermore, the symmetry conservation of the TMK method is confirmed once more. This is summarized below:

1. Demonstration of working with a two-particle model with Harmonic oscillator, Toda and Lennard-Jones potential.

2. Investigation of escape phenomenon with a three-particle model with the Lennard-Jones potential.

3. Investigation of symmetry loss with a five-particle model with periodic boundary conditions and the Lennard-Jones potential.

4. Investigation of time step size dependency of symmetry loss in Verlet with the five-particle model.

5. Investigation of symmetry loss with a (more chaotic) eight-particle model with periodic boundary conditions.

4.3.1 Demonstration of working for a two-particle model

In this section, we will demonstrate the performance of TMK, RK4, and Verlet for simple two-particle models without additional symmetry for several potentials. This section aims to demonstrate the working of the TMK method by presenting similar results as for the Verlet method. This will enhance our trust in implementing and applying the TMK method.

For the two-particle model, the Harmonic oscillator potential, the Toda potential, and the Lennard-Jones potential are used. The results of the two-particle model with the Harmonic oscillator potential are plotted in Figure 4.4. Furthermore, the outcomes of the two-particle model with a Toda potential are given in Figure 4.5. Similarly, using a Lennard-Jones potential, the outcomes are given in Figure 4.6. The initial displacement of the Toda potential is chosen to be $q_2 - q_1 = 8$, while the initial displacement for the Lennard-Jones and Harmonic oscillator potential is chosen to be $q_2 - q_1 = 2$. The initial momenta are zero for the Lennard-Jones and Harmonic oscillator potential and non-zero for the Toda potential. This is merely to explore different initial settings.

Displacement trajectories

From Figures 4.4(a), 4.5(a), and 4.6(a), it can be noted that the calculated displacements are similar for all three methods for all potentials. This enhances our trust in the working of the TMK method. Furthermore, it can be noted that the oscillation of the displacement with the Toda potential in Figure 4.5(a) is not symmetric with respect to the distance $r = q_2 - q_1$. Namely, it is clear that the repulsion for $r < 0$ is stronger than the attraction for $r > 0$. The repulsion for $r < 0$ of the Lennard-Jones potential in Figure 4.6(a) is even stronger with respect to its attraction for $r > 0$. This should be expected, looking at the slopes of the potentials in figure 3.3. Although the oscillation is still smooth, the sharper character due to the strong repulsion could induce larger errors.

Total energy

From Figure 4.4(c) one can note that the total energy is conserved exactly for all three time-integration methods for the harmonic oscillator potential within this time frame. For the Toda and Lennard-Jones potential, we note in Figure 4.5(b) and 4.6(c,d) the energy change has a periodic character for the TMK and Verlet method. The bounds within which this periodic behavior occurs are of a similar order of magnitude for the TMK and Verlet method, which is remarkable. From the theory in Chapter 2, we know that the methods are near-preserving of energy rather than exactly preserving. Therefore, this periodic behavior is expected and will remain within bounds for long-time simulations. For the Lennard-Jones potential, we note that the amplitude of the periodic energy oscillation is much larger compared to the Toda potential. This could be due to the Lennard-Jones potential's sharply increasing nature, which introduced high gradients into the problem that are always harder to capture. Furthermore, the peaks in the energy plots (Fig. 4.5(b),4.6(c)) correspond to the sharp oscillation peaks which are the result of the repulsion for the shortest distance $q_2 - q_1$.

For the fourth-order Runge-Kutta method, there appears to be no energy change for the Lennard-Jones and Toda potential in this order of magnitude plot. However, if we only inspect the energy

change of the RK4 method solely in Figure 4.6(e), we note that the energy drifts. The magnitude of the energy change for this short-time simulation is much smaller than the magnitude of the energy change of the TMK and Verlet method. However, those changes are bound, while the energy change of RK4 will likely increase and drift even further as longer-time simulations are done. The RK4 method is unsuitable for long-time MD simulations as it is not energy-conserving (Cf. section 2.2).

Total linear momentum

The total linear momentum is conserved exactly for all three Harmonic oscillator and Lennard-Jones potential methods (Figure 4.4(d), 4.6(b)). All methods conserve the total linear momentum up to machine precision for the Toda potential (Figure 4.5(c)). This simulation is the only one with non-zero initial momenta. This might induce the difference in conservation. Furthermore, as energy for the RK4 method is not conserved, it is expected that the momentum will not be conserved either for longer-time simulations. For the TMK and Verlet methods, the conservation of momentum is as expected.

Displacement error

For the quadratic potential of the Harmonic oscillator, an analytic solution is available. Therefore, we can compare our solutions to the analytic solution:

$$\text{Displacement Error } = \left|(\Delta q)_{numerical} - (\Delta q)_{analytical}\right| \tag{4.8}$$

where $r = \Delta q = q_2 - q_1$ and the analytical solution for two free particles with initially no momentum is given by:

$$(\Delta q)_{analytical} = 2\cos\left(t\sqrt{(\Delta q)_{initial}}\right) \tag{4.9}$$

The error of the three methods is plotted in figure 4.4(b). It can be noted that the TMK method has the largest error, followed by the fourth-order Runge-Kutta method. In this figure, the error of the Verlet method is not even visible. It is known that the global error of both TMK and Verlet increases linearly. However, it is clear that for the Harmonic oscillator potential, the error is much more significant for the TMK method with the same discretization. The difference in complexity of the methods could explain this. The TMK method consists of many calculation steps, as described in section 2.4. Many calculation steps, including a Newton solver and matrix inversion, could be responsible for more roundoff errors. The Verlet method, with only three lines of code, is much preferred here because of its simplicity.

Summary two-particle model

In conclusion, we observe that all three methods, TMK, Verlet, and RK4, obtain the correct trajectories for short-time simulations of two particles. The TMK method has a larger error than the Verlet method in the trajectory for the Harmonic oscillator potential. The momenta appear conserved for all methods, and the energy is bound for the TMK and Verlet method. Energy drift is present for the RK4 method, making it unsuitable for long-time MD simulations. We can conclude that the

TMK method appears suitable for MD simulations, but the Verlet method has better results for the smooth, integrable, harmonic oscillator.

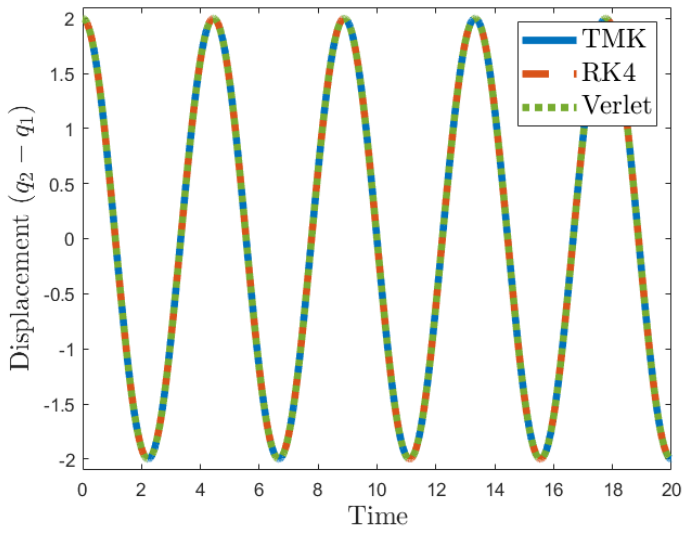

(a) Displacement $q_2 - q_1$.

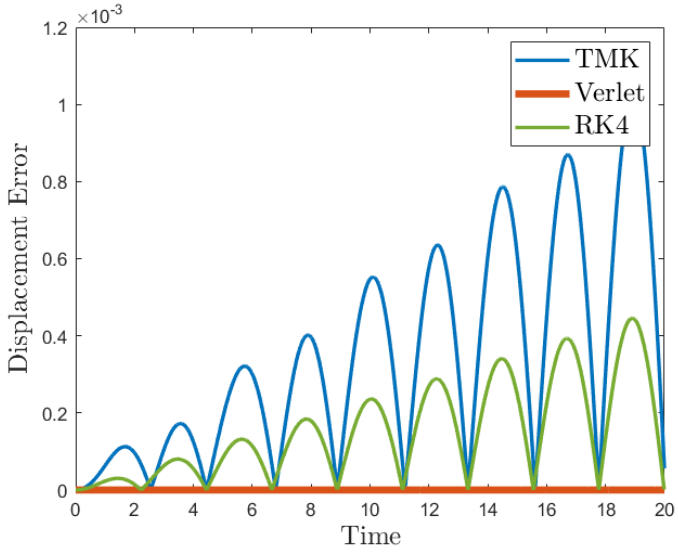

(b) Displacement error.

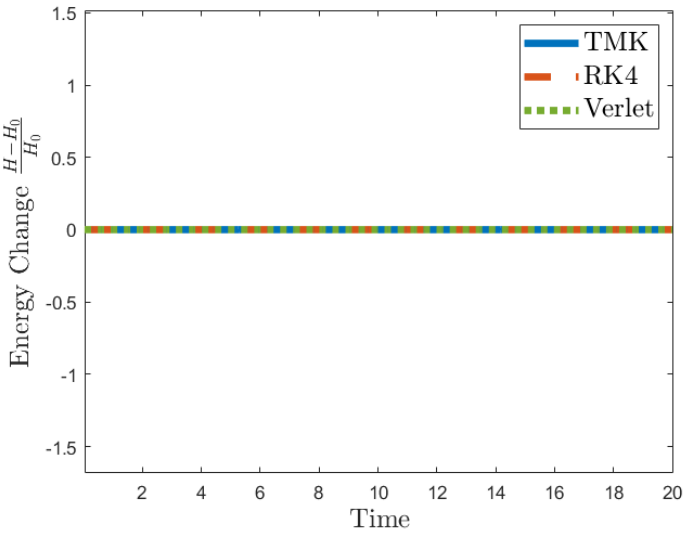

(c) Total energy change in percentages.

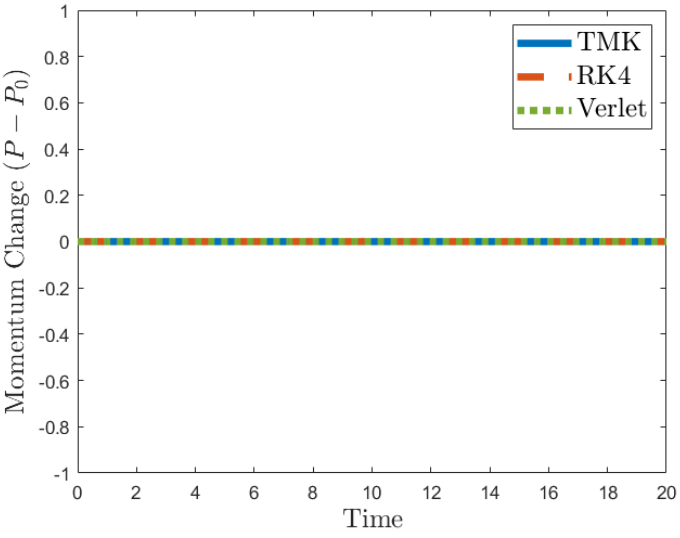

(d) Total momentum change.

Figure 4.4: Two particle model with the Harmonic oscillator potential, with $\Delta t = 10^{-2}$ and initial displacement $(q_2 - q_1) = 2$, and initial momenta $p_1 = p_2 = 0$.

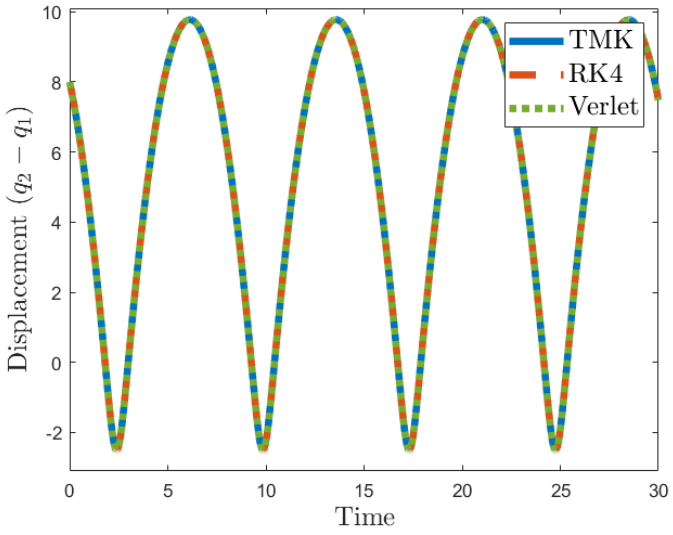

(a) Displacement $q_2 - q_1$.

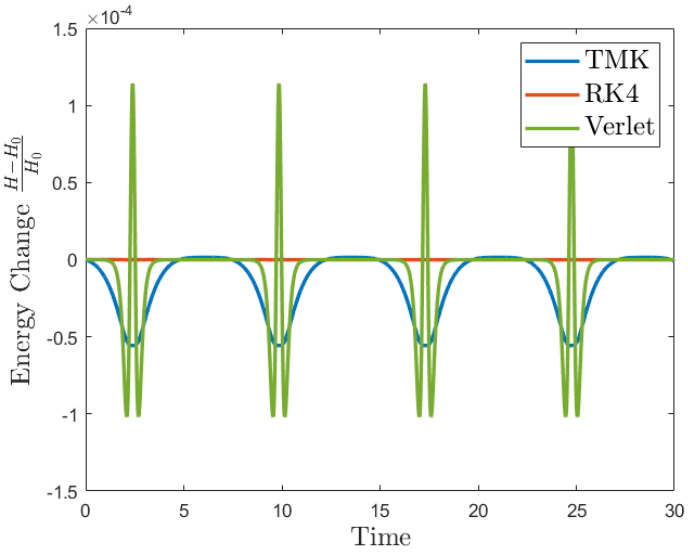

(b) Total energy change in percentages.

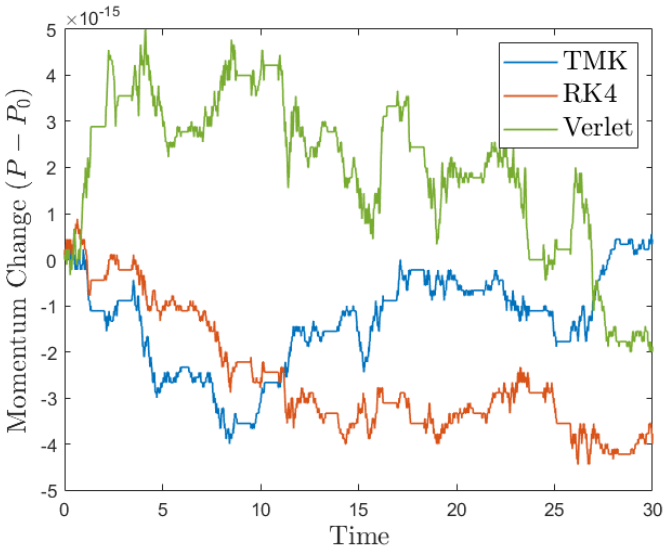

(c) Total momentum change.

Figure 4.5: Two particle model with the Toda potential, with $\Delta t = 10^{-2}$ and initial displacement $q_2 - q_1 = 8$, and initial momenta $p_1 = 2$, $p_2 = -\frac{2}{3}$.

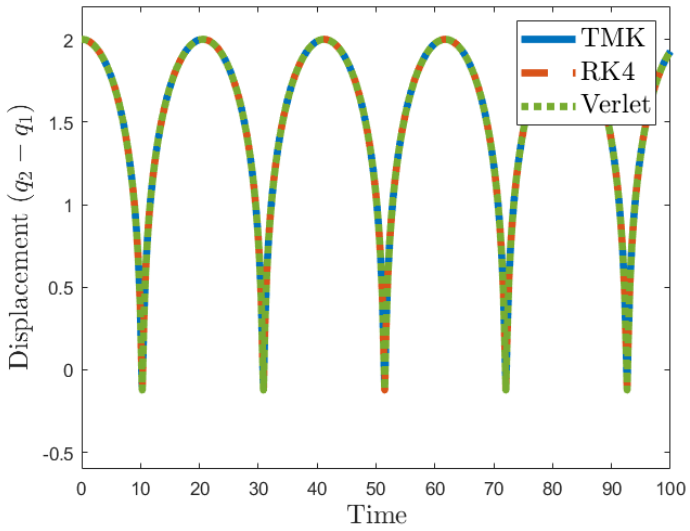

(a) Displacement $q_2 - q_1$.

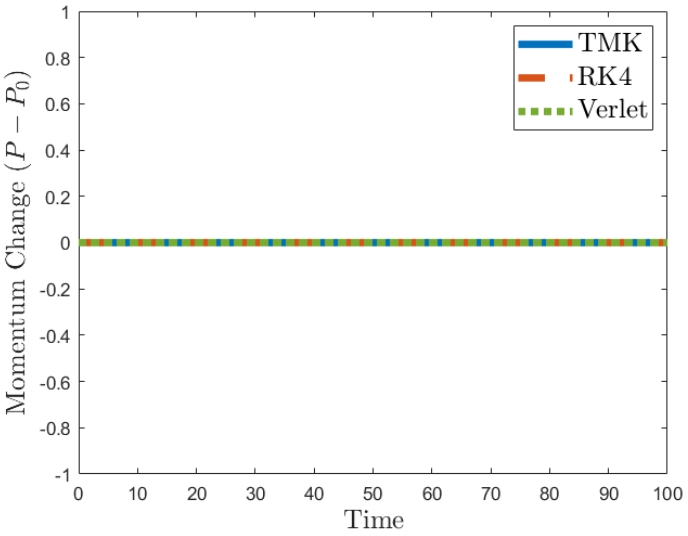

(b) Total momentum change.

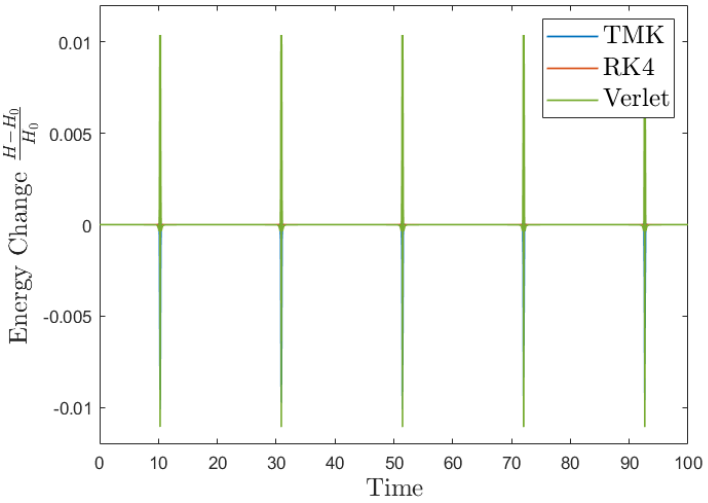

(c) Total energy change in percentages.

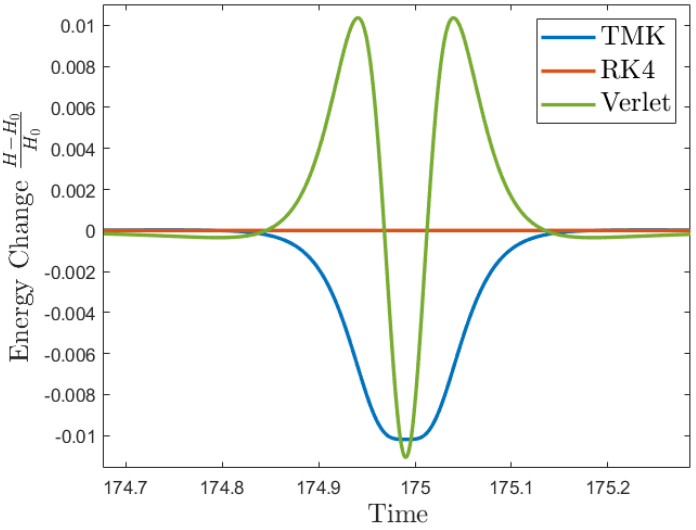

(d) Zoomed in on (c).

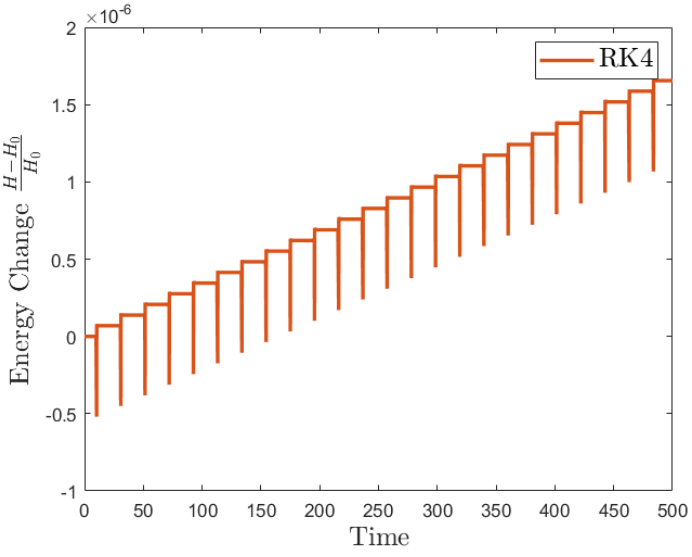

(e) Energy change of the Runge-Kutta method.

Figure 4.6: Two particle model with the Lennard-Jones potential, with $\Delta t = 10^{-2}$ and initial displacement $(q_2 - q_1) = 2$, and initial momenta $p_1 = p_2 = 0$.

4.3.2 Escape for a three-particle model

Let us now create a three-particle model in which symmetry as described in section 4.2 is present. Namely, the outer two particles have the same initial distance and velocities but with opposite directions, with respect to the middle particle. This is sketched in figure 4.3. Let us use the Lennard-Jones potential, as we expect the largest differences to be observed for this potential. The initial perturbed distances are chosen to be $r_1 = r_2 = 2^{1/6} + 1$. The initial potential energy should not be large enough for the particles to escape the potential in a symmetric manner. Instead, we expect a symmetric oscillatory motion for both distances r_1, r_2. The results are plotted in Figure 4.7.

Displacement trajectories

In Figure 4.7(a) we notice that the three methods do not recover the same or even similar trajectories. The behavior of the Verlet method is similar to the two-dimensional and three-dimensional cases described before. After some initial oscillations, a particle escapes with constant velocity with respect to the remaining two oscillating particles. The TMK and RK4 methods do not demonstrate this escape. Instead, the initial oscillations continue with these methods.

Total linear momentum and energy

Even though the trajectories display surprising and different behavior, the energy and momentum plots do not display erroneous behavior. The momentum of the Verlet system is still conserved, and the total energy is conserved within reasonably small bounds. If one looks closely, it can be noticed that the periodic behavior of the energy change of Verlet changes as the particle escapes. However, this would not be easily noticeable.

Symmetry

The difference between the displacements r_1 and r_2 is plotted in Figure 4.8. In Figure 4.8(a) we note that there is no symmetry loss for the TMK and RK4 methods. The differences are zero to machine precision. Furthermore, it can be noticed in the logarithmic plot, Figure 4.8(b), that the increasing differences of the Verlet method are not instantaneous upon escape but are building up starting at the first time step. With the first time steps, symmetry is lost with the Verlet method while preserved for time steps with the TMK and RK4 methods.

As described in section 4.1, the energy of an asymmetric system can be transferred between particles. In such a way, the energy of a single particle may become enough for an escape, while an escape was initially not possible. In section A.3.1 of the appendix the energy of each particle is plotted for the TMK and Verlet methods and energy transfer can be identified for the Verlet method, which allows for the escape of a particle after some time as if the system was asymmetric.

Escape for different initial conditions

In symmetric situations with enough energy or asymmetric situations with enough total energy, escape is a natural phenomenon. Furthermore, in asymmetric situations, an escape might occur due to the transfer of energy within the system. Let us map the escapes for different initial displacements $q_2 - q_1$, $q_3 - q_2$. All initial momenta are zero $p_1 = p_2 = p_3 = 0$. In Figure 4.9 these maps are given for the TMK and Verlet methods. Dark blue squares indicate no escape, while yellow squares indicate an escape. The escape is registered as having obtained a distance larger than the tolerated distance within a running time $t = 1000$. The maps may be different for even longer or shorter running times.

In Figures 4.9(a),(b) we notice that both TMK and Verlet indicate escapes for small distances $q_2 - q_1$, $q_3 - q_2$. This corresponds with the intuition that there is such a large repulsive initial potential energy for small distances between particles that escape is likely. The large repulsive energy apparently is large enough to escape the asymptotic gradual attractive force. Furthermore, we notice that for an 'intermediate' distance between particles, no escape is present for Verlet and TMK. This yellow region corresponds to having a total energy that is not large enough for a single particle to escape.
For larger distances in the asymmetric cases $r_1 \neq r_2$, the system's total energy is large enough such that transfer to a single particle may result in the escape phenomenon. In Figures 4.9(a),(b) it can be noted that escape indeed takes place for asymmetric cases with enough energy due to either rather small or rather large displacements or combinations thereof.

However, for symmetric cases, the particles should not transfer their energy. The initial energies of the individual particles are not enough to escape for large initial distances $q_2 - q_1$, $q_3 - q_2$. Therefore, the symmetric cases should not result in escape phenomena for larger distances. However, this is where a discrepancy between the TMK and Verlet map is observed. The TMK map has a diagonal of no escapes for $r > r_{sym-escp}$ where $r_{sym-escp}$ is given by $V_{LJ}(r_{sym-escp}) > 0$. We note that on this diagonal, the Verlet map indicates escapes.

Summary three-particle model

In conclusion, for the three-particle model with symmetry, the Verlet method demonstrates symmetry loss while the TMk method demonstrates symmetry conservation. This does not result in loss of total momentum or energy conservation. The asymmetry in the Verlet method is shown to build up from the first time step and may result in an escape phenomenon. This escape phenomenon is observed for asymmetric cases with both methods when the total energy is sufficiently large or in the symmetric case when initial individual energies are sufficiently large. However, in symmetric cases, the escape phenomenon always occurs with the Verlet method, while this does not happen with the TMK method. One should note that this additional symmetry is not pre-programmed into the TMK method. Only the initial conditions are changed.

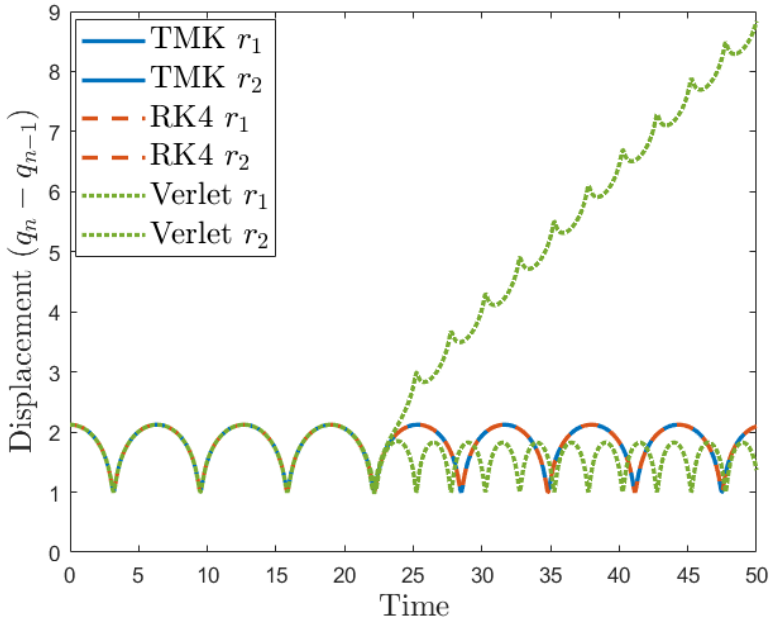

(a) Displacement $q_2 - q_1$.

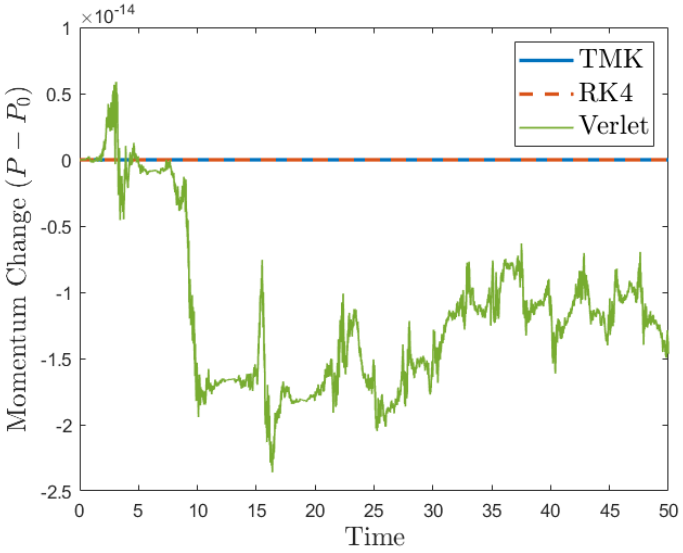

(b) Total momentum change,

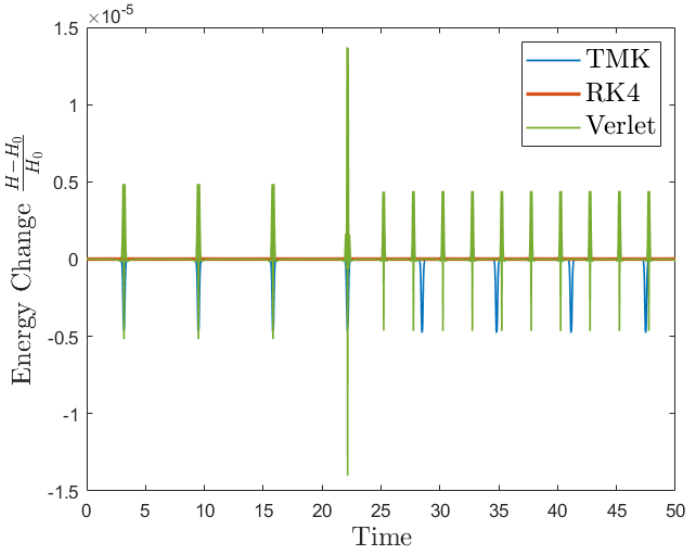

(c) Total energy change in percentages.

Figure 4.7: Three-particle model with the Lennard-Jones potential, with $\Delta t = 10^{-4}$ and initial displacement $r_1 = r_2 = 2^{1/6} + 1$, where $r_i = (q_{i+1} - q_i)$ and initial momenta $p_1 = p_2 = p_3 = 0$.

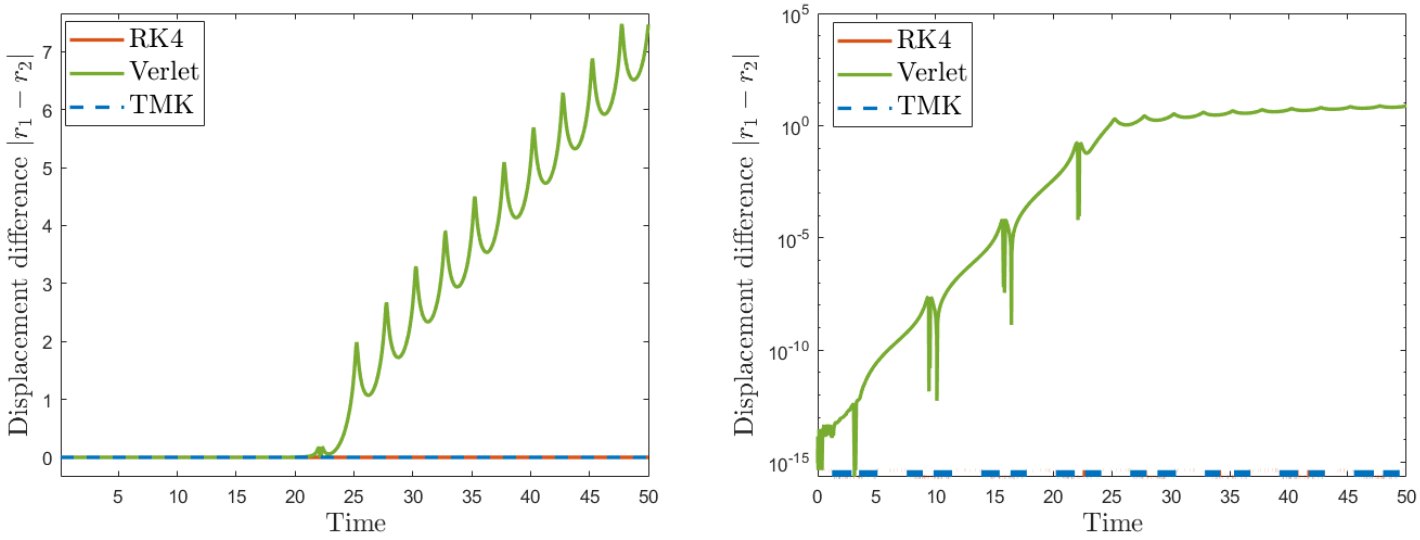

(a) Linear plot.

(b) Logarithmic plot.

Figure 4.8: Displacement difference $|r_1 - r_2|$ for the three-particle model with the Lennard-Jones potential, with $\Delta t = 10^{-4}$ and initial displacement $r_1 = r_2 = 2^{1/6} + 1$, where $r_i = (q_{i+1} - q_i)$ and initial momenta $p_1 = p_2 = p_3 = 0$.

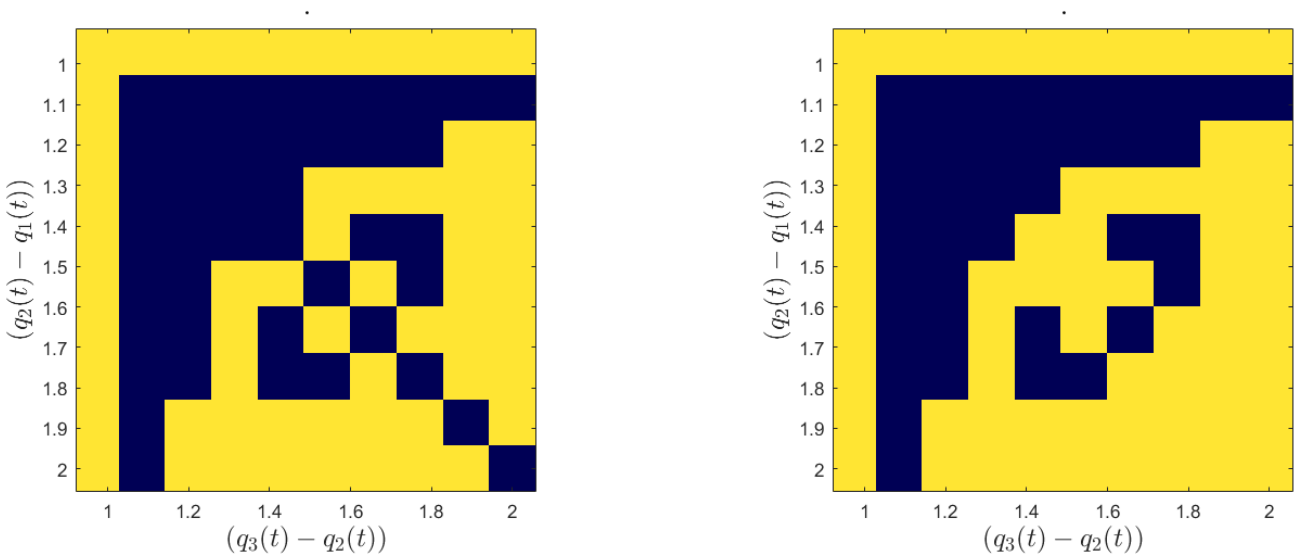

(a) TMK

(b) Verlet

Figure 4.9: Maps indicating escape of a particle (Yellow) or no escape (Blue) in a three-particle model with the Lennard-Jones potential and different initial displacements $r_1 = q_2 - q_1$, $r_2 = q_3 - q_2$ with same initial momenta $p_1 = p_2 = p_3 = 0$, with $\Delta t = 10^{-4}$.

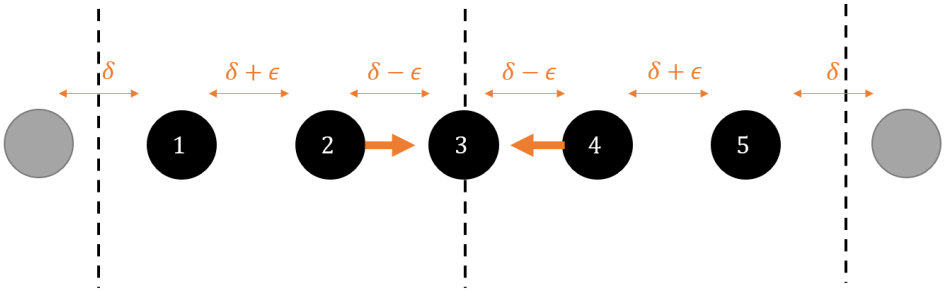

Figure 4.10: The five-particle model with periodic boundary conditions and symmetry with respect to its center particle. δ indicates the equilibrium distance and ϵ the perturbation with respect to the equilibrium distance.

4.3.3 Symmetry in a five-particle model with periodic boundary conditions

The five-particle ring is symmetric with respect to its middle particle. The positions of the two particles neighboring the center particle are perturbed with respect to the equilibrium distance. Such, the distance between the particles is given by:

$$q_2 - q_1 = r_1 = \delta + \epsilon \tag{4.10}$$
$$q_3 - q_2 = r_2 = \delta - \epsilon \tag{4.11}$$
$$q_4 - q_3 = r_3 = \delta - \epsilon \tag{4.12}$$
$$q_5 - q_4 = r_4 = \delta + \epsilon \tag{4.13}$$
$$q_{ghost} - q_5 = r_5 = \delta \tag{4.14}$$
$$q_1 - q_{ghost} = r_5 = \delta \tag{4.15}$$

where δ is the equilibrium distance for the potential and ϵ the perturbation. For the Lennard-Jones potential, the equilibrium distance is $\delta_{LJ} = 2^{1/6}$. The chosen perturbation is $\epsilon = 0.1$. The setup is sketched in Figure 4.10.

Displacement trajectories

We will not plot all trajectories for the five-particle ring in a single figure. Instead, let us inspect only the trajectory of the displacement r_4 for the different time-integration methods in Figure 4.12. It is clear that the TMK method and RK4 method result in a periodic oscillatory displacement. The Verlet method initially returns the same displacement trajectory but distorts clearly at $t \approx 200$.

Symmetry

In figure 4.13 we inspect the symmetry in the system by inspecting the difference of the left and right displacement with respect to the middle particle,$|r_2 - r_3|$. It can be noted that the TMK and RK4 methods result in zero symmetry loss in Figure 4.13(a). In Figure 4.13(b) one can note that

the Verlet method displays significantly increasing symmetry loss until $t = 250$. The asymmetry builds up from the first time step., but a maximum is reached. This is different from the symmetry loss for the thee-particle in Figure 4.8. The nature of the periodic boundary conditions can explain this. The boundary conditions do not allow a change in position outside of the periodic domain. Therefore, the possible differences in position, $(q_i - q_{i-1})$, is limited by the system.

Time step size dependency of symmetry loss

In Figure 4.11, the symmetry loss as a function of time is plotted for time step sizes of varying orders of magnitude. The model remains the same five-particle model with periodic boundary conditions. The initial conditions are kept constant and are the same as for the five-particle ring discussed before. For these time step sizes and intermediate step sizes, the maximum error within $t \in \{0, 400\}$ and their approximate time to reach asymmetry of order 10^{-1}, denoted $T_{10^{-1}}$, is given in table 4.1.

Δt	$\max\|r_2 - r_3\|$	$T_{10^{-1}}$
1×10^{-3}	0.2687	237
5×10^{-3}	0.2564	222
1×10^{-4}	0.2692	212
5×10^{-4}	0.2581	228
1×10^{-5}	0.2682	196

Table 4.1: Maximum symmetry loss $|r_2 - r_3|$ within $t \in \{0, 400\}$ and the approximate time it took for the symmetry loss to become 10^{-1} for different time step sizes for the five-particle model with periodic boundary conditions.

From Figure 4.11 and table 4.1 we note that a smaller time step does not correspond with a better result. Contrary to the intuition that a smaller time step solves all numerical errors, the smallest time step appears to have the fastest initial increase in symmetry loss.

For the smallest time step, more calculations are done within the same time frame. The increase in symmetry error appears to start at the computer's precision error and could start as an accumulation of rounding errors. In this line of reason, it is not strange that a smaller time step corresponds to a faster symmetry loss.

Summary five-particle model

For the five-particle model with symmetry and periodic boundary conditions, a build-up in asymmetry has been found for the Verlet method similar to the case of the three-particle model. However, due to the periodic boundary conditions, the location of the particles, and thus the difference therein is bounded. Furthermore, it has been demonstrated that decreasing the time step does not solve the asymmetry issue of the Verlet method. In contrast, the asymmetry is found to build up faster for a smaller time step.

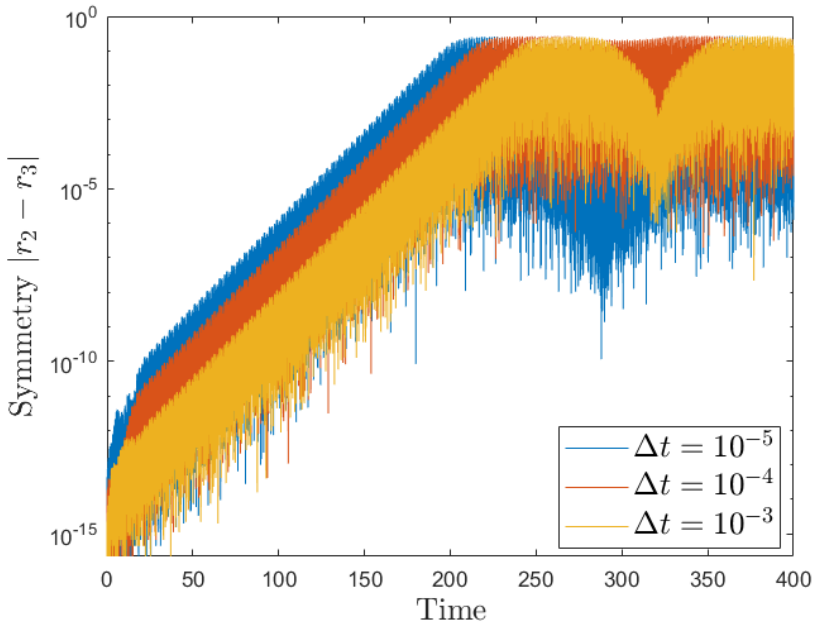

Figure 4.11: Displacement difference $|r_3 - r_2|$ for the five-particle model with the Lennard-Jones potential, with a varying time step size $\Delta t = \left(10^{-3}, 10^{-4}, 10^{-5}\right)$ and initial displacements $r_1 = r_4 = \left(2^{1/6} + 0.1\right)$, $r_2 = r_3 = \left(2^{1/6} - 0.1\right)$, $r_5 = r_{ghost} = \left(2^{1/6}\right)$, where $r_i = (q_{i+1} - q_i)$ and initial momenta $p_1 = p_2 = ... = p_5 = 0$.

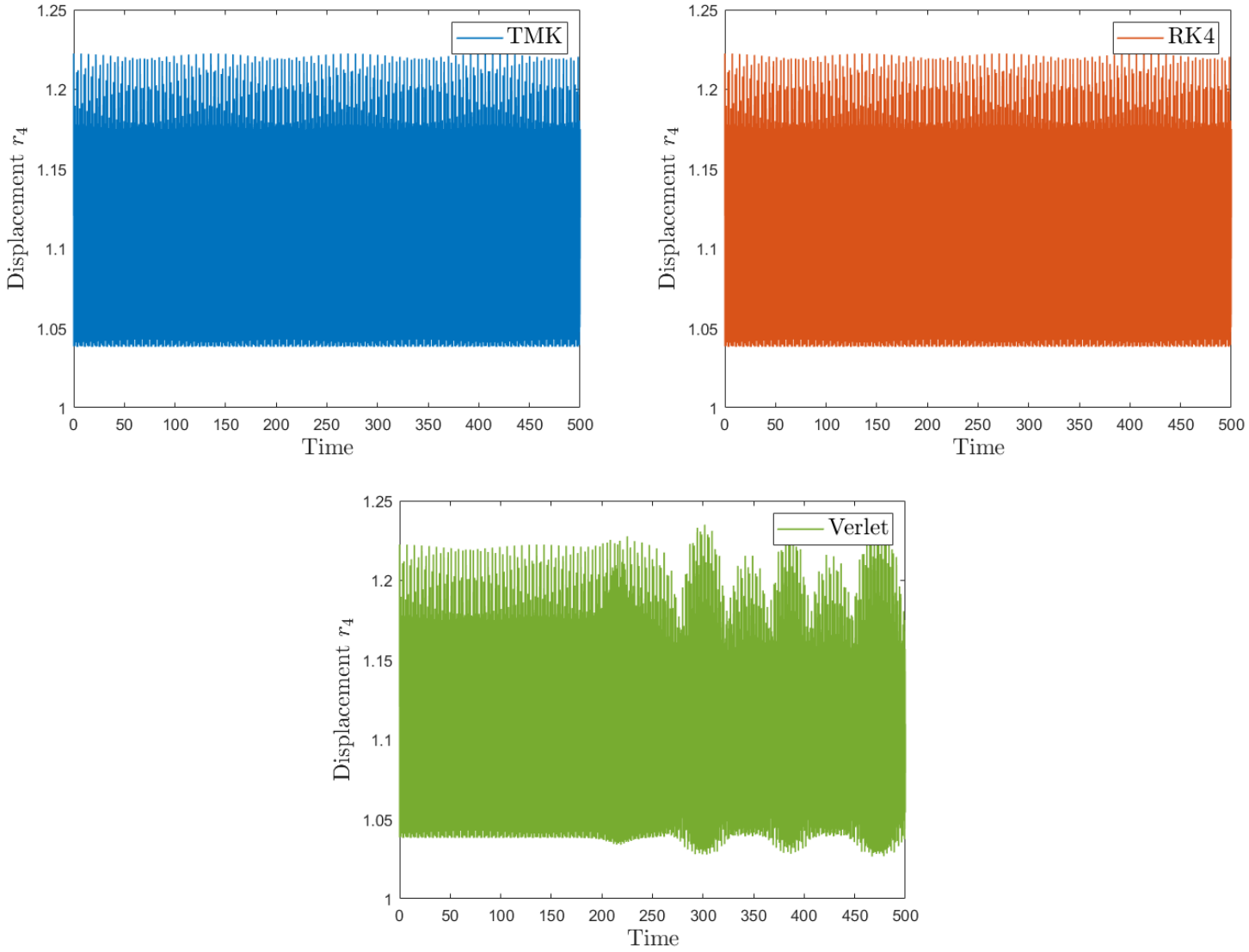

Figure 4.12: Five-particle ring with the Lennard-Jones potential, with $\Delta t = 10^{-4}$, and initial displacements $r_1 = r_4 = \left(2^{1/6} + 0.1\right)$, $r_2 = r_3 = \left(2^{1/6} - 0.1\right)$, $r_5 = r_{ghost} = \left(2^{1/6}\right)$, where $r_i = (q_{i+1} - q_i)$ and initial momenta $p_1 = p_2 = .. = p_5 = 0$.

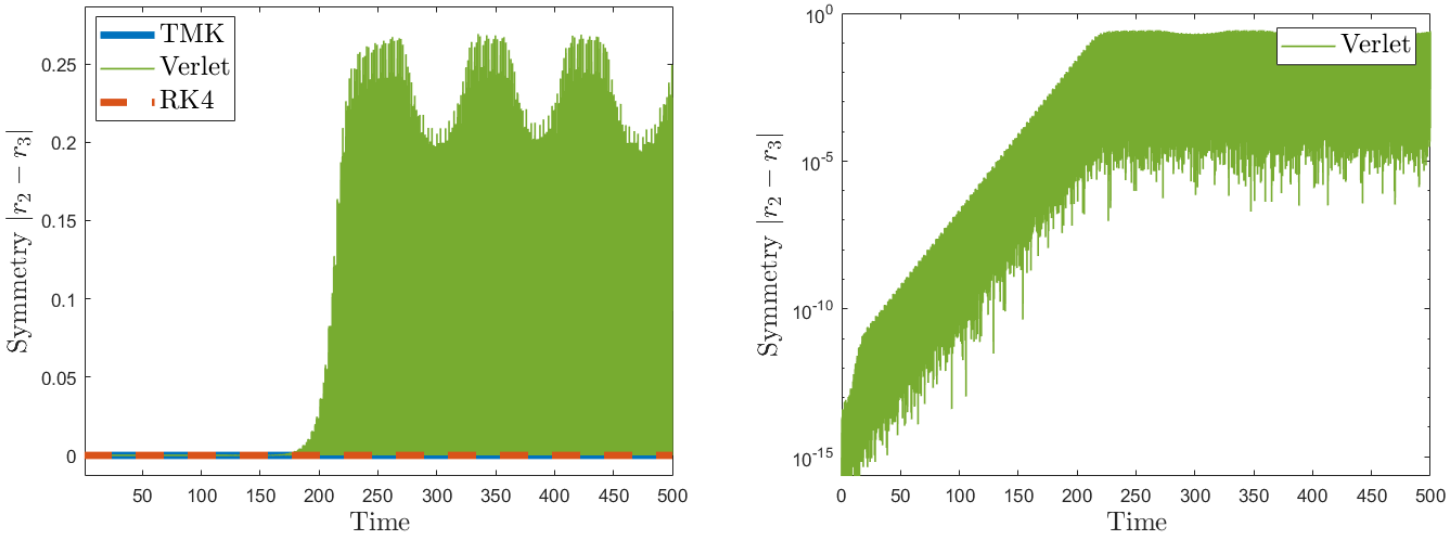

(a) Linear plot.

(b) Logarithmic plot.

Figure 4.13: Symmetry of the five-particle ring with the Lennard-Jones potential, with $\Delta t = 10^{-4}$, and initial displacements $r_1 = r_4 = \left(2^{1/6} + 0.1\right)$, $r_2 = r_3 = \left(2^{1/6} - 0.1\right)$, $r_5 = r_{ghost} = \left(2^{1/6}\right)$, where $r_i = (q_{i+1} - q_i)$ and initial momenta $p_1 = p_2 = .. = p_5 = 0$.

4.3.4 Symmetry in an eight-particle model with periodic boundary conditions

The eight-particle ring is symmetric with respect to a line between the middle particles. The positions of the two center particles are perturbed. Such, the distances between the particles are given by:

$$\begin{aligned} r_1 = r_2 = r_6 = r_7 = r_8 &= \delta \\ r_3 = r_5 &= \delta + \epsilon \\ r_4 &= \delta - 2\epsilon \end{aligned}$$

where δ is the equilibrium distance for the potential and ϵ the perturbation. For the Lennard-Jones potential, the equilibrium distance is $\delta_{LJ} = 2^{1/6}$. The chosen perturbation is $\epsilon = 0.1$. The setup is sketched in Figure 4.14.

Displacement trajectory

For the eight-particle ring, the displacement of only $r_4 = q_4 - q_3$ is plotted in Figure 4.15. One can note that the three methods do not yield the same trajectories. Their deviation starts relatively early in time; from $t \approx 30$ differences in all three methods are observed. For an even larger time, $t \approx 415$, we can see that the three methods surely do not result in the same trajectories. Also, it can be noted that the trajectories are chaotic. The Lyapunov instability may be the cause of these entirely different trajectories. Furthermore, we cannot indicate which of these might be the 'correct' trajectory and which may be wrong, if not all.

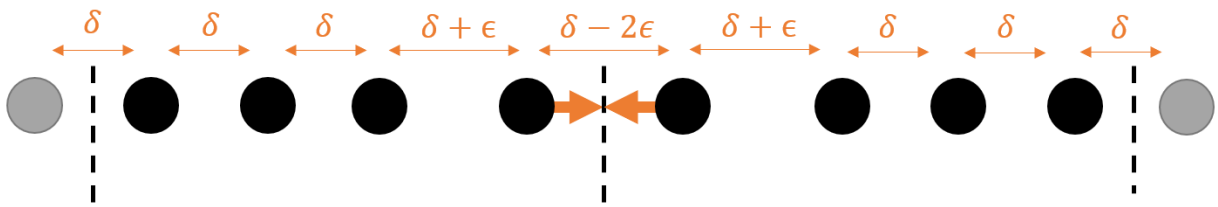

Figure 4.14: The eight-particle model with periodic boundary conditions and symmetry with respect to its center particles. δ indicates the equilibrium distance and ϵ the perturbation with respect to the equilibrium distance.

Symmetry

Although the trajectories do not indicate the time-integration method's correctness, the symmetry between the left and right parts can be measured. We do this by measuring the difference between the displacements left and right of the two middle particles, $|r_5 - r_3|$.[1] This is plotted in Figure 4.15(a),(b). In Figure 4.15(b) it can be noted that the asymmetry of the results of the Verlet method builds up from the first time step to significant amounts in the order of 10^{-1}. In contrast to what is seen before, the results of the RK4 method also lose its symmetry. The results computed with the TMK method, on the other hand, remain symmetric with $|r_3 - r_5|$ exactly zero for all time stepss.[2] This can be seen in Figure 4.15(a).

Summary eight-particle model

Symmetry loss with the Verlet and with the RK4 method similar to the five-particle model is observed for the eight-particle model with additional symmetry. The TMK method is observed to conserve this symmetry once again. Unlike the three-particle and five-particle models, it has become impossible to indicate a change from periodic to non-periodic behavior in the displacement plot, as the trends have become rather chaotic. However, as the RK4 and Verlet methods lose symmetry, these displacement trajectories may already be regarded as incorrect.

Summary of all results

In conclusion, without symmetry in the system, all three time-integration methods result in the same trajectories for simple three-particle models with periodic boundary conditions and short-time simulations. Even for a five-particle model with symmetry, initially, similar trajectories are observed. The Verlet method builds up asymmetry from the first time step, resulting in a trajectory distortion after some time. This feature is not resolved by decreasing the time step size. This is also observed for the RK4 method for a larger number of particles. In all cases, the TMK method

[1] This can also be chosen to be $|r_1 - r_7|$ or $|r_2 - r_6|$.

[2] Note that the TMK method is not plotted in the logarithmic plots. It is chosen to leave it out, as all zeros will not show in a logarithmic plot.

conserves symmetry exactly or up to machine precision. However, for models with a larger number of particles, the trajectories are not the same anymore, and identifying the 'correct' trajectory becomes impossible. The conservation or loss of symmetry might be a good indicator. Namely, if symmetry is lost, the trajectories can not be correct for sure. For models with less extreme initial displacements, the symmetry error takes longer to build up, but eventually, the same order of magnitudes of asymmetry will be recovered.

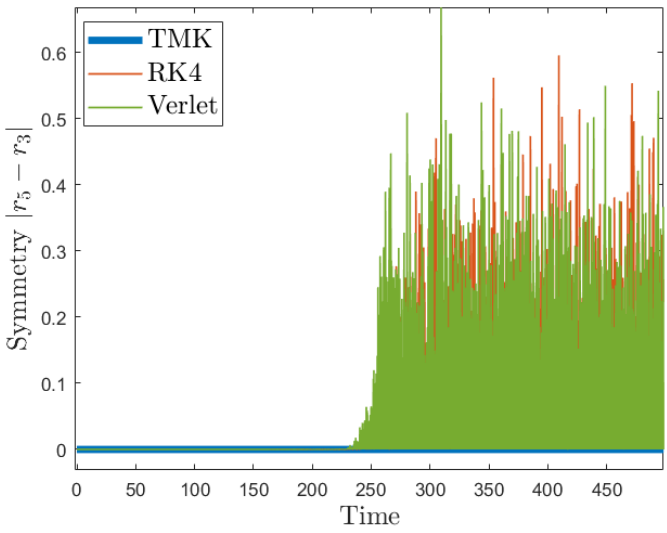

(a) Linear symmetry.

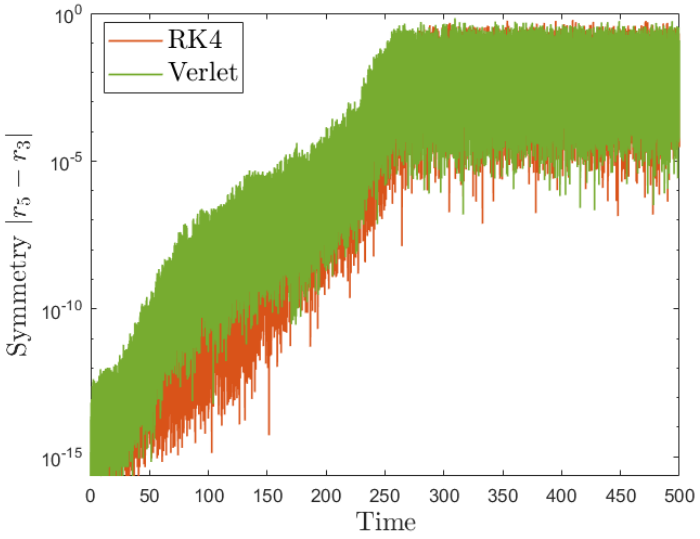

(b) Logarithmic symmetry.

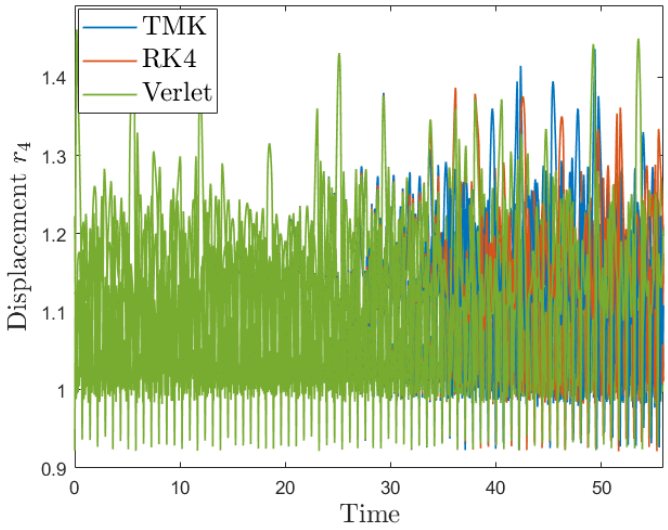

(c) Displacement for $t \in \{0, 55\}$.

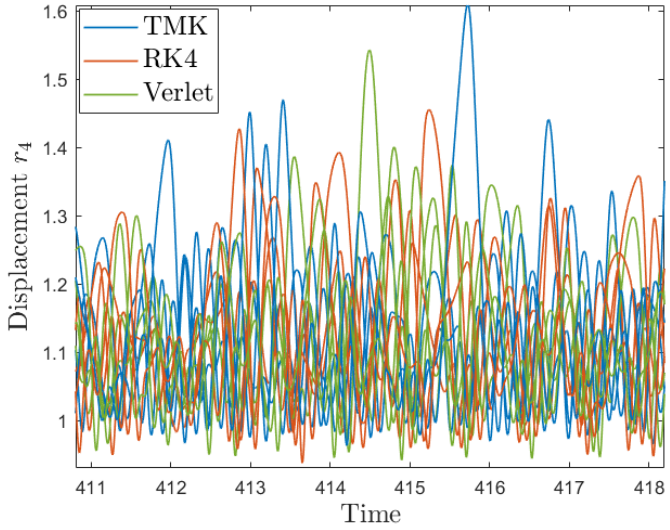

(d) Displacement for $t \in \{411, 418\}$.

Figure 4.15: Eight-particle ring with the Lennard-Jones potential, with $\Delta t = 10^{-4}$, and initial displacements $r_1 = r_2 = r_6 = r_7 = r_{ghost} = 2^{1/6}$, $r_3 = r_5 = \left(2^{1/6} + 0.1\right)$, $r_4 = \left(2^{1/6} - 0.2\right)$, where $r_i = (q_{i+1} - q_i)$ and initial momenta $p_1 = p_2 = .. = p_8 = 0$.

Chapter 5

Discussion and Conclusion

In this chapter, we will discuss and conclude the results of this thesis. Interpretation and discussion of the results are already given within Chapter 4. In the discussion section 5.1, rather than discussing the results we will discuss some issues arising from the work presented in this thesis. We will critically examine the approach taken in this work and give some remarks. In section 5.2, we will summarize and conclude the work presented in this thesis.

5.1 Discussion

This thesis investigates the suitability of the TMK method for MD simulations and demonstrates its performance compared to the well-known reference Verlet method. Some issues have not been investigated or addressed in detail and remain open for research. These aspects will be considered next.

First of all, in the thesis, the conservation of symmetry with the TMK method as opposed to the loss of symmetry when using the Verlet method is demonstrated with model simulations. These models provide us with a clear indication of the added value of using the TMK method as opposed to the Verlet method for MD simulations. However, this demonstration rests on example simulations and does not provide a rigorous proof of symmetry conservation when using the TMK method. This is an important open issue that needs theoretical consideration.

Secondly, the application of TMK in MD simulations might be limited by the computational costs of the method. It is mentioned that the TMK method is more costly than the Verlet method. A critical examination of the computation time and the complexity of the method will be extremely helpful for further development. Opportunities for dimension reduction with Lie group integrators could be an interesting line of work to pursue to avoid these costs.

Furthermore, the symmetry loss of the Verlet method as opposed to symmetry conservation with the TMK method has the most focus in this thesis. It would be of interest to look closer into the differences between the methods when near-symmetry is present. True symmetry might not be present in materials. Therefore, the results and arguments presented in this thesis should be developed further toward the requirements of actual MD applications.

Lastly, the relatively good performance of the fourth-order Runge-Kutta method in the model simulations may be observed. Energy drift is also demonstrated, which makes it a less suitable method for long-time MD simulations. However, it does demonstrate the advantages of higher-order methods for accurate solutions. The use of a higher-order Runge-Kutta-Munthe-Kaas method can be of interest. The TMK method is not the only option to consider.

Concluding this discussion, there is still some work to be done in proving the application of structure-preserving Lie group integrators in MD. However, a clear indication of an advantage of the TMK method as opposed to the Verlet method is given, and it would be interesting to investigate its extension to full MD simulations.

5.2 Conclusion

In this thesis, we have introduced a Lie group integrator, the Trapezoidal Munthe-Kaas integrator (TMK), to Molecular Dynamics (MD) simulations. We have demonstrated the use of this time integrator for one-dimensional model simulations and compared its outcomes with those computed with the Verlet and fourth-order Runge-Kutta (RK4) methods. The models used are one-dimensional lattices that build up from consisting only of two particles with free boundary conditions to eight particles with periodic boundary conditions. Several potentials are tested to observe the behavior of the integrators, namely, the Harmonic oscillator potential, the Toda potential, and the Lennard-Jones potential. The latter is used in most of our simulations as it can be argued to represent features of realistic force fields in MD simulations.

The Verlet and TMK methods are observed to preserve momentum and to near-preserve energy for all models, as expected for the N-body problem. Furthermore, an energy drift is observed for the RK4 method, which rules the RK4 method out for any long-time MD simulations. The computed trajectories for two- or three-particle models without additional symmetry are the same for all three methods for short-time simulations. Furthermore, we have seen that the Verlet method is more accurate for the Harmonic oscillator potential than the TMK or RK4 method. The number of computation steps is significantly lower for the Verlet method than for the TMK or RK4 method, reducing computational costs. Therefore, Verlet can be the cheapest and best integrator for simple problems without additional symmetry.

The Verlet method has been observed to fail to conserve symmetry for models with additional symmetries, which can not be resolved by decreasing the time step size. We have noted that this leads to incorrect trajectories and even incorrect break up of systems without periodic boundary conditions. The RK4 method has been shown to conserve this symmetry for some, but not all model simulations. The TMK method does conserve this symmetry in all tested cases. Models with a larger number of particles display chaotic behavior, and all three methods may result in different trajectories, but the TMK method was found to preserve the symmetry of the system, regardless.

The reader should note that the results computed in this thesis for the TMK method depend on the

implementation. The choice of the Lie group and the resulting allowed states of the system might be crucial to its performance. The added symmetry in the discussed models is not pre-installed into the TMK method. However, some structure about the lattice behavior is pre-installed. Depending on the exact system, this may reduce the dimensions of the problem and be of great additional value, for example, to reduce computational costs.

In conclusion, TMK is computationally more expensive but better performing than the commonly used Verlet method. For systems with additional symmetry, the Verlet method fails to conserve the additional symmetry and could compute incorrect outcomes independent of the time step size. The TMK method outperforms the Verlet method for the one-dimensional models with additional symmetry considered in this thesis, as it conserves these symmetries. We demonstrated the promising use of TMK for MD simulations. Namely, some structure may be assumed in MD simulations, and additional symmetries are usually present. Furthermore, the system is typically chaotic and enormous, and MD simulations are performed with periodic boundary conditions. We have demonstrated for a similar system that simulations break additional structural symmetry with the Verlet method and not with the TMK method. It remains to extend our approach to realistic MD simulations.

Chapter 6

Outlook

Further investigation following the results of this research could be numerous. This chapter will discuss future steps in section 6.1. Also, we would like to mention the possible use of learning methods with Lie group integrators for MD simulations in section 6.2. Furthermore, during the fruitful discussions leading up to this thesis, multiple ideas and approaches have been discussed that were not yet pursued. The main idea that might still be very interesting to pursue is the use of G-strands, which will be addressed shortly in section 6.4.

6.1 TMK as a time-integration method for MD

Future research we wish to conduct consists of expanding the current approach to real MD simulations. To that end, the next natural step to make would be to apply TMK to multi-dimensional systems. TMK for multi-dimensional models with lattice structures can be achieved with an approach similar to the one taken in this thesis for one-dimensional models. Additionally, the extension from nearest-neighbor potentials to potentials for m neighboring particles can be easily implemented and feasible for the TMK method. These additions will make MD simulations with potential forces calculated with TMK possible.

If multi-dimensional models with multiple particle potential interactions have been achieved, temperature fluctuations and the need for a thermostat for MD simulations may be investigated. An idea to implement the fluctuations can be achieved via the stochastic approach for the TMK solver as implemented by (Luesink et al., 2021).

Furthermore, the computational costs of the TMK method, as opposed to the Verlet method, have not been investigated yet in this thesis. It is discussed that the Verlet method is much cheaper and more simple, but exact measures are desirable. Namely, this could indicate when the additional value of the TMK method overrules its costs and indicate whether the use of the TMK method for large MD simulations is even feasible.

Another line of future research resulting from these results is a more theoretical one. Analysis of the methods should be performed such that we will not only demonstrate but also prove the

symmetry aspects of the two methods.

To summarize, an extension of the implementation of the TMK method is needed before realistic MD simulations can be performed. Apart from this, an analysis of its computational costs and an analysis of the symmetry conservation of the method is desired. Only then can we truly prove the potential of the TMK method for MD simulations.

6.2 Learning TMK for MD

Machine learning methods have been employed in MD simulations to construct force fields more efficiently (Lahnsteiner and Bokdam, 2022). However, learning methods to approach Hamiltonian systems can be combined with Lie group integrators of the Runge-Kutta Munthe-Kaas (RKMK) type, as shown in (Celledoni et al., 2023). Not only may we preserve structure when integrating the solutions in time, but we may also preserve structure when computing the force field of the system. This side of the MD simulations has not been discussed in this thesis.

6.3 Higher-order Lie group integrators

It could be of interest to consider higher-order Runge-Kutta methods as the basis of the Runge-Kutta-Munthe-Kaas method. In the model simulations, it is observed that the fourth-order Runge-Kutta method performs rather well, despite the observed energy drift. Therefore, a higher-order energy-conserving method as the basis of the RKMK method might be interesting to investigate.

6.4 G-strands for MD

Other approaches are possible to implement a Lie group integrator to MD simulations. An exciting approach would be to consider G-strands. G-strands have been constructed by (Holm et al., 2012) and can be thought of as coupled individual Lie groups. In a lattice formation, G-strands are called G-branes. Each unit cell of a material can be thought of as an individual heavy top, for example, that can be described with the Lie group $SE(3)$. The traveling of distortions through the unit cells can be represented by the coupling of individual $SE(3)$ elements. Similarly, phonon modes could be described by individual G-strands of which the coupling depends on the other G-strands. Choosing coupling and groups to represent the physical phenomena of a material would be challenging. Still, the correct implementation might be much more computationally efficient than the TMK implementation discussed in this thesis.

Aknowledgements

This thesis represents the current standpoint of an exciting journey. At the beginning of the project, we had many ideas, engaging discussions, and unexpected findings that shaped the direction of the project. Although the report appears complete, the work is far from finished. In fact, we are left with more questions to ask and research to pursue than at the very beginning. There are many ways to extend this work and even more other ideas that are yet to be explored. I feel like I have only scratched the surface of this field and have so much more to learn and there is so much more to be done. Apparently, this is inherent to learning and research in general, and I am eager to see where this journey will take me.

I want to express my gratitude to everyone who has helped and contributed to this project. Ever since I started working in the 3MS group, I have felt very welcome. I want to thank everyone for contributing to the enjoyable working environment present at the 3MS group: Arnout, Bernard, Erwin, Hyunjong, Kevin, Linda, Olena, Sagy, Sem, Stijn, and Viktoriia. The kind atmosphere is amazing and should not be taken for granted. I want to thank Arnout, Bernard, Erwin, and Menno for our meetings, discussions, and their many great ideas. Apart from helping me with insightful thoughts and critical comments, they have given me the freedom to explore multiple hunches and follow my own path within this project. This way, I have learned many things I could have never learned without this freedom. Special thanks go out to Erwin, who introduced me to the exciting world of Lie group integrators. His joy and passion for (this field in) mathematics are highly contagious. The road towards this project has not been the most straightforward, and I would like to thank Bernard for his guidance and support. He has given me great advice on the content of the work and everything that comes along with it. Furthermore, I thank Claudia Filippi and Felix Schwenninger for their time reading this (not-so-short) report and being committee members. At last, I would like to thank my family and friends, who had to endure my monologues on heavy tops and bouncing particles. Thank you for your support and patience.

Appendix A

Appendix

A.1 Example implementation group structure

Let us follow the steps described in section 3.3. We will demonstrate the process for $n = 3$ with free boundary conditions.

The state of the system is given by the following state vector:

$$\mu = (a_1, a_2, b_1, b_2, b_3) \tag{A.1}$$

For $n = 3$ a group element $g \in G$ and its inverse g^{-1} can be represented in matrix form as:

$$g = \begin{bmatrix} e^{\beta_2-\beta_1} & 0 & 0 & 0 & 0 \\ 0 & e^{\beta_3-\beta_2} & 0 & 0 & 0 \\ -\alpha_1 & 0 & 1 & 0 & 0 \\ \alpha_1 & -\alpha_2 & 0 & 1 & 0 \\ 0 & \alpha_2 & 0 & 0 & 1 \end{bmatrix}, \quad g^{-1} = \begin{bmatrix} e^{\beta_2-\beta_1} & 0 & 0 & 0 & 0 \\ 0 & e^{\beta_3-\beta_2} & 0 & 0 & 0 \\ \alpha_1 e^{\beta_2-\beta_1} & 0 & 1 & 0 & 0 \\ -\alpha_1 e^{\beta_2-\beta_1} & \alpha_2 e^{\beta_3-\beta_2} & 0 & 1 & 0 \\ 0 & -\alpha_2 e^{\beta_3-\beta_2} & 0 & 0 & 1 \end{bmatrix} \tag{A.2}$$

An element from the Lie algebra, $\xi \in \mathfrak{g}$, and an element from the dual Lie algebra, $\mu \in \mathfrak{g}^*$ can be denoted in matrix form as:

$$\xi = \begin{bmatrix} \xi_3 - \xi_4 & 0 & 0 & 0 & 0 \\ 0 & \xi_4 - \xi_5 & 0 & 0 & 0 \\ -\xi_1 & 0 & 0 & 0 & 0 \\ \xi_1 & -\xi_2 & 0 & 0 & 0 \\ 0 & \xi_2 & 0 & 0 & 0 \end{bmatrix}, \quad \mu = \begin{bmatrix} \mu_3 - \mu_4 & 0 & -\mu_1 & \mu_1 & 0 \\ 0 & \mu_4 - \mu_5 & 0 & -\mu_2 & \mu_2 \\ 0 & 0 & 0 & 0 & 0 \\ 0 & 0 & 0 & 0 & 0 \\ 0 & 0 & 0 & 0 & 0 \end{bmatrix} \tag{A.3}$$

The adjoint operator is constructed and written by the vector representation of $\mathfrak{g}$:

$$\mathrm{ad}_\xi \eta = [\xi, \eta] = \xi\eta - \eta\xi \tag{A.4}$$

$$\mathrm{ad}_\xi \eta = \begin{bmatrix} 0 & 0 & 0 & 0 & 0 \\ 0 & 0 & 0 & 0 & 0 \\ -\xi_1(\eta_3 - \eta_4) + \eta_1(\xi_3 - \xi_4) & 0 & 0 & 0 & 0 \\ \xi_1(\eta_3 - \eta_4) - \eta_1(\xi_3 - \xi_4) & -\xi_2(\eta_4 - \eta_5) + \eta_2(\xi_4 - \xi_5) & 0 & 0 & 0 \\ 0 & \xi_2(\eta_4 - \eta_5) + \eta_2(\xi_4 - \xi_5) & 0 & 0 & 0 \end{bmatrix} \tag{A.5}$$

$$\begin{bmatrix}(\mathrm{ad}_\xi\eta)_1\\(\mathrm{ad}_\xi\eta)_2\\(\mathrm{ad}_\xi\eta)_3\\(\mathrm{ad}_\xi\eta)_4\\(\mathrm{ad}_\xi\eta)_5\end{bmatrix} = \begin{bmatrix}\xi_1(\eta_3-\eta_4)-\eta_1(\xi_3-\xi_4)\\\xi_2(\eta_4-\eta_5)+\eta_2(\xi_4-\xi_5)\\0\\0\\0\end{bmatrix} \tag{A.6}$$

The Adjoint action is constructed and written by the vector representation of $\mathfrak{g}$:

$$\mathrm{Ad}_g\xi = g\xi g^{-1} \tag{A.7}$$

$$\mathrm{Ad}_g\xi = \begin{bmatrix}(\xi_3-\xi_4) & 0 & 0 & 0 & 0\\0 & (\xi_4-\xi_5) & 0 & 0 & 0\\e^{\beta_2-\beta_1}(-\alpha_1(\xi_3-\xi_4)-\xi_1) & 0 & 0 & 0 & 0\\e^{\beta_2-\beta_1}(\alpha_1(\xi_3-\xi_4)+\xi_1) & e^{\beta_3-\beta_2}(-\alpha_2(\xi_4-\xi_5)-\xi_2) & 0 & 0 & 0\\0 & e^{\beta_3-\beta_2}(\alpha_2(\xi_4-\xi_5)+\xi_2) & 0 & 0 & 0\end{bmatrix} \tag{A.8}$$

$$\begin{bmatrix}(\mathrm{Ad}_g\xi)_1\\(\mathrm{Ad}_g\xi)_2\\(\mathrm{Ad}_g\xi)_3\\(\mathrm{Ad}_g\xi)_4\\(\mathrm{Ad}_g\xi)_5\end{bmatrix} = \begin{bmatrix}e^{\beta_2-\beta_1}(\alpha_1(\xi_3-\xi_4)+\xi_1)\\e^{\beta_3-\beta_2}(\alpha_2(\xi_4-\xi_5)+\xi_2)\\\xi_3\\\xi_4\\\xi_5\end{bmatrix} \tag{A.9}$$

Let us use this to find the Coadjoint action:

$$\left\langle \mathrm{Ad}_g^*\mu, \xi\right\rangle = \langle \mu, \mathrm{Ad}_g\xi\rangle \tag{A.10}$$

$$\begin{aligned}\langle \mu, \mathrm{Ad}_g\xi\rangle =& \mu_1(\mathrm{Ad}_g\xi)_1 + \mu_2(\mathrm{Ad}_g\xi)_2 + \mu_3(\mathrm{Ad}_g\xi)_3 + \mu_4(\mathrm{Ad}_g\xi)_4 + \mu_5(\mathrm{Ad}_g\xi)_5\\ =& \mu_1\left(e^{\beta_2-\beta_1}\left(\alpha_1(\xi_3-\xi_4)+\xi_1\right)\right) + \mu_2\left(e^{\beta_3-\beta_2}\left(\alpha_2(\xi_4-\xi_5)+\xi_2\right)\right) + \mu_3\xi_3 + \mu_4\xi_4 + \mu_5\xi_5\\ =& \left(\mu_1 e^{\beta_2-\beta_1}\right)\xi_1 + \left(\mu_2 e^{\beta_3-\beta_2}\right)\xi_2 + \left(\mu_1 e^{\beta_2-\beta_1}\alpha_1 + \mu_3\right)\xi_3 + ..\\ & .. + \left(-\mu_1 e^{\beta_2-\beta_1}\alpha_1 + \mu_2 e^{\beta_3-\beta_2}\alpha_2 + \mu_4\right)\xi_4 + \left(-\mu_2 e^{\beta_3-\beta_2}\alpha_2 + \mu\right)\xi_5\end{aligned}$$

By rewriting the expression, we identify the elements of the Coadjoint action.

$$\begin{bmatrix}(\mathrm{Ad}_g^*\xi)_1\\(\mathrm{Ad}_g^*\xi)_2\\(\mathrm{Ad}_g^*\xi)_3\\(\mathrm{Ad}_g^*\xi)_4\\(\mathrm{Ad}_g^*\xi)_5\end{bmatrix} = \begin{bmatrix}\mu_1 e^{\beta_2-\beta_1}\\\mu_2 e^{\beta_3-\beta_2}\\\mu_1 e^{\beta_2-\beta_1}\alpha_1 + \mu_3\\-\mu_1 e^{\beta_2-\beta_1}\alpha_1 + \mu_2 e^{\beta_3-\beta_2}\alpha_2 + \mu_4\\-\mu_2 e^{\beta_3-\beta_2}\alpha_2 + \mu_5\end{bmatrix} \tag{A.11}$$

In matrix form, the Coadjoint action follows the dual Lie algebra mapping:

$$\begin{bmatrix}(3)-(4) & 0 & -(1) & (1) & 0\\0 & (4)-(5) & 0 & -(2) & (2)\\0 & 0 & 0 & 0 & 0\\0 & 0 & 0 & 0 & 0\end{bmatrix} \tag{A.12}$$

Now, we have obtained the group actions that are needed to implement the TMK integrator for the case of $n = 3$ with free boundary conditions.

A.2 Additional model simulations

A.2.1 Three-particle ring

The three-particle ring has asymmetric initial conditions with $r_1 = \left(2^{1/6}\right)$, $r_2 = \left(2^{1/6} - \frac{1}{10}\right)$ and $r_3 = \left(2^{1/6} + 1\right)$. For the three-particle ring, we observe similar results in Figure A.1 as before for cases without additional symmetry. The TMK, RK4, and Verlet methods result in the same displacement trajectories. We do note that the system becomes rather chaotic. The trajectories are not as neatly periodic as seen in other examples. This is also observed in the energy change. Although it is not as elegant as before, the total energy still appears to be near-conserved, and the total momentum is conserved up to machine precision as seen before.

A.2.2 Eight-particle ring with less extreme initial conditions

In Figure A.2, the symmetry of the eight-particle ring with smaller distortion is plotted for the different methods. The distortion of the initial displacements is half of the eight-particle model observed before. It can be noted that the asymmetry builds up for the RK4 and Verlet methods but takes a much longer time to become of significant magnitude. The TMK method does not show the build-up in asymmetry.

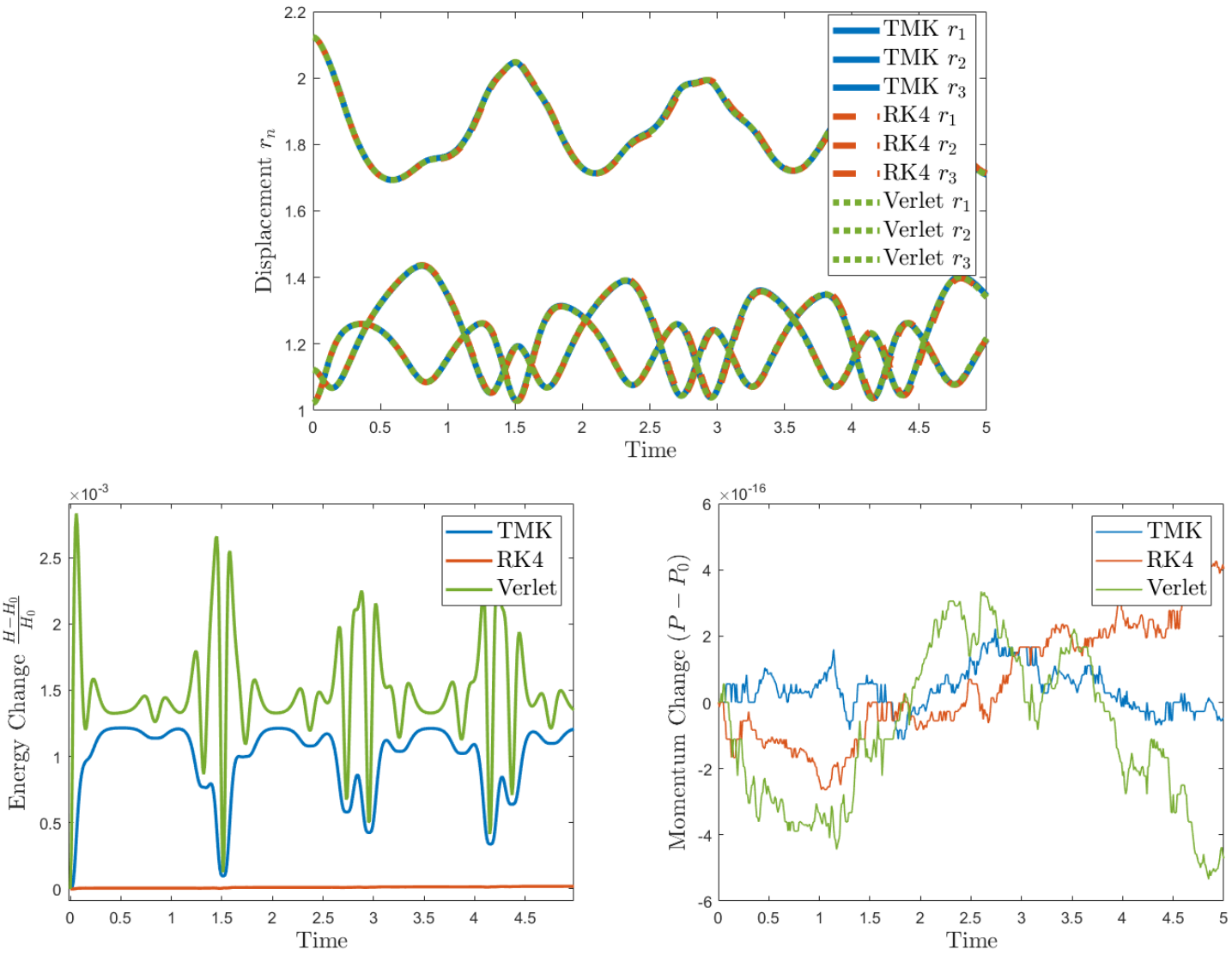

Figure A.1: Three-particle ring with the Lennard-Jones potential, with $\Delta t = 10^{-2}$, and initial conditions $r_1 = \left(2^{1/6}\right), r_2 = \left(2^{1/6} - 1/10\right), r_3 = \left(2^{1/6} + 1\right)$, $p_1 = p_2 = p_3 = 0$.

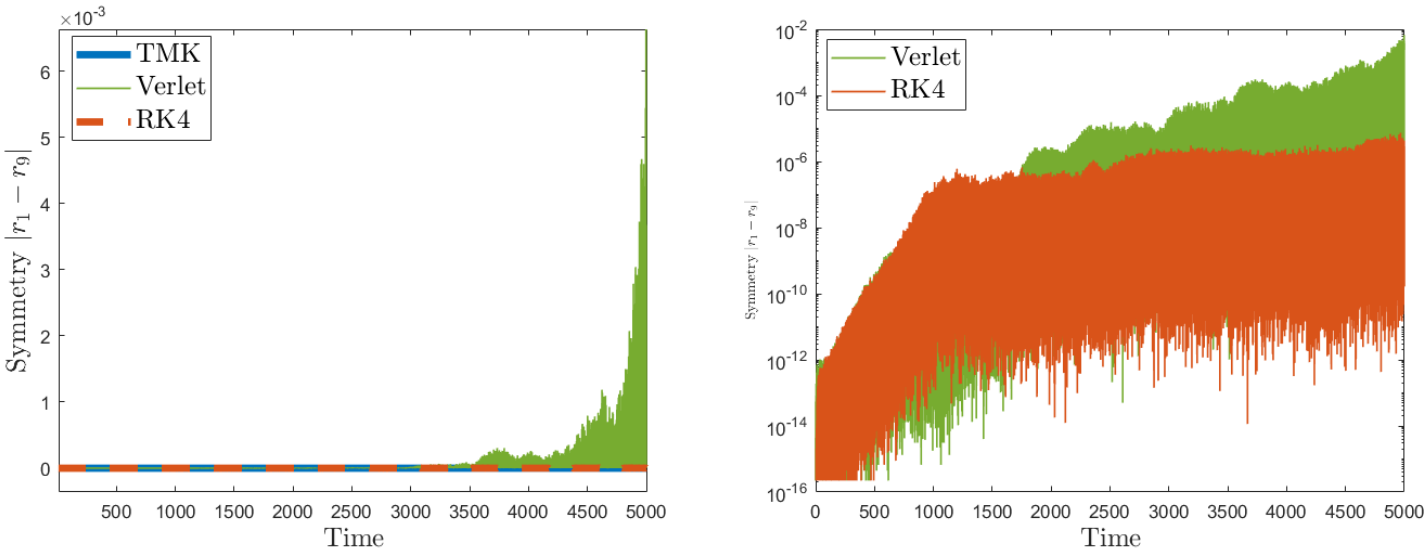

Figure A.2: Symmetry of the eight-particle ring with the Lennard-Jones potential, with $\Delta t = 10^{-4}$, and initial conditions$r_1 = r_2 = r_6 = r_7 = r_{ghost} = 2^{1/6}$, $r_3 = r_5 = \left(2^{1/6} + 0.05\right)$, $r_4 = \left(2^{1/6} - 0.1\right)$, $p_1 = p_2 = .. = p_8 = 0$.

A.3 Additional figures

This section provides the reader with additional figures for the model simulations discussed in Chapter 4.

A.3.1 Energy conversion - three particles on a line

For the three-particle model without periodic boundary conditions, one can illustrate the energy transfer from the left to the right particle, E_1 to E_3. The oscillatory energy of E_2 is due to the oscillatory potential energies. However, the left and right particles should have the same constant energy $E_1 = E_3$. It can be seen that indeed the distribution of energy changes in the Verlet method corresponding to the escape of one particle leaving an oscillating binary system.

The difference between energies E_1 and E_3 are plotted in Figure A.3.

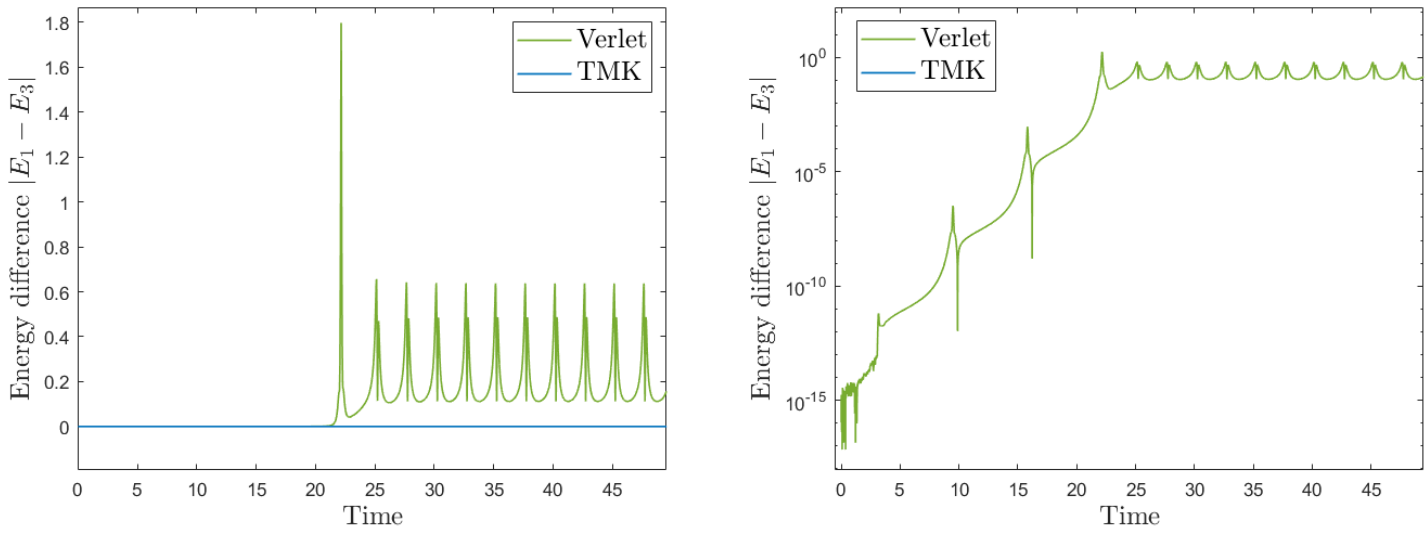

(a) Linear plot.

(b) Logairthmic plot.

Figure A.3: Energy difference $|E_1 - E_3|$ for the three-particle model with the Lennard-Jones potential, with $\Delta t = 10^{-4}$ and initial conditions $r_1 = r_2 = 2^{1/6} + 1$, $v_1 = v_2 = v_3 = 0$.

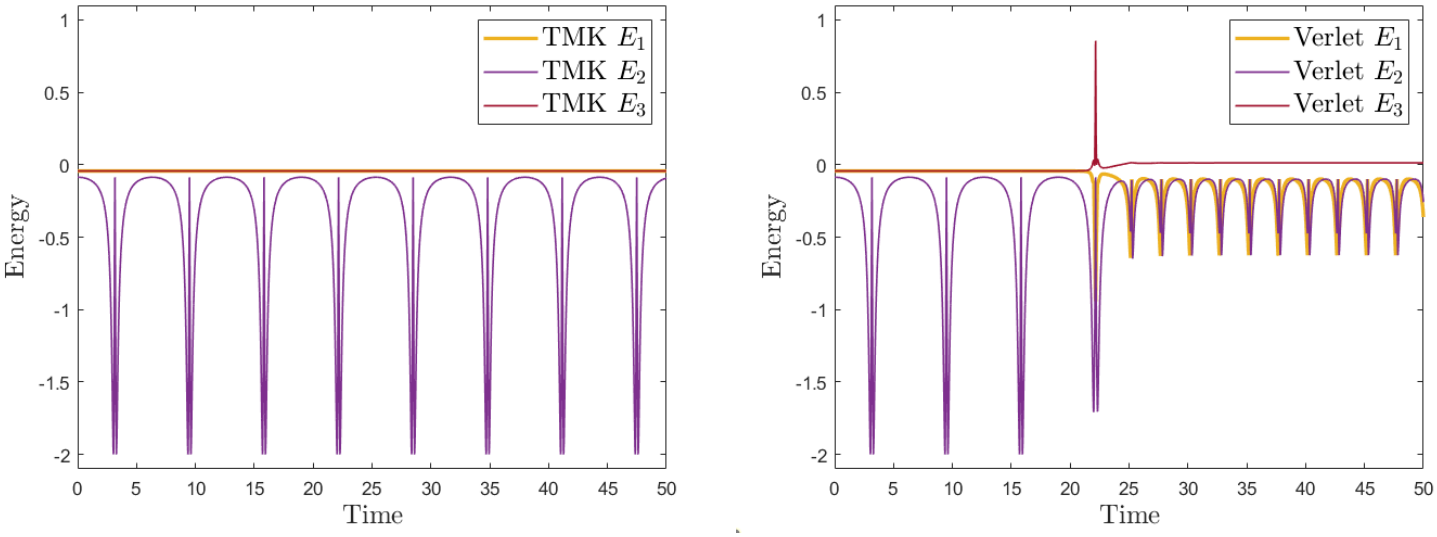

(a) TMK.

(b) Verlet.

Figure A.4: Energies E_1, E_2, E_3 for the three-particle model with the Lennard-Jones potential, with $\Delta t = 10^{-4}$ and initial conditions $r_1 = r_2 = 2^{1/6} + 1$, $v_1 = v_2 = v_3 = 0$.

Bibliography

G. Benettin and A. Giorgilli. On the hamiltonian interpolation of near-to-the identity symplectic mappings with application to symplectic integration algorithms. Journal of Statistical Physics, 74:1117–1143, 1994.

A. M. Bloch, F. Gay-Balmaz, and T. S. Ratiu. The geometric nature of the flaschka transformation. Communications in Mathematical Physics, 352:457–517, 2017.

E. Celledoni, R. I. McLachlan, D. I. McLaren, B. Owren, G. R. W. Quispel, and W. M. Wright. Energy-preserving runge-kutta methods. ESAIM: Mathematical Modelling and Numerical Analysis, 43(4):645–649, 2009.

E. Celledoni, H. Marthinsen, and B. Owren. An introduction to lie group integrators–basics, new developments and applications. Journal of Computational Physics, 257:1040–1061, 2014.

E. Celledoni, A. Leone, D. Murari, and B. Owren. Learning hamiltonians of constrained mechanical systems. Journal of Computational and Applied Mathematics, 417:114608, 2023.

A. Coretti, T. Baird, R. Vuilleumier, and S. Bonella. Mass-zero constrained dynamics for simulations based on orbital-free density functional theory. The Journal of Chemical Physics, 157(21):214110, 2022.

P. E. Crouch and R. Grossman. Numerical integration of ordinary differential equations on manifolds. Journal of Nonlinear Science, 3:1–33, 1993.

R. De Vogelaere. Methods of integration which preserve the contact transformation property of the hamilton equations. Technical report (University of Notre Dame. Dept. of Mathematics), 1956.

P. Dereń, A. Bednarkiewicz, P. Goldner, and O. Guillot-Noël. Laser action in la al o 3: Nd 3+ single crystal. Journal of Applied Physics, 103(4):043102, 2008.

K. Engø and S. Faltinsen. Numerical integration of Lie–Poisson systems while preserving coadjoint orbits and energy. SIAM journal on numerical analysis, 39(1):128–145, 2001.

H. Flaschka. The toda lattice. ii. existence of integrals. Physical Review B, 9(4):1924, 1974a.

H. Flaschka. On the toda lattice. ii: inverse-scattering solution. Progress of Theoretical Physics, 51 (3):703–716, 1974b.

D. Frenkel and B. Smit. Understanding molecular simulation: from algorithms to applications, volume 1. Elsevier, 2001.

Y. Gao, Y. Wu, H. Lu, C. Chen, Y. Liu, X. Bai, L. Yang, W. Y. William, Q. Dai, and Y. Zhang. Cspbbr3 perovskite nanoparticles as additive for environmentally stable perovskite solar cells with 20.46% efficiency. Nano Energy, 59:517–526, 2019.

A. Gotzias. Water to cyclohexane transfer free energy calculations for a carbon nanotube. Carbon Trends, 9:100215, 2022.

E. Hairer and C. Lubich. Energy conservation by stormer-type numerical integrators. CHAPMAN AND HALL CRC RESEARCH NOTES IN MATHEMATICS, pages 169–190, 2000.

E. Hairer, C. Lubich, and G. Wanner. Geometric numerical integration illustrated by the störmer–verlet method. Acta numerica, 12:399–450, 2003.

E. Hairer, C. Lubich, and G. Wanner. Geometric Numerical Integration: Structure-Preserving Algorithms for Ordinary Differential Equations, volume 31. Springer Science & Business Media, 2006.

D. D. Holm. Geometric Mechanics-Part II: Rotating, Translating and Rolling. World Scientific, 2011.

D. D. Holm and A. M. Lucas. Toda lattice g-strands. arXiv preprint arXiv:1306.2984, 2013.

D. D. Holm, T. Schmah, and C. Stoica. Geometric mechanics and symmetry: from finite to infinite dimensions, volume 12. Oxford University Press, 2009.

D. D. Holm, R. I. Ivanov, and J. R. Percival. G-strands. Journal of Nonlinear Science, 22:517–551, 2012.

J. R. Hook and H. E. Hall. Solid state physics. John Wiley & Sons, 2013.

A. Iserles, H. Z. Munthe-Kaas, S. P. Nørsett, and A. Zanna. Lie-group methods. Acta numerica, 9: 215–365, 2000.

J. Lahnsteiner and M. Bokdam. Anharmonic lattice dynamics in large thermodynamic ensembles with machine-learning force fields: Cs pb br 3, a phonon liquid with cs rattlers. Physical Review B, 105(2):024302, 2022.

S. Lie. Begründung einer invarianten-theorie der berührungs-transformationen. Mathematische Annalen, 8(2):215–303, 1874.

E. Lindahl. Molecular dynamics simulations. Molecular modeling of proteins, pages 3–26, 2015.

E. Luesink, S. Ephrati, P. Cifani, and B. Geurts. Casimir preserving stochastic lie-poisson integrators. arXiv preprint arXiv:2111.13143, 2021.

J. Luo, J.-H. Im, M. T. Mayer, M. Schreier, M. K. Nazeeruddin, N.-G. Park, S. D. Tilley, H. J. Fan, and M. Grätzel. Water photolysis at 12.3% efficiency via perovskite photovoltaics and earth-abundant catalysts. Science, 345(6204):1593–1596, 2014.

V. Manwadkar, B. Kol, A. A. Trani, and N. W. Leigh. Testing the flux-based statistical prediction of the three-body problem. Monthly Notices of the Royal Astronomical Society, 506(1):692–708, 2021.

J. E. Marsden and T. S. Ratiu. Introduction to mechanics and symmetry: a basic exposition of classical mechanical systems, volume 17. Springer Science & Business Media, 1999.

J. Michl, M. Sega, and C. Dellago. Phase stability of the ice xvii-based co2 chiral hydrate from molecular dynamics simulations. The journal of chemical physics, 151(10):104502, 2019.

H. Munthe-Kaas. High order runge-kutta methods on manifolds. Applied Numerical Mathematics, 29(1):115–127, 1999.

E. Noether. Invariant variation problems. Transport theory and statistical physics, 1(3):186–207, 1971.

X.-Y. Qu, X.-F. Gou, and T.-G. Wang. A highly accurate interatomic potential for lamno3 perovskites with temperature-dependence of structure and thermal properties. Computational Materials Science, 193:110406, 2021.

P. K. Schelling, S. R. Phillpot, and D. Wolf. Mechanism of the cubic-to-tetragonal phase transition in zirconia and yttria-stabilized zirconia by molecular-dynamics simulation. Journal of the American Ceramic Society, 84(7):1609–1619, 2001.

S. D. Stranks and H. J. Snaith. Metal-halide perovskites for photovoltaic and light-emitting devices. Nature nanotechnology, 10(5):391–402, 2015.

M. Toda. Waves in nonlinear lattice. Progress of Theoretical Physics Supplement, 45:174–200, 1970.

M. Valtonen and H. Karttunen. The three-body problem. Cambridge University Press, 2006.

L. Verlet. Computer" experiments" on classical fluids. i. thermodynamical properties of lennard-jones molecules. Physical review, 159(1):98, 1967.

Q. You, S. Gu, and X. Gou. The highly accurate interatomic potential of cspbbr3 perovskite with temperature dependence on the structure and thermal properties. Materials, 16(5):2043, 2023.

H. Yu and P. A. Dalby. A beginner's guide to molecular dynamics simulations and the identification of cross-correlation networks for enzyme engineering. In Methods in enzymology, volume 643, pages 15–49. Elsevier, 2020.